University of Massachusetts Amherst
ScholarWorks@UMass Amherst

Doctoral Dissertations | Dissertations and Theses

March 2016

Translocations of Ring and Linear Polymers & Polyelectrolyte Brush in Salty Solution

Ning Ouyang
University of Massachusetts - Amherst

Follow this and additional works at: https://scholarworks.umass.edu/dissertations_2

 Part of the Physics Commons

Recommended Citation

Ouyang, Ning, "Translocations of Ring and Linear Polymers & Polyelectrolyte Brush in Salty Solution" (2016). *Doctoral Dissertations*. 593.
https://scholarworks.umass.edu/dissertations_2/593

This Open Access Dissertation is brought to you for free and open access by the Dissertations and Theses at ScholarWorks@UMass Amherst. It has been accepted for inclusion in Doctoral Dissertations by an authorized administrator of ScholarWorks@UMass Amherst. For more information, please contact scholarworks@library.umass.edu.

TRANSLOCATIONS OF RING AND LINEAR POLYMERS & POLYELECTROLYTE BRUSH IN SALTY SOLUTION

A Dissertation Presented

by

NING OUYANG

Submitted to the Graduate School of the
University of Massachusetts Amherst in partial fulfillment
of the requirements for the degree of

DOCTOR OF PHILOSOPHY

February 2016

Physics

© Copyright by Ning Ouyang 2016

All Rights Reserved

TRANSLOCATIONS OF RING AND LINEAR POLYMERS & POLYELECTROLYTE BRUSH IN SALTY SOLUTION

A Dissertation Presented

by

NING OUYANG

Approved as to style and content by:

Murugappan Muthukumar, Chair

Adrian Parsegian, Member

Narayanan Menon, Member

Harry Bermudez, Member

Rory Miskimen, Department Chair
Physics

ACKNOWLEDGMENTS

First of all, I would like to express my sincere appreciation and gratitude to my advisor Dr. Murugappan Muthukumar for his instruction and influence on broad aspects of my academic life ever since I started my graduate study at UMass. He has always been encouraging and supportive without reservation. I also would like to thank my committee members: Dr. Adrian Parsegian, Dr. Narayanan Menon and Dr. Harry Bermudez, for their help and suggestions on my thesis writing. I am greatly in debt to my colleague Dr. Mithun K. Mitra for his collaboration, especially on topics in Chapter 5. I am sincerely grateful to all current members of Muthu group: Hamidreza Shojaei, Harsh Katkar, Byoung-Jin Jeon, Anand Rahalkar, Svetlana Morozova, Michael Leaf, Brendan R. Ondra, Debasish Mondal, Sabin Adhikari, Sadhana Chalise, Prabhat Tripathi, Kiran S. Iyer, and former members: Jin Hua, Yanbo Wang, Bo Peng, Sunil P. Singh, Jyoti Prakash Mahalik, Stephen Mirigian, Benjamin Mohr, for their valuable friendship and inspiring discussion during my years in Amherst. Last but not least, I am thankful to my parents and my husband Han Li for their love and support.

ABSTRACT

TRANSLOCATIONS OF RING AND LINEAR POLYMERS & POLYELECTROLYTE BRUSH IN SALTY SOLUTION

FEBRUARY 2016

NING OUYANG

B.Sc., TIANJIN UNIVERSITY, CHINA

M.Sc., UNIVERSITY OF MASSACHUSETTS AMHERST

Ph.D., UNIVERSITY OF MASSACHUSETTS AMHERST

Directed by: Professor Murugappan Muthukumar

We study the electric-field-driven translocation of polymers with ring architecture, i.e. circular polymers, in comparison with their linear counterpart. We construct the free energy landscape for ring and linear polymer translocations respectively, in the context of Fokker-Planck formalism. Non-monotonicity of translocation time as function of polymer length is observed from ring polymer, which is enhanced by pore-polymer attraction. The external electric driving force and pore-polymer interaction are the tuning parameter of relative translocation time of ring and linear polymers.

We study the polyelectrolyte brush in monovalent salt using self-consistent-field-theory. We confirmed the step-function polymer profile in strong-stretched state. We examine the ion distribution and assure the trapping counterions by the brush. We also study the polyelectrolyte brush in divalent salt using explicit Donnan equilibrium and free energy minimization. We calculation the brush height and degree

of ionization self-consistently as function divalent salt concentration. We explained the non-monotonic behavior of brush height versus salt concentration (observed in experiment) by charge reversal.

TABLE OF CONTENTS

LIST OF TABLES

Table **Page**

LIST OF FIGURES

Figure **Page**

CHAPTER 1

OUTLINE

Polymer translocation is an important process to study polymer dynamics and a number of works have been done in linear polymer translocation. Recently circular DNA, i.e. a closed form of charged polymer, has attracted more and more interests. Half of this work is devoted to the study of translocation dynamics, focusing on the comparison of translocations of ring and linear polymers.

In the past couple of decades, polymer brush, which is composed of densely grafted chains on a wall, becomes a more and more interesting research subject due to its practical use in surface modification. More recently the charged polymer brush keeps attracting attentions, as long-range electric interaction among chains leads to even richer phenomena. The second half of this work develops theory on polyelectrolyte brush.

Both subjects of polymer translocations and polymer brushes use the ideas and concepts of polymer near surfaces, which we discuss extensively in chapter 2. The first chapter also outlines the basic theories involved in the study of polymer translocation, including partition sum of polymer conformations near surfaces and Fokker-Planck formalism. The chapter 3 aims to understand the physics and differences of translocations of ring and linear polymer in general with scaling theory. To compare the two topologically different objects, we carefully examine their conformational entropy. We also found the pore and polymer interaction plays an important role in the translocation dynamics. A non-monotonic behavior of translocation time as a function of polymer length is observed for ring polymer, which is absent in linear polymer translo-

cation. In chapter 4, we present some existing theory on both neutral and charged polymer brushes. We study the polyelectrolyte brush immersed in monovalent salt with self-consistent-field theory in chapter 5. We compute the distribution of all species of molecules in the system as well as the brush height and degree of ionization self-consistently. Backed up by the results of SCFT, we construct a free energy in a more straightforward way by using the Donnan equilibrium conditions explicitly in chapter 6. We get consistent results as SCFT. We are able to apply the same method to divalent salt case and to explain some experimental results by the concept of charge reversal.

CHAPTER 2

POLYMER TRANSLOCATION THEORY

2.1 Introduction

Polymer translocation is an important physical model extracted from real biological systems and processes[**?**]. It is a process of charged polymer moving from one region to another through a confined opening. A wide range of examples include the DNA/RNA translocating through nuclear pores[**?**], gene swapping from virus to bacteria[**?**], injection of genomes from virus into a host cell, and transportation of protein across membranes. The topic of polymer translocation has been attracting considerable interest in the past few decades, especially with the emergence of well controlled experiments in molecular level. For instance, the synthetic charged polymer (NaPSS) or DNA/RNA are driven by electric force through a protein (αHL) pore or a solid-state nanopore in experiments[**?** **?** **?** **?** **?**]. Substantial research works have been contributing to the area of polymer translocations, not only due to its practical promise in DNA sequencing [**?**], but also due to the fundamental inquiries about macromolecule dynamics. Variety of numerical works by molecule dynamics simulations have been done on this subject too[**?** **?** **?** **?** **?** **?** **?**]. Both experiments and simulations endeavored to examine the effects due to the macromolecules and the pore on the dynamical process.

Polymers forced through a narrow pore are subjected to an entropic barrier. This is because the entering to a restricted space reduces the number of possible conformations that are allowed by free space[**?**]. Muthukumar[**?**] implemented the concepts of crystal nucleation and growth to analogize the process of a polymer translocat-

ing from donor compartment to receiver compartment through the hole. To make a successful translocation, a polymer has to overcome such a barrier, which is similar to the nucleation of crystals. In this context, the entropic barrier along with other energetic contributions from intra-chain interaction, pore-polymer interaction, and external driving force, makes a complete free energy landscape of the translocation process. Under the full free energy landscape, the polymer can move back-and-forth under thermal fluctuation. The stochastic nature of this process which falls into the Markov process category, allows us to use Fokker-Planck formalism[**?**]. Our discussion of polymer translocation kinetics will base on this theoretical foundation. Some theoretical discussion has been made following this model[**?**]. Other variation of this theoretical model were also reported in literatures[**? ?**].

Polymer translocation incorporates many aspects of polymer physics[**?**]. Firstly, as the entropy barrier coming from conformation suppression plays an important role, we have to understand the structure of macromolecules under different circumstances, such as polymers near surfaces, inside a pore or a sphere, polymers with excluded volume interaction and bending energy, etc. In bio-systems, for example a cell, polymers are mostly charged and immersed in electrolyte solution. The long-range, electric interaction and ion flows make this problem even more complicated. In this chapter, we investigate the configurations of polymers near a impenetrable wall, as well as difference between linear and closed chain architectures. We also summarize the Fokker-Planck formalism used to approach numerical analytics of translocation process. At the end we give one example of free energy landscape of polymer translocation through a hole.

2.2 Polymers near surfaces

A polymer translocation process starts with a chain approaching a surface where the pore is sitting. Some conformations of a chain are suppressed during this process

compared with a chain in a free space. The polymer system is no long isotropic, as the symmetry in the perpendicular direction is broken by the presence of an impenetrable surface. The polymer properties associate with this geometry itself is a fundamental problem [**?**]. As the polymer length, i.e. the number of monomers N becomes very large, there some universal power laws. For example[**?**], in the mean end-to-end distance $< R^2 > \propto N^{\nu}$, $\nu = 0.59$ (for a free chain in bulk) is universal. While in the number of configurations of a chain with free end $\mathscr{Z}_N \propto N^{\gamma'-1} z^N$, although z is a lattice-dependent quantity, the critical exponent $\gamma' = 0.5$ (for an ideal chain in bulk) is also universal. How does these numbers change at the presence of a surface? We discuss in three situations: ideal chain, self-avoiding chain, and semi-flexible chain.

2.2.1 Ideal (Gaussian) chains near surfaces

We start with non-interactive chain (also called ideal chain or Gaussian chain), where the interaction among monomers are ignored. The only variable comes from the chain connectivity, which accounts for the entropy of a chain. We can simply count the number of possible conformations by viewing it as a chain of subsequent, freely-jointed bonds.

2.2.1.1 One-dimensional ideal chain on a lattice

In a lattice model, a ideal chain with N bonds starts at position A ($z = z_A$) and ends at position B ($z = z_B$). The chain conformation mimics the random walk of N steps. First consider the simplest case of one dimension. Define the number of steps going right to be N_R and the number of steps going left to be N_L. There are two equations governing this scenario:

$$\begin{cases} N_R - N_L = z_B - z_A, \\ N_R + N_L = N. \end{cases} \tag{2.1}$$

Solve N_A and N_B from the above equations, we have

$$\begin{cases} N_R = \frac{N+(z_B-z_A)}{2}; \\ N_L = \frac{N-(z_B-z_A)}{2}. \end{cases} \tag{2.2}$$

The total number of possible conformations of the path (examples in Figure**??**) can be expressed as [**?** **?**]:

$$\mathscr{Z}_N(z_A, z_B) = \binom{N}{N_R} = \frac{N!}{N_R!N_L!} \approx 2^N \sqrt{\frac{2}{\pi N}} \exp\left[-\frac{(z_B - z_A^2)}{2N}\right] \tag{2.3}$$

by Sterling approximation.

2.2.1.2 Reflection principle

For a random walk (i.e. the path of an idea chain), the number of paths from position A to postition B via position C is equal to the number of paths from the mirror image of A (A') to B via C [**?**]. A' is the mirror image of A respect to C. Every path going from A to B via C has a counterpart with starting point reflected by C. The one-dimensional case is shown in Figure**??**. A path in green color from A through C to B always has a image path in blue from A' to B through C. It is equivalent to the statement that, the number of paths from A to B without crossing C is equal to the number of paths from A to B minus the number of path from A' to B in the absence of C. Suppose $z_C = -1$, the image of A is at $z_{A'} = 2 - z_A$. Therefore, the partition sum of conformations in half space is:

$$\begin{aligned} \mathscr{Z}_N^{half}(z_A, z_B) =& \mathscr{Z}_N(z_B - z_A) - \mathscr{Z}_N(z_B - z_{A'}) \\ =& \binom{N}{\frac{N+(z_B-z_A)}{2}} - \binom{N}{\frac{N+(z_B-z_A+2)}{2}}. \end{aligned} \tag{2.4}$$

This can be easily generalized to 3D path with C being on a flat mirror surface.

2.2.1.3 Continuum description of ideal chains

The contour of a ideal chain can be viewed as a path of particle under diffusion. We can use a partial differential equation to describe the probability that the chain starts at $\mathbf{r_A}$ and ends at $\mathbf{r_B}$ [**?**] as:

$$\frac{\partial}{\partial N}G(\mathbf{r_A},\mathbf{r_B},N)-\frac{l}{6}\nabla^2 G(\mathbf{r_A},\mathbf{r_B},N)=\delta(N)\delta(\mathbf{r_A}-\mathbf{r_B}), \tag{2.5}$$

where l is the bond (step) length. G is the Green's function for the diffusion equation with the diffusion coefficient $l/6$. The length of the chain is in place of the time under diffusion. In infinite space, the Green's function that is also called the propagator, is solved as a Gaussian distribution.

$$G(\mathbf{r_A},\mathbf{r_B},N)=\left(\sqrt{\frac{3}{2\pi N l^2}}\right)^3\exp\left[-\frac{3(\mathbf{r_B}-\mathbf{r_A})^2}{2Nl^2}\right] \tag{2.6}$$

2.2.1.4 Proper boundary conditions

However, when there is a boundary, we should solve it under proper boundary conditions. Suppose we place an imaginary absorbing surface one layer behind the boundary and then remove the physical surface (Figure **??**). When a monomer touches the absorbing surface, this path will disappear. In this way all the paths across the boundary will be eliminated. Therefore, the proper boundary condition for a non-penetrating boundary is $G(\mathbf{r} = \textit{boundary}) = 0$. This is called absorbing boundary in the context of a ordinary diffusion equation. The solution to the diffusion equation under absorbing condition is equivalent to place a negative source at A', i.e. the image position of A:

$$\begin{aligned}&\mathscr{Z}_N^{half}(\mathbf{r_A},\mathbf{r_B})\approx G^{half}(\mathbf{r_A},\mathbf{r_B},N)\\&=\left(\sqrt{\frac{3}{2\pi N l^2}}\right)^3\left(\exp\left[-\frac{3(\mathbf{r_B}-\mathbf{r_A})^2}{2Nl^2}\right]-\exp\left[-\frac{3(\mathbf{r_B}-\mathbf{r_{A'}})^2}{2Nl^2}\right]\right).\end{aligned} \tag{2.7}$$

2.2.1.5 Partition sum of ideal chain grafted at surface

Consider the boundary to be a flat surface and put the adsorbing surface at origin $z = 0$. We want to know what the partition sum of a chain grafted at the physical boundary (at $z = l$;) is. Therefore, the chain starts at $z_A = l$, and could possibly end at any place with $z > 0$. The is rendered to a one dimensional problem, as the x and y direction is intact and trivial. After integrating out x and y dependence in full range ($-\infty$ to ∞), the propagator in z direction is

$$G^{half}(z_A, z_B, N) = \sqrt{\frac{3}{2\pi N l^2}} \left(\exp\left[-\frac{3(z_B - z_A)^2}{2Nl^2} \right] - \exp\left[-\frac{3(z_B + z_A)^2}{2Nl^2} \right] \right).$$

To derive the partition sum, z dependent is integrated over the positive half space (0 to ∞):

$$\begin{aligned} \mathscr{Z}_N^{half} &\approx \int_0^\infty G^{half}(l, z, N) dz \\ &= \int_0^\infty \sqrt{\frac{3}{2\pi N l^2}} \left(\exp\left[-\frac{3(z-l)^2}{2Nl^2} \right] - \exp\left[-\frac{3(z+l)^2}{2Nl^2} \right] \right) dz \\ &= erf(\frac{3l}{2N}) \end{aligned}$$

For long chain limit, there are two kinds of chain architectures in which we are interested (as shown in Figure**??**). One is the linear tail sticking out of the surface, which has a partition sum scales with polymer length N as:

$$\mathscr{Z}_N^{half} \approx \frac{3l}{\sqrt{\pi} N} \propto N^{-0.5}. \tag{2.8}$$

Another is a loop in which the two ends of a chain both attach to the surface and have $z_A = z_B = l$. The partition sum of such a loop is:

$$\mathscr{Z}_N^{half,loop} \approx \sqrt{\frac{3}{2\pi N l^2}} \left(1 - \exp\left[-\frac{3(2l)^2}{2Nl^2} \right] \right) \propto N^{-1.5}. \tag{2.9}$$

	Ideal Chain	Self-avoiding Chain
linear form	$\gamma_l' = 0.5$	$\gamma_h' = 0.69$
loop form	$\gamma_h' = -0.5$	$\gamma_h' = -0.38$

Table 2.1. Critical exponent

2.2.2 Self-avoiding chains near surfaces

The polymer chain with excluded volume interaction cannot be solved exactly due to non-linear interaction among monomers. Fortunately, the connection between the polymer statistics and the correlation function in the n-vector model of magnets as $n \to \infty$, makes it possible to borrow the techniques developed in the critical phenomenon of semi-infinite systems. The critical exponent γ' is one of the universal properties that calculated numerically and confirmed by Monte Carlo simulations[**?**]. The following table presents the critical exponents for self-avoiding chain and ideal chain in both linear and loop form respectively:

2.2.3 Semiflexible chains near surfaces

Many biopolymers have stiff backbones. For example dsDNA has a persistent length of about $50nm$ under physiological conditions. Some synthetic polyelectrolytes can be stiff in low salt concentration. Especially when the chain length decreases, the chain stiffness becomes a major concern. Many pioneers have done seminal work in this area, to name a few[**? ? ? ? ?**]. We will treat the semiflexible chain following the path integral methodology.

2.2.3.1 Path integral of a semiflexible chain

The partial differential equation description (Equation **??**) of a non-interacting, flexible chain has an equivalent path integral representation[**?**]:

$$G(\mathbf{r_0}, \mathbf{r_L}, L) = \int_{\mathbf{r_0}}^{\mathbf{r_L}} \mathscr{D}[\mathbf{r}(s)] \exp\left(-\int_0^L \frac{3}{2l}\dot{\mathbf{r}}(s)^2 ds\right). \tag{2.10}$$

Define a unit vector $\mathbf{u}(s)$ tangent to the contour $\mathbf{r}(s)$ as:

$$\mathbf{u}(s) = \frac{d\mathbf{r}(s)}{ds}, \tag{2.11}$$

with $|\mathbf{u}(s)| = 1$ and $\mathbf{R} = \mathbf{r_L} - \mathbf{r_0} = \int_0^L \mathbf{u}(s)ds$. The bending energy can be expressed through the local curvature $1/\dot{\mathbf{r}}(s)$ of the chain contour by:

$$\frac{E}{k_B T} = \frac{\alpha}{2} \int_0^L \dot{\mathbf{u}}(s)^2 ds, \tag{2.12}$$

where $\alpha = 1/l_p$, l_p being persistent length. Thus the path integral of a semiflexible chain can be written as

$$G(\mathbf{u_0}, \mathbf{u_L}, L) = \int_{\mathbf{u_0}}^{\mathbf{u_L}} \mathscr{D}[\mathbf{u}(s)] \exp\left(- \int_0^L \left[\frac{3}{2l} \mathbf{u}(s)^2 + \frac{\alpha}{2} \dot{\mathbf{u}}(s)^2 \right] ds \right),$$

with the constraint of $|\mathbf{u}(s)| = 1$. Neither this constrained path integral nor corresponding differential equation can be solved exactly. A number of attempts have been made to accommodate the inextensibility constraint[**?** **?**]. We follow the lines of [**?**] to incorporate local inextensibility in an average sense by modifying the path integral in this way:

$$G(\mathbf{u_0}, \mathbf{u_L}, L) = \int_{\mathbf{u_0}}^{\mathbf{u_L}} \mathscr{D}[\mathbf{u}(s)] \exp\left(- \int_0^L \left[\frac{3}{2l} \mathbf{u}(s)^2 + \frac{\alpha}{2} \dot{\mathbf{u}}(s)^2 + \delta(\mathbf{u_0}^2 + \mathbf{u_L}^2) \right] ds \right).$$

With fixed end-to-end vector $\mathbf{R}$, it becomes:

$$\begin{aligned} G(\mathbf{R}, \mathbf{u_0}, \mathbf{u_L}, L) = \int_{\mathbf{u_0}}^{\mathbf{u_L}} \mathscr{D}[\mathbf{u}(s)] \delta \left(\mathbf{R} - \int_0^L \mathbf{u}(s) ds \right) \\ \exp\left(- \int_0^L \left[\frac{3}{2l} \mathbf{u}(s)^2 + \frac{\alpha}{2} \dot{\mathbf{u}}(s)^2 + \delta(\mathbf{u_0}^2 + \mathbf{u_L}^2) \right] ds \right). \end{aligned}$$

The Fourier transform of the semiflexible propagator is[**?**]:

$$I(\mathbf{k},\mathbf{u_0},\mathbf{u_L},L)=\int_{\mathbf{u}_0}^{\mathbf{u}_L}\mathscr{D}[\mathbf{u}(s)]\exp\left(-\int_0^L\left[\frac{3}{2l}\mathbf{u}(s)^2+\frac{\alpha}{2}\dot{\mathbf{u}}(s)^2+\delta(\mathbf{u_0}^2+\mathbf{u_L}^2)-i\mathbf{k}\cdot\mathbf{u}(s)\right]ds\right)$$
$$=G(\mathbf{u_0}-\frac{i\mathbf{k}l}{3},\mathbf{u_L}-\frac{i\mathbf{k}l}{3},L)\exp(-\frac{Ll\mathbf{k}^2}{6}).$$

2.2.3.2 Path integral of a harmonic oscillator

The Green's function $G(\mathbf{u_0},\mathbf{u_L},L)$ has the same form as the path integral of a harmonic oscillator whose Lagrangian is $\mathscr{L}=\frac{m}{2}\dot{x}^2-\frac{mw^2}{2}x^2$. Its path integral has been solve as[**?**]:

$$K=\int\mathscr{D}[x(t)]\exp\left(\frac{i}{\hbar}\int_{t_a}^{t_b}\mathscr{L}(x,\dot{x},t)dt\right)$$
$$=\left(\frac{mw}{2\pi i\hbar\sin(wt)}\right)^{1/2}\exp\left(\frac{imw}{2\hbar\sin(wt)}\Big[\cos(wt)(x_a^2+x_b^2)-2x_ax_b\Big]\right).$$

With proper substitution of variables, we can derive the path integral of semiflexible chain as:

$$G(\mathbf{u_0},\mathbf{u_L},L)=\left(\frac{b}{\pi\sin(a)}\right)^{3/2}\exp\left(-\frac{b}{\sin(a)}\Big[\cosh(a)(\mathbf{u}_0^2+\mathbf{u}_L^2)-2\mathbf{u}_0\cdot\mathbf{u}_L\Big]\right)$$

where $a=\frac{\sqrt{3}N}{\sqrt{\widetilde{l_p}}}$, $b=\frac{\sqrt{3\widetilde{l_p}}}{2}$, with $\widetilde{l_p}=\frac{l_p}{l}$.

2.2.3.3 Partition sum of a semiflexible chain

The Fourier transform of $G(\mathbf{R},\mathbf{u_0},\mathbf{u_L},L)$ is derived as:

$$I(\mathbf{k},\mathbf{u_0},\mathbf{u_L},L)=\left(\frac{b}{\pi\sin(a)}\right)^{3/2}\exp\left(-(\delta+b\coth(a))(\mathbf{u}_0^2+\mathbf{u}_L^2)+\frac{2b}{\sin(a)}\mathbf{u}_0\cdot\mathbf{u}_L\right)$$
$$\exp\big(-A\mathbf{k}^2+iB\mathbf{k}\cdot(\mathbf{u}_0+\mathbf{u}_L)\big)$$

where $A = \frac{Ll}{6}\left[1 - \frac{2}{a}\tanh\left(\frac{a}{2}\right)\right]$, $B = \frac{L}{a}\tanh\left(\frac{a}{2}\right)$. Integrate over $\mathbf{u_0}$ and $\mathbf{u_L}$,

$$\begin{aligned} I(\mathbf{k}, L)d\mathbf{u_0}d\mathbf{u_L} &= \int I(\mathbf{k}, \mathbf{u_0}, \mathbf{u_L}, L)d\mathbf{u_0}d\mathbf{u_L} \\ &= \left(\frac{b}{\pi \sin(a)}\right)^{3/2} \left(\frac{\pi^2}{(\delta + b\coth(a))^2 - b^2/\sinh(a)^2}\right)^{3/2} \\ &\quad \exp\left(-\mathbf{k}^2\left(A + \frac{B^2/2}{\delta + b\coth(a) - b^2/\sinh(a)^2}\right)\right). \end{aligned}$$

Therefore, the mean end-to-end distance is the coefficient of $\mathbf{k}^2$ times 6. With $\delta = b$ [**?**], the end-to-end distance has the same form as Kratcky-Porod model (worm-like-chain model) [**?**]:

$$\begin{aligned} < R^2 > &= 6\left(A + \frac{B^2/2}{\delta + b\coth(a) - b^2/\sinh(a)^2}\right) \\ &= Ll\left(1 - \frac{\tanh(a/2)}{a/2}\right) + \frac{3L^2}{a^2 b}\left(\frac{\tanh^2(a/2)}{1 + \tanh(a/2)}\right) \\ &= Ll - \frac{Ll}{a}(1 - e^{-a}) \\ &= Ll - l^2\sqrt{\frac{\widetilde{l_p}}{3}}(1 - e^{-\sqrt{3}N/\sqrt{\widetilde{l_p}}}). \end{aligned} \tag{2.13}$$

After integrating out the spacial dependence, the partition sum of a semiflexible chain becomes:

$$\begin{aligned} \mathscr{Z}_N &= \int I(\mathbf{k}, L)d\mathbf{k} \\ &= \left(\frac{b}{\pi \sin(a)}\right)^{3/2} \left(\frac{\pi^2}{(\delta + b\coth(a))^2 - b^2/\sinh(a)^2}\right)^{3/2} \\ &= \left(\frac{\pi}{2b}e^{-a}\right)^{3/2}. \end{aligned} \tag{2.14}$$

For a linear, semiflexible chain grafted on a impenetrable surface can be derived following the reflecting principle used for Gaussian chain:

$$\mathscr{Z}_N^{half} = \frac{\mathscr{Z}_N}{\sqrt{< R^2 >}} = \left(\frac{\pi}{2b}e^{-a}\right)^{3/2} / (Ll(1 - \frac{1}{a}(1 - e^{-a})))^{1/2}. \tag{2.15}$$

For a semiflexible chain making a loop, the partition sum reads as:

$$\mathscr{Z}_N^{half,loop} = \frac{\mathscr{Z}_N}{< R^2 >^{3/2}} = \left(\frac{\pi}{2b}e^{-a}\right)^{3/2} /(Ll(1-\frac{1}{a}(1-e^{-a})))^{3/2}. \tag{2.16}$$

2.3 Fokker-Planck formalism

In general, the translocation process encounters a free energy barrier when a chain tries to squeeze into a pore. Under thermal fluctuation the chain would move back and forth until it overcomes the barrier and the rest of the chain moves to the receiver compartment in a downhill manner. This process is same as that of forming a crystal from a seed[**?**]. The crystal grows or diminishes as the material and energy exchange with the environment. Once it reaches some critical crystallization size, it will finally form a macroscopically large crystal. Figure**??** depicts the nucleation mechanism, where m is the number of monomers pass through the pore into receiver compartment at some time. This is also an indicator of the status of the process. By recognizing the analogy with the nucleation process, the transportation of a chain through a pore can by described by the Fokker-Planck equation[**? ?**].

2.3.1 Translocation kinetics

The translocation process is a stochastic process, as the chain can move back and forth through the pore. We use $W(m,t)$ to denote the probability of finding m monomers in the receiver compartment at time t. The change of this probability in unit time is the derivate of $W(m,t)$, which equals the negative sum of probability flux flowing from state m away to the adjacent state $m-1$ and $m+1$ [**?**]:

$$\frac{\partial W(m,t)}{\partial t} = -\left(J(m,t) - J(m-1,t)\right),$$
$$J(m,t) = k_m W(m,t) - k'_{m+1} W(m+1,t),$$

where k_m is the rate of translocating forward and pushing the state from m to $m+1$, while k'_{m+1} is the rate of moving backwards from state $m+1$ to m. The ratio between these two competing rate is dictated by the free energy difference of the two states:

$$\frac{k_m}{k'_{m+1}} = e^{-(F(m+1)-F(m))/k_BT}. \tag{2.17}$$

By Taylor expansion of $J(m,t)$, $W(m,t)$ and $e^{-(F(m+1)-F(m))/k_BT}$,

$$\begin{aligned}
J(m,t) =& k_m W(m,t) - k_m e^{F(m+1)-F(m)} W(m+1,t) \\
=& k_m W(m,t) - k_m(1 + F(m+1) - F(m) + ...)W(m+1,t) \\
=& -k_m(W(m+1,t) - W(m,t)) - \frac{k_m}{k_BT}(F(m+1) - F(m))(W(m,t) + ...) \\
\approx& -k_m \frac{\partial W(m,t)}{\partial t} - \frac{k_m}{k_BT}\frac{\partial F(m)}{\partial m} W(m,t) + ...
\end{aligned}$$

we have

$$J(m,t) = -k_m \frac{\partial W(m,t)}{\partial t} - \frac{k_m}{k_BT}\frac{\partial F(m)}{\partial m} W(m,t), \tag{2.18}$$

and

$$\frac{\partial W(m,t)}{\partial t} = -\frac{\partial J(m,t)}{\partial m}, \tag{2.19}$$

which is in accordance with conservation law. Substitute Equation**??** into Equation**??** and we have explicit Fokker-Planck equation for $W(m,t)$:

$$\frac{\partial W(m,t)}{\partial t} = -\frac{\partial}{\partial m}\left(-k_m \frac{\partial}{\partial m}\frac{F(m)}{k_BT} + \frac{\partial k_m}{\partial m}\right) W(m,t) + \frac{\partial^2}{\partial m^2}\left(k_m W(m,t)\right). \tag{2.20}$$

The Fokker-Planck equation is used to describe the diffusion under field. The first term depicts "drift" motion under external field and the second term comes purely from "diffusion" under thermal fluctuation. As a result, k_m can be identified as the diffusion coefficient of the mth monomer. For homopolymer, suppose all monomers are identical, then the diffusion coefficient can be expressed by a constant that is independent of monomer index.

2.3.2 Fokker-Planck equation

With a constant monomer diffusion coefficient $k_m \equiv k_0$, the Fokker-Planck equation becomes:

$$\frac{\partial W(m,t)}{\partial t} = \frac{\partial}{\partial m}\left(k_0 \frac{\partial F(m)}{\partial m} W(m,t) + k_0 \frac{\partial W(m,t)}{\partial m}\right), \tag{2.21}$$

where m is the translocation coordinate, i.e. the number of monomers transport from donor compartment to receiver compartment; $W(m,t)$ is the probability of finding the polymer chain in state m at time t; and $F(m)$ is the free energy landscape of the process.

2.3.3 First passage time

Once we have the free energy landscape, the polymer translocation problem is well defined by Fokker-Planck Equation**??**. The mean translocation time can be calculated by the first passage time of the Markov process[**?**]. It is also shown that the conditional probability $W(m,t;m_0,0)$ obeys the same equation as[**?**]

$$\frac{\partial W(m,t;m_0,0)}{\partial t} = k_0 \frac{\partial}{\partial m}\left(\frac{\partial F(m)}{\partial m} W(m,t;m_0,0) + \frac{\partial W(m,t;m_0,0)}{\partial m}\right). \tag{2.22}$$

To solve this equation, we need only a proper initial condition and boundary conditions at $m = m_0$ (the starting state) and $m = m_{max}$ (the ending state). The initial condition is usually depicted by putting one monomer at the pore mouth, and it can be written as a delta function:

$$W(m, t = 0; m_0, 0) = \delta(m - m_0). \tag{2.23}$$

There are two kinds of boundary conditions usually used in this context to mimic the experimental conditions. They are reflecting and absorbing boundary conditions.

When a chain could bounce back to the donor compartment under thermal fluctuation, the absorbing boundary condition is used:

$$\begin{cases} W(m = m_0, t; m_0, 0) = 0; \\ W(m = m_{max}, t; m_0, 0) = 0. \end{cases} \tag{2.24}$$

When there is a strong electric field, for example, nearly all translocation events are successful. The probability flux J at the entrance $m = m_0$ is 0:

$$\begin{cases} J(m = m_0, t; m_0, 0) = \left(\frac{dF(m)}{dm} W(m, t; m_0, 0) + \frac{\partial W(m,t;m_0,0)}{\partial m}\right) |_{m=m_0} = 0; \\ W(m = m_{max}, t; m_0, 0) = 0. \end{cases} \tag{2.25}$$

We mainly concern with the translocation time of all successful translocation events with reflecting boundary condition. In the context of Fokker-Planck equation, the mean translocation time under reflecting boundary condition can be evaluated by[**?**]:

$$k_0 < \tau >= \int_{m_0}^{m_{max}} \int_0^y \exp(F(y) - F(z)) dz dy. \tag{2.26}$$

Our time τ is alway a scaled time $k_0\tau$. Because of the exponential nature, the translocation time is dominated by the free energy barrier if there is any. As well, the slope of free energy can tell something about the translocation speed. It will be discussed in detail when it comes to the generalized force from free energy landscape.

2.3.4 Probability distribution of translocation time

The mean translocation time is the first moment of probability distribution function of translocation time. To get the distribution, we need to solve the Fokker-Planck equation numerically under its boundary condition, where we use the Crank-Nicolson

finite difference method with reflecting boundary condition, and the following equation:

$$g(m_0,t) = -\frac{d}{dt}\int_{m_0}^{m_{max}} W(m,t;m_0,0)dm. \tag{2.27}$$

To solve the Fokker-Plank equation**??** numerically, we employ the Crank-Nicolson method, i.e. a finite-difference method, which is unconditionally stable. It is a combination of the forward Euler method and the backward Euler method at a subsequent time. We discretized space by $i = 0, 1, 2, ..., J$ and time by $j = 0, 1, 2, ..., I$, with increment of Δx and Δt respectively, and the Equation **??** is approximated as

$$\begin{aligned}\frac{W_i^{j+1} - S_i^j}{\Delta t} =& \frac{1}{2}\left(\frac{dF_{i+1}W_{i+1}^{j+1} - dF_{i-1}W_{i-1}^{j+1}}{2\Delta x} + \frac{dF_{i+1}W_{i+1}^{j} - dF_{i-1}W_{i-1}^{j}}{2\Delta x}\right) \\ &+ \frac{1}{2}\left(\frac{W_{i+1}^{j+1} - 2W_i^{j+1} + W_{i-1}^{j+1}}{\Delta x^2} + \frac{W_{i+1}^{j} - 2W_i^{j} + W_{i-1}^{j}}{\Delta x^2}\right)\end{aligned}$$

with dF_i is the discrete version of the derivative of $F(x)$. After sorting the equation and defining $D = \frac{\Delta t}{2\Delta x^2}$ and $G_i = dF_i\frac{\Delta t}{4\Delta x} + D$, we have

$$(1+2D)W_i^{j+1} - G_{i+1}W_{i+1}^{j+1} + S_{i-1}W_{i-1}^{j+1} = (1-2D)W_i^j + G_{i+1}W_{i+1}^j - S_{i-1}W_{i-1}^j$$

To approximate the original equation in this way automatically maintains the conservation of probability $\sum_{i=0}^{I} W_i^j$ at any time j. One can check the conservation of probability by summing all I equations at time j, and find that $\sum_{i=0}^{I} W_i^{j+1} = \sum_{i=0}^{I} W_i^j$. To involve the initial condition, we prescribe

$$W_i^0 = \begin{cases} 0 \text{ (if } i \neq x_0), \\ \dfrac{1}{\Delta x} \text{ (if } i = x_0). \end{cases}$$

The corresponding boundary conditions are:

$$W^j_{i=I}=0 \text{ and } \begin{cases} W^j_{i=0}=0 \text{ (Absorbing BC)}, \\ dF_{i=0}W^j_{i=0}+\dfrac{W^j_{i=1}-W^j_{i=0}}{\Delta x}=0 \text{ (Reflecting BC)}, \end{cases} \quad \text{for any time } j.$$

2.4 Free energy landscape

We assumed that the diffusion of a homopolymer has constant diffusion coefficient of monomers. Then what dictates the translocation dynamics is the free energy landscape. We have discussed the physics of polymer near surfaces, because in the problem of polymer translocation we always have the scenario that part of the chain sticking out of the pore and constrained by the wall. Besides, we also encounter the situation of chain partitioned by the wall, as well as part of the chain confined in the pore. We will discuss the origins of entropic barrier from partitioning and the construction of free energy landscape in the rest of this chapter and the following chapter systematically. Here we give one examples of translation through a hole.

2.4.1 Entropic barrier

When a linear chain passes through a hole in single-file manner, the chain is partitioned by the membrane on which the hole is sitting. The free energy can be modeled by tails grafted on the wall and restricted only in half infinite space. The entropy of a polymer partitioning through a hole can be modeled by two tails grafted at the same spot on the wall, as pictured in Figure**??**. The partition sum of such a anchored chain in half space is[**?**]

$$F^L_{en}(j)=(1-\gamma'_l)\ln j, \tag{2.28}$$

where j is the number of monomer in the tail, and $\gamma'_l=0.69$[**?**] is the critical exponent for a self-avoiding chain. While the half space self-avoiding loop near a wall

can be used for the ring polymer cases (lower half in Figure**??**). The partition sum of such a anchored loop is[**?**]

$$F_{en}^{R}(j) = (1 - \gamma_h')\ln j, \tag{2.29}$$

with j being the number of monomers in the loop, and $\gamma_h' = -0.38$[**?**] for a self-avoiding loop.

At a certain moment in the translocation process, the coordinate m is defined to be the number of monomers in the receiver compartment. Thus there are $N - m$ monomers left in donor compartment for a chain with N monomers in total. The free energies for linear and ring polymer respectively are

$$F_{en}^{L}(m) = (1 - \gamma_l')\ln(m(N - m)), \tag{2.30}$$

$$F_{en}^{R}(m) = (1 - \gamma_h')\ln(m(N - m)), \tag{2.31}$$

which are plotted in Figure**??**, with green curve for linear chain and red curve for ring chain. The entropic barrier peaks at $N/2$, as the free energy is symmetric in translocation coordinate m. For both linear and ring chain, the barrier height increases with the polymer length N as

$$F_{en}^{R*} = F_{en}^{R}(m^* = \frac{N}{2}) = (1 - \gamma_h')\ln(\frac{N}{4}), \tag{2.32}$$

$$F_{en}^{L*} = F_{en}^{L}(m^* = \frac{N}{2}) = (1 - \gamma_l')\ln(\frac{N}{4}). \tag{2.33}$$

However, the ring has larger pure entropic barrier than its linear counterpart with ratio of

$$\frac{F_{en}^{R*}}{F_{en}^{L*}} = \frac{1 - \gamma_h'}{1 - \gamma_l'} = \frac{1.38}{0.31}. \tag{2.34}$$

It is also possible to have hairpin configurations in linear polymer translocation. Therefore during the translocation process of a linear polymer, there are three kinds

of possible configurations: linear on both sides and loop on either side , as shown in Figure**??**. We have already discussed the linear mode. Now we will look into the hairpin mode. In the hairpin configuration, it always has two tails sticking out one one side. The entropic free energy with two tails grafted on the wall of length j and $J-j$ respectively and J monomers in total on this side is

$$F_{en}(j,J) = (1-\gamma_l')\ln(j(J-j)), \tag{2.35}$$

with j ranges from 0 to J. Therefore, the total possibility for having two tails on one side summing up to J monomers is

$$P_{en}(J) = \int_0^J \exp(-F_{en}(j,J))dj = AJ^{2\gamma_l'-1}, \tag{2.36}$$

with[**?**]

$$A = \frac{\pi^{\frac{3}{2}}\csc(\pi\gamma_l')2^{1-2\gamma_l'}}{\Gamma(1-\gamma_l')\Gamma(\frac{1}{2}+\gamma_l')} = \frac{\Gamma^2(\gamma_l')}{\Gamma(2\gamma_l')}. \tag{2.37}$$

$j = 0$ represents only one tail outside the pore, which recovers the linear mode. Taking all possible configurations into consideration, the total entropic free energy of the linear chain partition can be written as

$$F_{en,tot}^{L}(m) = -\ln\left[((N-m)m)^{\gamma_l'-1} + A(N-m)^{2\gamma_l'-1}m^{\gamma_h'-1} + A(N-m)^{\gamma_h'-1}m^{2\gamma_l'-1}\right].$$

It is plotted in Figure**??** in a blue curve, which almost overlaps that of the ring polymer. This implies that the loop conformational barrier is quite high and dominant in both hairpin pass and ring pass. When the linear chain makes hairpin passage the entropic free energy resembles that of the ring polymer.

2.4.2 Hole in a wall

A simple model for polymer translocating is to take a polymer chain through a small hole in a wall which divides the space into two compartments (Figure**??**). A

chain is sent from the donor compartment and can only reach the receiver compartment through the hole. To construct the free energy of the whole process, we start with an arbitrary, intermediate state, when there are m monomers in the receiver compartment, and $N-m$ left in the donor. The partition sum of the configurations of this state is $\mathscr{Z} = \mathscr{Z}_{Rec}\mathscr{Z}_{Don}$. The partition sum of a tail with n monomers near a surface is given by[**?**]

$$\mathscr{Z}_N^{half} = N^{\gamma'-1}e^{-\mu N/k_BT}. \tag{2.38}$$

where μ is the chemical potential per monomer in the half space, and γ' is the critical exponent discussed in previous section. The total partition sum is written as

$$\mathscr{Z}(m) = \mathscr{Z}_{Rec}\mathscr{Z}_{Don} = m^{\gamma'-1}e^{-\mu_{Rec}N/k_BT}(N-m)^{\gamma'-1}e^{-\mu_{Don}(N-m)/k_BT}. \tag{2.39}$$

The free energy is

$$F(m) = -k_BT\ln\mathscr{Z}(m) = (1-\gamma')\ln[m(N-m)] - \frac{m\Delta\mu}{k_BT}, \tag{2.40}$$

with $\Delta\mu = \mu_{Rec} - \mu_{Don}$ being the difference in chemical potential in receiver and donor compartment. Three free energy landscapes are given in Figure**??** for different chemical potential difference. The corresponding translocation times as function of N are also plotted in Figure**??**.

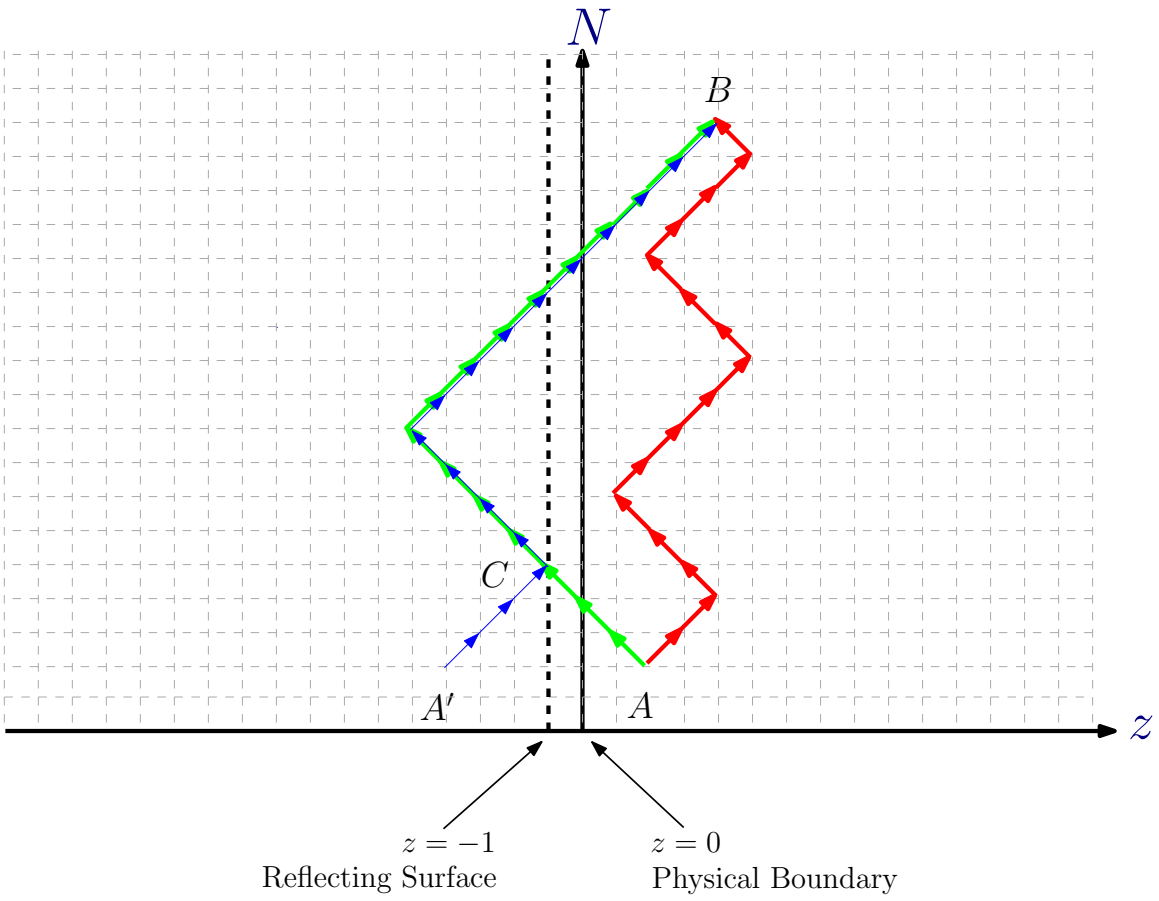

Figure 2.1. Demonstration of one-dimension random walks. The red path is allowed in semi-infinite space $z > 0$. The green path is allowed in free space, but not allowed by the physically impenetrable boundary at $z = 0$. Such a path has a one-to-one counterpart, which is indicated by the blue path. The blue path is the image path of the green path reflected by surface at $z = -1$.

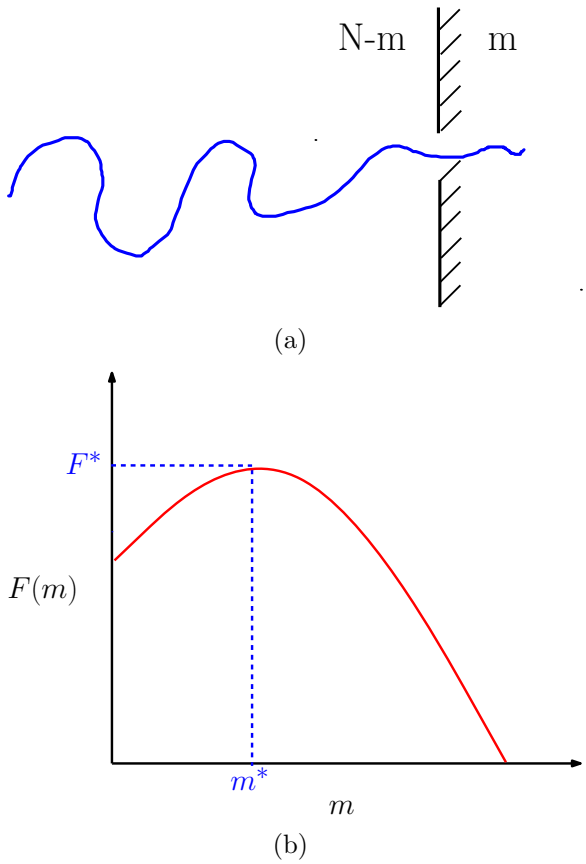

Figure 2.2. Demonstration of nucleation stage of polymer translocation. The nucleation stage of polymer translocation has similar mechanism as crystallization, which has to overcome a free energy barrier and proceeds a growth in a downhill manner.

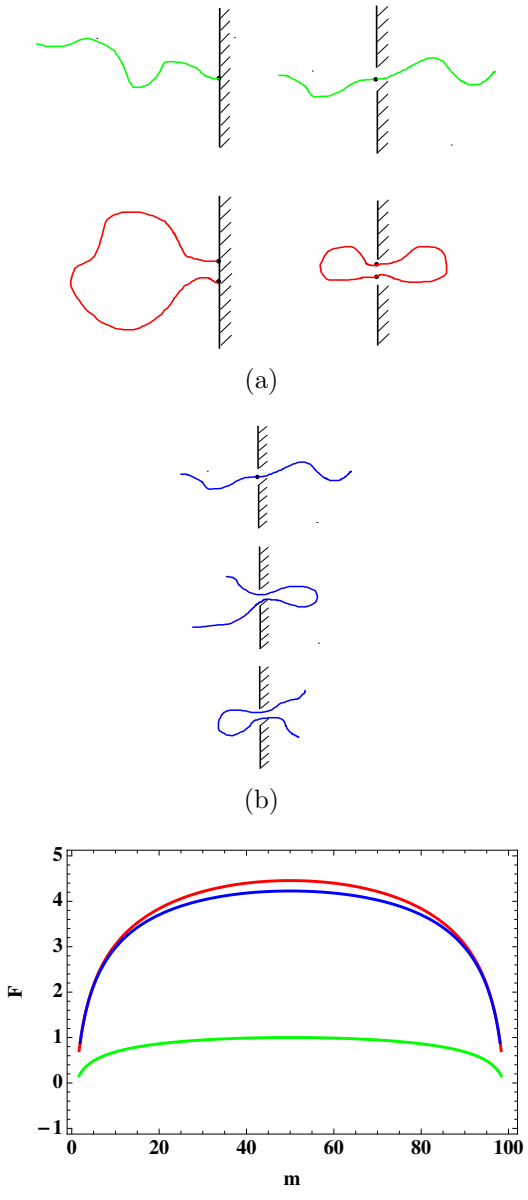

Figure 2.3. Entropic barrier due to chain partitioning by a hole in a wall.

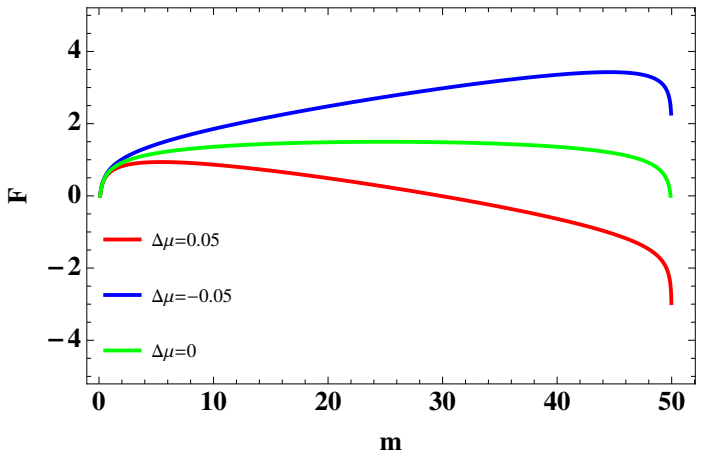

(a)

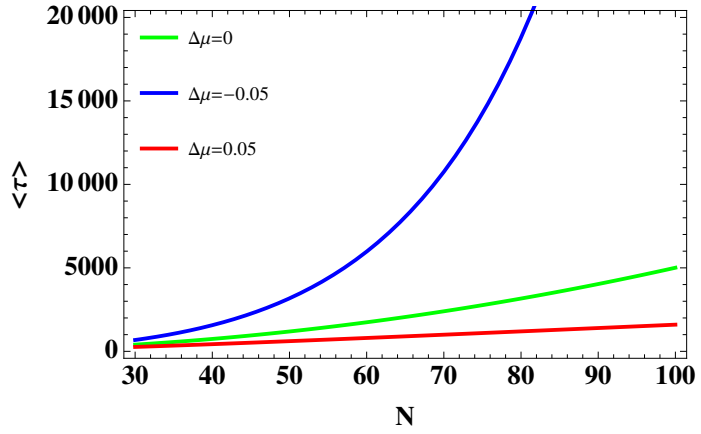

(b)

Figure 2.4. (a)Free energy landscape of the simple model of polymer translocating through a hole (as in Figure**??** for different chemical potentials). (b)Corresponding translocation time.

CHAPTER 3

COMPARISON OF TRANSLOCATION PROCESSES OF RING AND LINEAR POLYMERS

3.1 Introduction

Both experimental and simulational efforts have been made to examine the effects due to the macromolecules and the pore in translocation process. Most of these works deal with linear polymers; however, such dynamical process associated with ring-like polymer has not been investigated as thoroughly as linear polymers. This is an interesting and fundamental topic related to ring polymer, as certain DNA molecules have been found in nature in a circular form for a long time[**?** **?**]. In the example of gene swapping, the genes residing on a ring-shape plasmid would be cut open into a linear-shape DNA before being transferred to the inhibited bacteria cell[**?**]. Such biological phenomena makes us interested in the fundamental questions: How does the configuration of polymer influence the translocation dynamics? Which translocation mode is preferred in terms of translocation time?

The cyclization of polymers has been extensively studied both analytically and experimentally. Jacobson and Stockmayer calculated the rate of loop formation in the context of polycondensation in polymer solutions[**?**]. Meanwhile, experiments had been done to qualitatively verify the theoretical predictions[**?**]. On the other hand, the diffusion controlled cyclization in dilute solution without excluded volume interaction was formulated by Wilemski and Fixman[**?**], and the cyclization rate was calculated[**?**]. Subsequently the formalism was simplified by Doi using variational principle[**?** **?**], and further by Szabo et al with first passage time approach[**?**].

Experimentally, methods were developed to synthesize and purify high molecular weight ring polystyrenes[?]. Recently, simulations were implemented to investigate the loop formation and stability of self-avoiding polymer chains[? ?].

Some dynamical phenomenon of ring polymers have been discussed in the literature. For example, the theorists used simple scaling theory to study the dynamics of a ring polymer without excluded volume interaction in a gel[?], which is considerably different from its linear counterpart with fixed obstacles[?]. The diffusional dynamics of circular polymer are affected by its topology, which has been demonstrated in experimental endeavors[? ? ?].

We conjectured that the conformational differences between ring and linear polymer are responsible for their differences in translocational dynamics. There have been many works dedicating to the comparison of conformational differences between linear and ring polymers due to different topologies. Self-consistent-field-theory[? ?], as well as simulations[?], were used to compute the difference in adsorption on a surface between ring and linear polymers. This is related to the conformations of polymer chains outside the pore in translocation process. It also has been discussed about the conformations of self-avoiding ring and linear polymers under confinements, especially cylindrical confinement[? ?].

A few interesting results related to ring polymer translocation have been obtained from both theoretical and experimental perspectives. The experiments were able to detect the folded and unraveled mode in DNA translocations through nanopores[? ?]. It was found in theoretical work on linear polymer translocations with hairpins that, the conformational differences during the nucleation (entering) stage dramatically affect the free energy barrier, and hence the translocation time[?]. In a numerical simulation, the ejection of polymer from a cylindrical nanochannel has been studied and the confinement differences between ring and linear polymer have been taken into account[?]. The relative translocation times of ring and linear polymers were

compared for different polymer lengths. However, the entropy of chain part outside the pore and the possible hairpin mode were not considered yet.

The process that a polymer passes through a pore can be divided into four steps[**?**]. The first step is for a polymer to find the pore mouth. In the second step the chain is filling the pore to full. Then the chain threads from donor compartment to receptor compartment in the third step. Finally, in fourth step, the rest part of the chain is expelled out of the pore. This paper is concerned with the translocation process starting from the second step after the chain is captured by the pore. An overview of the 3-step process is pictured in Figure **??**. In this chapter, we mainly focus on discussing the translocations of self-avoiding chains, especially the translocation time counted starting from the chain captured by the pore. We construct the free energy landscape of the translocation process and calculate the mean translocation time and its distribution function for the linear polymer and ring polymer respectively. We examine the effects of entropy barrier, chain length, and pore-polymer interaction on the translocation time. It is also found that the ring conformations could give rise to a non-monotonic dependence of translocation time on polymer length. While polymer-pore interaction has been investigated in translocation setting both simulations[**?**], theory[**?**] and experiments[**? ? ? ? ?**]. This effect is amplified by increasing polymer-pore attraction. The relative translocation time of linear and ring polymer translocation can be also tuned by the pore-polymer interaction. These results may provide us with clues about how a bio-system chooses to process certain type of polymers: ring or linear.

In order to see the pathway and entropy effects separately, we will discuss two models of translocations through narrow pore and wider pore. In narrow-pore model, we only consider single-file passage of linear polymer; while in wider pore model, we consider double-file passage for both ring and linear polymer. We see that the deference from the pathways of ring and linear polymer in a narrow pores affects the

translocation time dramatically, as well as entropy and energy. However, when the pathway effect is suppressed in wider pores, the entropy and energy effects are more transparent.

3.2 Narrow-pore model

In this model, the pore diameter is small and only allows two monomers to pass side by side. The ring polymer translocates in double-filed manner. For linear polymer, it prefers single-filed passage to double-filed passage in such a narrow pore. Thus, in this model we mainly compare translocation of ring polymer with the linear mode of linear chain. We assume that the successful translocations of linear polymer are single-filed. Therefore, the three step translocation is depicted in Figure **??**.

3.2.1 Model description

For linear polymer, the first step starts with one end of the chain finds the pore and ends up filling up the whole length of the pore. In this step, the range of the translocation coordinate m is $[0, M]$, where M is the maximum number of monomers inside the pore and represents the length of the pore. The second step is also called threading step, in which the chain's forepart threads out till the last monomer fits in the pore, with m ranging from M to N. We always take polymer chain longer than the pore, so that there are portions of chain outside both entrance and exit in the second step. While in the third step, the whole chain exit the pore till the last monomer get out of the pore completely. Differently m is the number of monomers have already passed the entrance (i.e. the length of the chain N), plus the number of monomers pass the exit in this step. Thus m ranges from N to $N + M$. The number of monomers outside the exit is $m - M$, while the number inside is $N + M - m$.

While for ring polymer, it makes double-filed passage. We define m to be the number of monomers in one strand in the double strands that passes the pore entrance.

Therefore, the three intervals for three steps are different from those of linear polymer. They are $0 \leq m \leq M$, $M < m < \frac{N}{2}$, and $\frac{N}{2} \leq m \leq \frac{N}{2} + M$.

3.2.2 Free energy landscape

The free energy is composed of the entropy of the chain part outside the pore, the electric energy, and the pore-polymer interaction energy of the confined part of the chain. The free energy of the portion of a chain outside the pore is[**?**]

$$F_{en}(m) = (1 - \gamma') \ln(N - m), \tag{3.1}$$

where m is the number of monomers in the pore, N is polymer length and γ' is the critical exponential. For a self-avoiding loop $\gamma'_h = -0.38$; for a tail $\gamma'_l = 0.69$ [**?**]. We remark here that, this polymer model as mentioned before, does not account for stiffness of chains that is important for DNA. However, when chain length is significantly longer than its persistent length, we can still approximate semiflexible chain by freely joint chain with appropriate Kuhn bond length.

We assume that the electric field across the pore is E. The electric free energy is quadratic in the number of monomers inside the pore[**?**], i.e. $-\frac{fm^2}{2}$ for single-file passage and $-fm^2$ for double-file passage, with $f = \frac{eEl}{k_B T}$, e being unit charge, l being the monomer size, k_B being the Boltzmann constant, and T being the absolute temperature. We also consider that the pore-polymer interaction and express it through the parameter ϵ, which is the interaction energy felt by one monomer when it is in the pore. When the chain enters the receiver compartment, this portion of the chain is subjected to an electric chemical potential difference. This chemical potential per monomer is denoted by $\mu = -fM$.

Therefore, our free energy of the translocation process can be written as a segmental function including the three steps.

For the ring polymer:

$$\begin{cases} \text{(Step 1)} 0 \le m \le M : \\ F_1^R(m) = (1-\gamma_h')\ln(N-2m) - fm^2 + 2\epsilon m; \\ \text{(Step 2)} M < m < \frac{N}{2} : \\ F_2^R(m) = (1-\gamma_h')\ln((N-2m)(m-M)) - fM^2 - 2fM(m-M) + 2\epsilon M; \\ \text{(Step 3)} \frac{N}{2} \le m \le \frac{N}{2} + M : \\ F_3^R(m) = (1-\gamma_h')\ln 2(m-M) - f(M^2 - (m-\frac{N}{2})^2) - 2fM(m-M) + 2\epsilon(M+\frac{N}{2}-m). \end{cases}$$

For the liner polymer:

$$\begin{cases} \text{(Step 1)} 0 \le m \le M : \\ F_1^R(m) = (1-\gamma_l')\ln(N-m) - \frac{fm^2}{2} + \epsilon m; \\ \text{(Step 2)} M < m < N : \\ F_2^R(m) = (1-\gamma_l')\ln((N-m)(m-M)) - \frac{fM^2}{2} - fM(m-M) + \epsilon M; \\ \text{(Step 3)} N \le m \le N + M : \\ F_3^R(m) = (1-\gamma_l')\ln(m-M) - \frac{f}{2}(M^2 - (m-N)^2) - fM(m-M) + \epsilon(M+N-m). \end{cases}$$

3.2.3 Comparison of the linear and ring polymer

3.2.3.1 Pathway effect

Under strong confinement, the pore size is not favored by hairpin passage, but enough to allow the ring polymer to pass. In this circumstance the pathway of ring polymer is shorter than that of linear chain, as linear chain mainly takes the single-file passage while ring chain takes the double-file passage. In the experiments of DNA translocation through solid-state nanopore[**?**], it is shown that there are two levels of current blockages, and the event durations are concentrated in two

clusters (Figure**??**). The current blockages with narrower, deeper signal are believed to belong to the single-file passage mode. While the broader, shallower ones are from the double-file mode among the translocation events.

To compare with the above experimental results with our theory, using the free energy from Equations**??** and Equations**??**, we plot the free energy landscape in Figure**??** with $f = 0.05, \epsilon = 0$, and $N = 80$ and calculate the mean translocation time for both chains in Figure**??**. Under this relatively stronger electric field, the translocation is nearly a downhill process, and it takes the ring polymer much shorter time than linear polymer. This is consistent with the observations in [**?**].

3.2.3.2 Partition entropic barrier

When there is no electric field ($f = 0$) or polymer-pore interaction ($\epsilon = 0$), the barrier height in the second step (Figure**??**) is increasing with polymer length N, but decreasing with pore length M as

$$F_{en}^{R*} = F^R(m^* = \frac{1}{2}(\frac{N}{2} + M)) = (1 - \gamma_h') \ln(\frac{1}{4}(\frac{N}{2} - M)), \tag{3.2}$$

$$F_{en}^{L*} = F^L(m^* = \frac{N}{2}) = (1 - \gamma_l') \ln(\frac{1}{4}(N - M)). \tag{3.3}$$

Since the ring polymer has higher barrier than linear polymer (Figure **??**), when the electric force becomes weaker, the entropy effect will start to show up in the free energy landscape and the translocation time. In Figure **??** (compared to Figure **??**), with much weaker field, the entropy barrier reduces their pathway difference in terms of translocation time. Because this partition barrier increases faster with polymer length N for ring polymer than linear polymer. The relative translocation time of linear and ring polymer reverses for longer chain, as shown in Figure **??**.

Thus when the electric force becomes weaker, the entropy effect will start to appear in the translocation time. In Figure**??** and Figure**??**, with much weaker fields, the

entropy barrier reduces the difference between linear chain and ring chain in terms of translocation time.

3.2.3.3 Non-monotonicity of translocation time

We also observe non-monotonicity of ring polymer's translocation time in terms of polymer length N for attractive pore($\epsilon < 0$), shown as in Figure **??**. In general, the translocation time is longer for longer chains. However, the third step in ring polymer translocation takes shorter time to complete for longer chains. This competing effect is amplified when the pore is attractive. We will discuss this phenomenon in details in the next section.

3.2.3.4 Pore-polymer interaction effect

The pore-polymer interaction can tune the relative translocation time for ring and linear polymers too. As shown in Figure **??**, with neutral pore, the pathway effect is dominating, thus ring polymer translocation is faster than linear polymer. With interactive pore, the entropic effect in the first or the third step is amplified. Since ring polymer has higher entropic free energy, it is retarded by the pore-polymer interaction more than linear polymer is. We will discuss pore-polymer interaction effect in next section in details.

The confinement energy is not considered explicitly in the free energy. However, we can assume that the confinement energy is proportional to the number of monomers inside the pore. As a result we can absorb the confinement energy in the pore-polymer interaction energy, which is equivalent to a positive contribution to ϵ.

3.2.3.5 Competition between entropy and pathway

To examine the effects of experimental conditions other than the foregoing polymer length effect, we plot the mean translocation time as functions of the electric field strength f, the pore-polymer interaction ϵ, and the pore length M. As shown in

the Figure**??**, the stronger the electric field the more pathway effect appears; The longer the pore, the lower the barrier height thus the less salient the entropy. Only in some region of these parameters, the shorter pathway of ring polymer shortens the translocation time. Therefore, in real bio-system, by tuning these parameters, for instance, changing the cross membrane potential, decoration of charges inside the pore and/or the thickness of the membrane, linear or ring polymer may be favored over the other in terms of translocation time.

3.3 Wider pore model

In the experiments, to increase the successful translocation events for ring polymer, the size of the pore should be moderately larger to allow more monomers passing side by side. Meanwhile, the hairpin passage mode from linear chain becomes more feasible, whose pathway resembles ring polymer as shown in the Figure **??**. Therefore, without the advantages in pathway, we would like to see the other effects on the ring polymer translocation, compared to the linear polymer case.

3.3.1 Model description

In the experiments, to increase the successful translocation events for ring polymer, the diameter of the pore should be moderately larger to allow more monomers passing side by side. Meanwhile, the hairpin passage mode from linear chain becomes more feasible, whose pathway resembles ring polymer. Therefore, without the advantages in pathway, we would like to see the other effects on the ring polymer translocation, in contrary to the linear polymer case.

Compared to the "narrow-pore model", this "wider pore model" assumes the pore size is large enough for the polymer strands to form blobs under confinement (Figure **??**). The confinement free energy is given by de Gennes' blobs[**? ?**]:

$$F_{conf}(m) = \frac{m}{d^{\frac{1}{\nu}}}, \tag{3.4}$$

where m is the number of monomers inside the pore, d is the ratio of diameter of the pore to the monomer size l, and $\nu = 0.59$ is the size exponential for self-avoiding chain. The free energy is proportional to the number of blobs in the pore $m/d^{\frac{1}{\nu}}$. Here we assume the pore diameter is large enough to allow the two strands in the pore to relax and form the blobs with nearby monomers regardless of which strand they come from; but also small for the pore to play the role as a confinement. Therefore, under the electric field, the blobs aligns in the pore. This assumption leads to the same confinement free energy term for both ring and linear polymer. By assuming uniform electric field along the pore, the electric free energy is[**?**]:

$$F_{elec}(m) = -\frac{fm^2}{2d^{\frac{1}{\nu}-1}}. \tag{3.5}$$

The three-step intervals are the same for both ring and linear polymers:

$$\begin{cases} \text{Step 1: } 0 \leq m \leq M, \\ \text{Step 2: } M < m < N, \\ \text{Step 3: } N \leq m \leq N + M. \end{cases} \tag{3.6}$$

3.3.2 Free energy landscape

In this section, we will show how to construct the free energy landscape for ring and linear polymer respectively in details.

3.3.2.1 Free energy for a ring polymer

The three-step process is depicted in Figure**??**.

3.3.2.1.1 Step 1 The first step starts with fixing one monomer at the pore entrance and ends up with one monomer getting to the exit of the pore. In this step,

the range of m is $[0, M]$, where M is number of monomers filling the pore to full and represents the length of the pore. In the translocation problem, we always have the chain longer than the pore, so that we have portions of the chain outside both ends of the pore in second step. In each step, there are four major sources of free energy. One is the entropy of the loop outside the entrance; another is the confinement free energy of the part of chain squeezed in the pore; the third part is the energy gain due to the electric field; the fourth part is from the interaction between the pore and chain. The first and fourth part are the same with the previous section. The free energy of the portion of a chain outside the pore is

$$F_{en}(m) = (1 - \gamma_h') \ln(N - m), \tag{3.7}$$

where m is the number of monomers in the pore, N is polymer length and $\gamma_h' = -0.38$ for a self-avoiding loop. The attractive interaction between the pore and monomer can be expressed by a linear free energy term

$$F_{attr}(m) = \epsilon m, \tag{3.8}$$

where ϵ is negative for attractive pore and positive for repulsive pore. We will discuss the effects of ϵ and claim that the attractive interaction enhances the non-monotonic behavior of translocation time as a function of polymer length N in the results section. The confinement free energy is given by de Gennes' blob model[**?** **?**] as discussed before:

$$F_{conf}(m) = \frac{m}{d^{\frac{1}{\nu}}}. \tag{3.9}$$

The electric free energy can be shown to be quadratic in the number of monomers m in the pore[**?**], by assuming uniform electric field along the pore, which is the case in experiment situation[**?**].

$$F_{elec}(m) = -\frac{fm^2}{2d^{\frac{1}{\nu}-1}}. \tag{3.10}$$

Therefore, the total free energy for the first step is

$$F_1^R(m) = (1-\gamma_h')\ln(N-m) + \frac{m}{d^{\frac{1}{\nu}}} - \frac{fm^2}{2d^{\frac{1}{\nu}-1}} + \epsilon m. \tag{3.11}$$

3.3.2.1.2 Step 2 The second step starts from first monomer passing the exit to the last monomer passing the entrance, while m is still the number of monomers have passed the entrance and ranges from $M+1$ to $N-1$. There are four terms similar to Step 1 in free energy, i.e. entropy of chains outside both ends of pore, confinement, pore interaction and electric free energy of M monomers inside the pore. There are $N-m$ monomers outside entrance and $m-M$ monomers outside the exit. In addition, there is one more term arrises due to the chemical potential that $m-M$ monomers gain due the the electric potential difference across the pore.

$$F_2^R(m) = (1-\gamma_h')\ln((N-m)(m-M)) + \frac{M}{d^{\frac{1}{\nu}}} - \frac{fM^2}{2d^{\frac{1}{\nu}-1}} + \epsilon m + \mu(m-M),$$

where $\mu = -fL$ is the chemical potential of a monomer in the exit compartment, and $L = \frac{M}{d^{\frac{1}{\nu}-1}}$ is ratio of the pore length to monomer size.

3.3.2.1.3 Step 3 The third step follows up the second step util the last monomer expelled out of the pore, while m here is the number of monomers have already passed the entrance, i.e. the length of the chain N, plus the number of monomers would pass the exit in this step. Thus m ranges from N to $N+M$. The number of monomers outside the exit is $m-M$, while the number inside is $N+M-m$. Similarly, we have

$$F_3^R(m) = (1-\gamma_h')\ln(m-M) + \frac{N+M-m}{d^{\frac{1}{\nu}}} - \frac{f}{2d^{\frac{1}{\nu}-1}}(M^2-(m-N)^2) + \epsilon(N+M-m) + \mu(m-M).$$

Finally, we have the free energy landscape as a piecewise function,

$$F^R(m) = \begin{cases} F_1^R(m) \text{ if } 0 \leq m \leq M, \\ F_2^R(m) \text{ if } M+1 \leq m \leq N-1, \\ F_3^R(m) \text{ if } N \leq m \leq N+M. \end{cases} \tag{3.12}$$

3.3.2.2 Free energy for a linear polymer

Since the pore size is large enough to allow hairpin in translocation process, the possible conformations of chain are shown in Figure**??**. Here we assume the portion of chain segments inside the pore make blobs under pore confinement, i.e. the free energy of chain inside the pore is the same for both ring and linear polymer.

3.3.2.2.1 Step 1 ($0 \leq m \leq M$) Since hairpin allowed in translocation process, it is possible in the first step to make linear translocation with one tail, hairpin with two tails and loop, as shown in Figure**??**. The entropic free energy for linear mode with m monomers inside the pore is

$$F_{1a}(m) = -\ln((N-m)^{\gamma_l'-1}). \tag{3.13}$$

The entropic free energy for hairpin mode with two tails of length j and $N-m-j$ is

$$F_{1b}(m,j) = -\ln((j(N-m-j)^{\gamma_l'-1}), \tag{3.14}$$

with j ranges from 0 to $N-m$. Therefore, the total possibility for hairpin mode is

$$P_{1a}(m) = \int_0^{N-m} \exp(-F_1 1(m,j)) = A(N-m)^{2\gamma_l'-1}, \tag{3.15}$$

with[**?**]

$$A = \frac{\pi^{\frac{3}{2}} \csc(\pi\gamma_l') 2^{1-2\gamma_l'}}{\Gamma(1-\gamma_l')\Gamma(\frac{1}{2}+\gamma_l')} = \frac{\Gamma^2(\gamma_l')}{\Gamma(2\gamma_l')}. \tag{3.16}$$

The entropic free energy for loop mode with m monomers inside the pore is

$$F_{1c}(m) = -\ln((N-m)^{\gamma_h'-1}). \tag{3.17}$$

Taking all possible configurations into consideration, the total entropic free energy of the first step is

$$F_{1en}^L(m) = -\ln(P_{1a}(m) + P_{1b}(m) + P_{1c}(m)),$$

$$F_{1en}^L(m) = -\ln((N-m)^{\gamma_l'-1} + A(N-m)^{2\gamma_l'-1} + (N-m)^{\gamma_h'-1}).$$

Similar to ring polymer translocation, there are also confinement free energy due to m monomers inside the pore and free energy gain due to electric field and pore interaction. Therefore, the free energy for first step is summed up as

$$F_1^L(m) = -\ln((N-m)^{\gamma_l'-1}+A(N-m)^{2\gamma_l'-1}+(N-m)^{\gamma_h'-1})+\frac{m}{d^{\frac{1}{\nu}}}-\frac{fm^2}{2d^{\frac{1}{nu}-1}}+\epsilon m. \tag{3.18}$$

3.3.2.2.2 Step 2 ($M+1 \le m \le N-1$) As shown in Figure**??**, there are four possible translocation modes. Summing over all entropic and enthalpic energy, we have free energy for the second step

$$\begin{aligned} F_2^L(m) = &-\ln(((N-m)(m-M))^{\gamma_l'-1} + ((N-m)(m-M))^{\gamma_h'-1} \\ &+A(m-M)^{2\gamma_l'-1}(N-m)^{\gamma_h'-1} + A(N-m)^{2\gamma_l'-1}(m-M)^{\gamma_h'-1}) \\ &+\frac{M}{d^{\frac{1}{\nu}}} - \frac{fM^2}{2d^{\frac{1}{nu}-1}} - \mu(m-M) + \epsilon M. \end{aligned} \tag{3.19}$$

3.3.2.2.3 Step 3 ($N \le m \le N+M$) Symmetrically to first step, we derive the free energy for the third step as

$$\begin{aligned} F_3^L(m) = &-\ln((m-M)^{\gamma_l'-1} + A(m-M)^{2\gamma_l'-1} + (m-M)^{\gamma_h'-1})+ \\ &\frac{N+M-m}{d^{\frac{1}{\nu}}} - \frac{f(M^2-(m-N)^2)}{2d^{\frac{1}{\nu}-1}} - \mu(m-M) + \epsilon(N+M-m). \end{aligned} \tag{3.20}$$

3.3.3 Comparison of linear and ring polymers

3.3.3.1 Polymer length effects

3.3.3.1.1 Results for ring polymer The free energy varies with the choice of parameters, such as polymer length N and pore-polymer interaction ϵ. By applying a uniform electric field along the pore, the overall translocation is a downhill process, while the pore-polymer interaction and the chain partitioning induce free energy barriers during the process.

To find the polymer length effect, we plot the free energy of each step for different N (Figure**??**). It is straightforward that the second step, i.e. the threading step, would spend more time with longer chain, since both the barrier height and pathway increase with polymer length (as shown in Figure **??**). However, interesting things happen to the third step in ring polymer case, and to the first step in linear polymer case. It is worth mentioning that chain length only affects the free energy of chain parts outside the pore. Therefore, we mainly focus on the entropy term in the first and third step:

$$\begin{cases} \text{Step 1: } F^R_{1en}(m) \sim (1-\gamma'_h)\ln(N-m), \\ \text{Step 3: } F^R_{3en}(m) \sim (1-\gamma'_h)\ln(m-M). \end{cases} \tag{3.21}$$

Then, the negative derivative of free energy is the generalized force:

$$\begin{cases} \text{Step 1: } -\frac{\partial F^R_{1en}}{\partial m} \sim \frac{1-\gamma'_h}{N-m}, \\ \text{Step 3: } -\frac{\partial F^R_{3en}}{\partial m} \sim -\frac{1-\gamma'_h}{m-M}. \end{cases} \tag{3.22}$$

We can see that, the force due to the pure entropy of the chain outside the entrance is positive and pulling polymer into the pore, while the entropy of chain outside the exit is negative and holding the polymer back. The magnitude of the pulling force decreases with the polymer length N, which makes the pore filling process slower with longer chain. As shown in Figure **??**, the free energy is flatter for longer chain. Thus

the first step translocation time is longer with increasing polymer length (Figure **??**). However, the chain experiences the retarding force which decreases with N while existing the pore. As shown in Figure **??**, the barrier holding the chain back is decreasing with polymer length. Thus the third step translocation time is decreasing with N.

The corresponding translocation time for each step is shown in Figure **??**. The competing effect from third step gives rise to the non-monotonicity of translocation time (Figure **??**). We can also see the non-monotonicity in the distribution of translocation time in Figure **??**. Polymer with intermediate length has the narrowest profile towards shorter translocation time.

3.3.3.1.2 Results for Linear Polymer The generalized forces for linear polymer of three different configurations are:

$$\begin{cases} \text{Step 1: } -\frac{\partial F^L_{1en}}{\partial m} \sim \frac{1-\gamma'_l}{N}, \frac{1-2\gamma'_l}{N}, \frac{1-\gamma'_h}{N}; \\ \text{Step 3: } -\frac{\partial F^L_{3en}}{\partial m} \sim -\frac{1-\gamma'_l}{N}, -\frac{1-2\gamma'_l}{N}, -\frac{1-\gamma'_h}{N}. \end{cases} \tag{3.23}$$

The three-step free energy of a linear polymer is similar to that of a ring polymer, though differs in several ways. In contrary to ring polymer, the free energy barrier and slope decrease with polymer length N in the first step, but increase in the third step. This polymer length effect is also seen in translocation times of these two steps in Figure **??**. However, the decreasing effect in first step arises from the hairpin mode in the translocation process. The free energy of a linear chain entering the pore with hairpin conformations is

$$F^L_{1en} \sim (1 - 2\gamma'_l) \ln(N - m). \tag{3.24}$$

And the generalized force due to the the hairpin free energy is

$$-\frac{\partial F^L_{1en}}{\partial m} \sim \frac{1-2\gamma'_l}{N-m}. \tag{3.25}$$

Compared with ring polymer translocation, the pulling force of linear polymer in first step decreases with N at the rate of $|1-2\gamma'_l| = 0.38$, which is much smaller than the rate of ring polymer in third step, Equation **??**, $1-\gamma'_h = 1.38$. Besides, the opposite effect from other conformations in step 1 neutralizes the hairpin effect. Although the translocation time of first step for linear polymer is decreasing with N, the effect is much weaker than the third step of ring polymer, as discussed in Free energy section. Thus the total translocation time is monotonically increasing with polymer length. One example is shown in Figure **??**. Another example of how pore-polymer interaction changes the translocation is also shown in Figure **??**.

3.3.3.2 Pore-polymer interaction effects

With long chain approximation, we can show that the free energy is quadratic in m. As for entropic free energy, we have the following for step 1 and 3 in long chain limit:

$$\begin{aligned} F^R_{1en}(m) &= (1-\gamma'_h)\left(\ln(\frac{N-m}{N}) + \ln N\right) \\ &\propto (1-\gamma'_h)\ln\left(1-\frac{m}{N}\right) \\ &\approx -(1-\gamma'_h)\frac{m}{N}, \end{aligned} \tag{3.26}$$

$$\begin{aligned} F^R_{3en}(m) &= (1-\gamma'_h)\left(\ln\left(\frac{m-M}{N}\right) + \ln N\right) \\ &\propto (1-\gamma'_h)\ln\left(1-\frac{N+M-m}{N}\right) \\ &\approx (1-\gamma'_h)\frac{m}{N}. \end{aligned} \tag{3.27}$$

Therefore, the total free energy can be written as:

$$\begin{aligned} F_1^R(m) &= (1-\gamma_h')\ln(N-m) + \frac{m}{d^{\frac{1}{\nu}}} - \frac{fm^2}{2d^{\frac{1}{\nu}-1}} + \epsilon m \\ &\approx -Cm^2 + (\epsilon_{en} + \epsilon_{conf} + \epsilon)m; \end{aligned} \tag{3.28}$$

$$\begin{aligned} F_3^R(m) &= (1-\gamma_h')\ln(m-M) + \frac{N+M-m}{d^{\frac{1}{\nu}}} - \frac{f}{2d^{\frac{1}{\nu}-1}}(M^2-(m-N)^2) \\ &+ \epsilon(N+M-m) + \mu(m-M) \\ &\approx Cm^2 - (2C(M+N) + \epsilon_{en} + \epsilon_{conf} + \epsilon)m. \end{aligned} \tag{3.29}$$

where $C = \frac{f}{2d^{\frac{1}{\nu}-1}}$, $\epsilon_{conf} = \frac{1}{d^{\frac{1}{\nu}}}$ and $\epsilon_{en} = -\frac{1-\gamma_h'}{N}$.

3.3.3.2.1 Effective pore-polymer interactions We know that the electric free energy is quadratic in m, while the confinement free energy and the pore-polymer interaction are linear in m, as well as the chemical potential appearing in step 2 and step 3. It is obvious for ring polymer that, with long chain approximation, the leading term in entropy is linear too (Equation **??** and **??**). It should also be true for different modes in linear polymer translocation. Thus the total free energy is essentially a quadratic function in m as in Equation **??** and **??**. We can view ϵ_{en} as effective pore-polymer interaction from entropy, and ϵ_{conf} as effective pore-polymer interaction from confinement energy. What matters here is $\epsilon_{tot} = \epsilon_{en} + \epsilon_{conf} + \epsilon$ (as in Figure **??**). If $\epsilon_{tot} < 0$, in the third step $F_3^R(m)$ has a barrier; if $\epsilon_{tot} > 0$, in the first step $F_1^R(m)$ has a barrier. We know from the theory that the translocation process will spend most of the time in the step which has a barrier. The translocation time is dominated by the time spent in that step. Therefore, the properties in the dominating step will be amplified by the barrier, namely by the non-zero ϵ_{tot} value.

3.3.3.2.2 Pore-polymer interaction effect enhances the non-monotonicity For ring polymer, by increasing the attractive interaction between the pore and poly-

mer, the free energy barrier in third step is amplified and so is the decreasing trend of translocation time. Meanwhile, the first step becomes more downhill and quicker, thus less pronounced in determining the total translocation time. This ϵ effect on free energy landscape is clearly shown in Figure **??**. For ring polymer, the increase of pore-polymer interaction enhances the non-monotonicity in the dependence of polymer length in translocation time(Figure **??**). For linear polymer, with varying ϵ we still do not see any non-monotonic trend(Figure **??**).

3.3.3.2.3 Asymmetric translocation time Imaging that a single particle translating through a pore, its travel time would be symmetric with respect to zero pore-particle interaction. Namely, either attractive or repulsive pore would slow down the process equally. Similarly in polymer problem, the translocation time would be symmetric with respect to the total effective pore-polymer interaction $\epsilon_{tot} = 0$. However, the symmetry about $\epsilon = 0$ is broken (as shown in Figure **??**), as the other effective pore-polymer interaction from entropy and confinement energy are non-zero ($\epsilon_{en} \sim -10^{-2}$ and $\epsilon_{conf} \sim 10^{-1}$).

3.3.3.3 More comparisons

Figure **??** shows the interaction between pore and polymer acting as a parameter tuning the relative translocation time of ring and linear polymer. When the pore is more attractive, the ring polymer translocation is slowed down, which makes way for linear polymer translocation. While the pore starts to repel the chain, the ring polymer is prevailing in faster translocation events.

This result can be also predicted from the free energy comparison shown in Figure **??**. The second step for linear polymer is dominated by the configuration with loops of both sides, which is very similar to ring polymer configuration. The comparison of ring and linear polymer free energy focuses on the first and the third step. Because of the symmetry in these two steps, the interaction between pore and polymer varies

in such a way that it makes either entering step or the expulsion step experience a free energy barrier. As well, the comparison of generalized forces of Equation **??** and Equation **??**, implies the pulling force in first step and the holding force in third step of ring polymer are all stronger than that of linear polymer. Therefore, when the free energy barrier appears in the first step, it takes longer for linear polymer to translocate; when that appears in third step, it takes longer for ring polymer to translocate. At some point (for some particular value of ϵ), the two forces in these two steps balance, there we see linear polymer and ring polymer have same translocation time.

Figure **??** implies that the polymer length could also be another tuning parameter, for instance, in a bio-system which processes both linear and ring polymer by different translocation time. It is shown that for shorter chain, ring polymer has much longer translocation time than linear polymer. However, this difference is minimized as the chain becomes longer. There are three reasons for this. Firstly for fixed pore length M, the path for step 1 and step 3 are both M, while the path for step 2 would increase with polymer length N. The shorter the chain, the difference in entropy (step 1 & 2) is more dominative (Figure **??**). Secondly, the entropic effect comes in through the effective parameter$\epsilon_{en} = -\frac{1-\gamma'_h}{N}$. For long chains, this parameter decreases, which means the entropic effect diminishes. Thirdly, for shorter chain it is much easier to make linear translocation, so that it takes much shorter time to translocate, which is also mentioned in[**?**]. While for longer chains, it is tend to make a hairpin translocation, which resembles ring polymer translocation and minimize the difference between ring and linear polymer translocation times.

3.4 Conclusion and Discussion

We have developed the formalism to compare the translocations of ring and linear polymers in two scenarios: narrow pore and wider pore. Common phenomenon of

non-monotonicity of translocation time as function of polymer length is observed for both models. The pore-polymer interaction is playing an important role in the translocation process. The repulsive pore induces free energy barrier in the first step; while the attractive pore induces barrier in the third step. It can tune the relative translocation time of ring and linear polymer, by putting emphasis on the first step or last step.

However, there are some differences and advantages of the two models. In wider pore model, we approximated the confinement energy by simple blob argument and assumed that in spite of the translocation mode, the confined part of the chain would form blobs with the same size. For instance, when the part of ring polymer gets in the pore, it is assumed that the monomers in that two strands feel the confinement equally and they form blobs just like the monomers in one strand of the linear polymer. The same argument applies to hairpin model of the linear chain too. This assumption would be valid as long as the confinement of the pore is not too strong to the polymer. Because when the pore diameter becomes too small and only two monomers are allowed to pass side by side, this is reduced to narrow-pore model.

In narrow-pore model, the pathway effect is profound, as the single-file passage is preferable for linear polymer in small pore. The longer pathway makes the linear translocation slower (Figure **??**). However, in wide-pore model, The linear polymer can also make double-file passage. The difference of pathways between linear and ring polymer translocations is largely reduced due to hairpin mode through wider pore that resembles ring translocation. Moreover, the entropy difference between ring and linear polymer is more pronounced, and slows down the ring polymer translocation (Figure **??**).

The pore-polymer interaction also has different effect on translocation time for these two models. From Figure **??**, both repulsive and attractive narrow-pore model would slow down ring polymer translocation more than linear polymer. This is be-

cause the double-filed ring polymer experiences the pore-polymer interaction energy twice as much as linear chain does. The resistant effect from pore-polymer interaction is always stronger on ring polymer in a narrow pore. However, when the chain feels no difference in confinement from wider pore, the ring polymer is more sensitive to attractive pore, while linear polymer is more sensitive to repulsive pore (Figure **??**). This result comes from the difference in ϵ_{en}, i.e. the effective pore-polymer interaction from the entropy of dangling chain part, which are defined in Equation **??** and **??**.

We have to remark here that, supercoiling is common for helical DNA[**?** **?** **?** **?**]. However, the above theoretical prediction of ring polymer translocation applies to DNA without supercoiling structure. It is known that, certain enzymes such as topoisomerases are able to tune the extension of supercoiling. They break the DNA backbone, so that the DNA strands can relax before they reseal the breaks. Therefore, in experiment, such enzymes can be used to control the unwanted supercoiling. On the other hand, the semiflexibity of DNA chains has not been addressed by our model. To be pertinent to the questions raised in the beginning(Section**??**), we require that polymer chains (DNA) should be long enough so that it approaches self-avoiding chain. In this scenario, our prediction should still hold.

Our prescription of electric potential across the pore is about $1.25mV \sim 12.5mV$ (equivalent to $f = \frac{eEl}{k_BT} = 0.005 \sim 0.05$). In order to see the entropy effect, the experimental driving force should not be too high to blot out the delicate entropic effect. In this regard, the theory could potentially shed some light on gene swapping scheme mentioned in [**?**]. Since gene swapping takes place between two similar bacteria, the electric potential difference should not be too high.

On the other hand, if we consider long, semiflexible chain, we have to replace l by l_p. Thus the model is scaled up as the unit length l is scaled up to l_p. For longer, semiflexible chain, the higher bound of electric potential (in order to see entropic effect) can be much more higher than that for flexible chain.

It should also be remarked that the prevailing discussion of free energy of the chain in equilibrium is based on the assumption that, the relaxation time scale of the polymer chain is much shorter than the translocation time scale. Then the equilibrium free energy would be valid at every time step in the whole process.

Another remark to make is that the partition sum of the a polymer chain with length $N-m$ is in a complete form, $Z = (N-m)^{\gamma'-1}c^{N-m}$, with c being the constant chemical potential of each monomer in the dangling chain outside the pore. In the free energy, the linear term of $c(N-m)$ can be adsorbed in the pore-polymer interaction energy term ϵm.

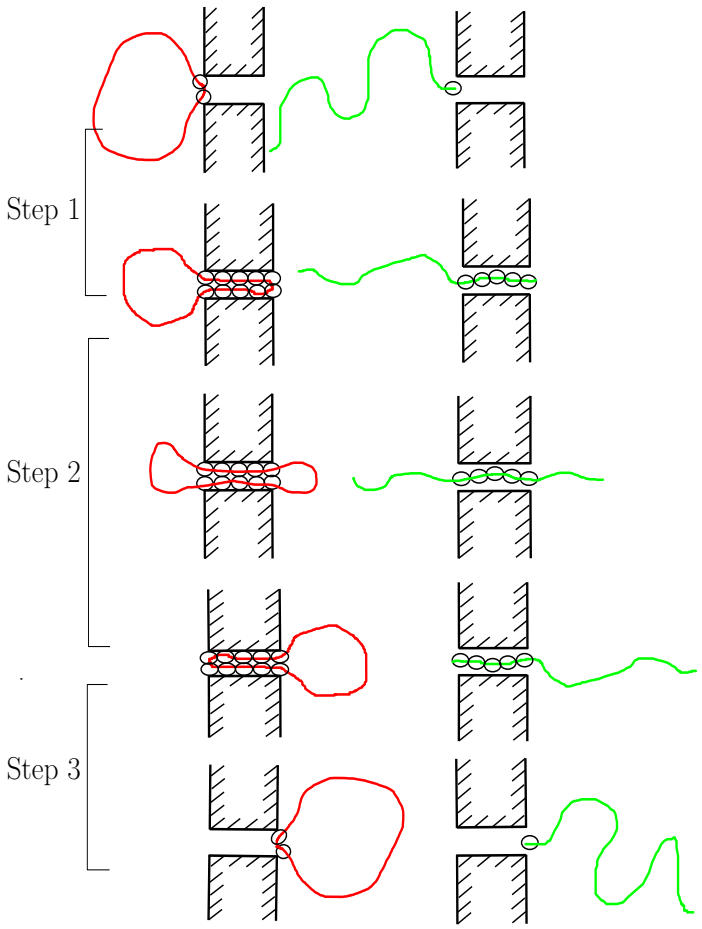

Figure 3.1. Three steps through a narrow pore.

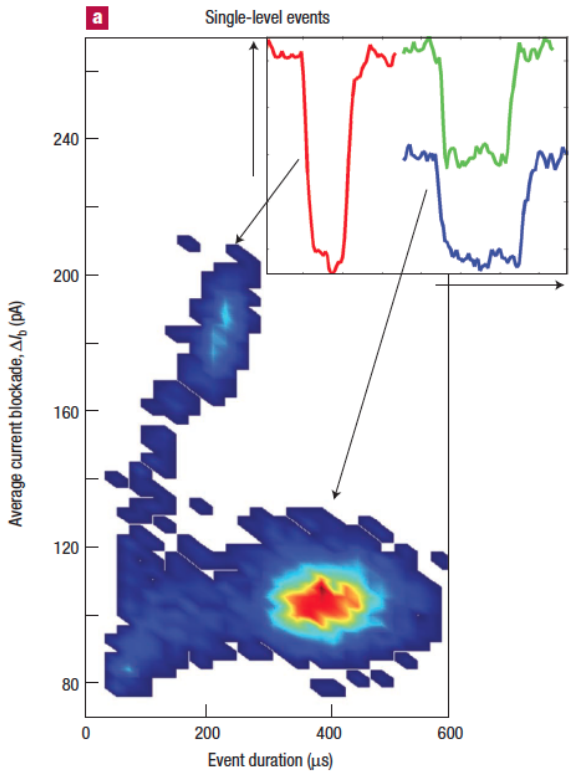

(a)

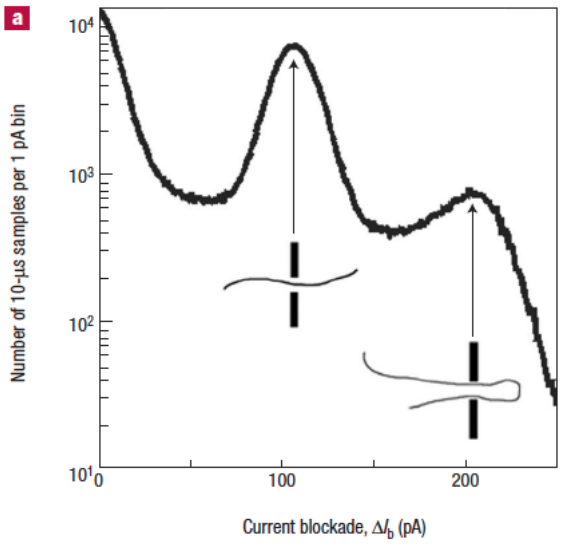

(b)

Figure 3.2. DNA translocation through solid-state nanopore[**?**]. (**??**) single-file and double-file events. (**??**) current blockage analysis.

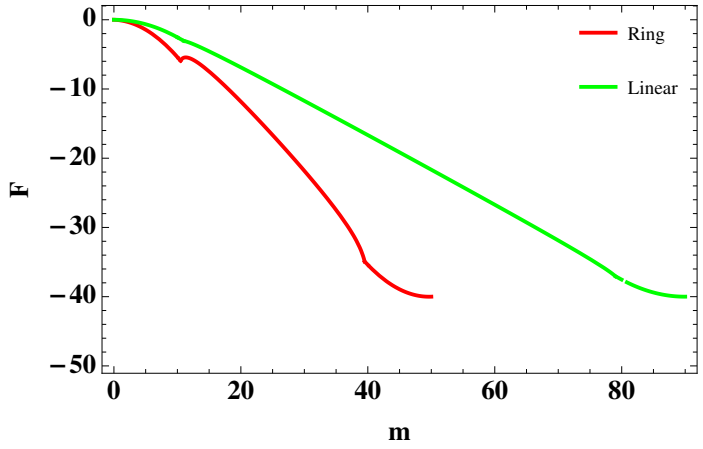

(a)

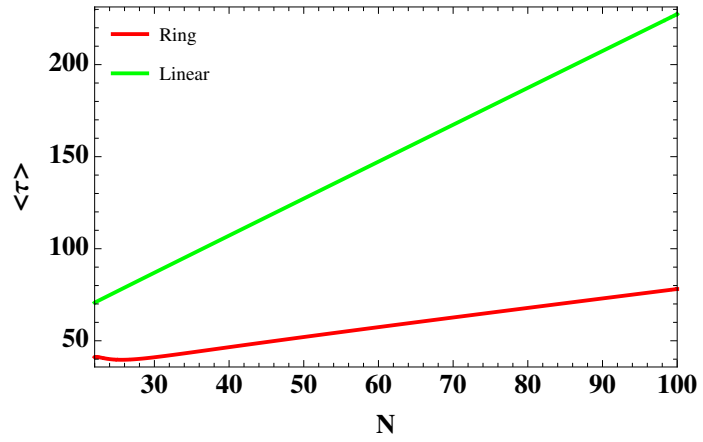

(b)

Figure 3.3. Comparison of ring and linear polymer translocation with $f = 0.05, \epsilon = 0$. (**??**) Free energy landscape with $N = 80$. (**??**) Translocation time as a function of N.

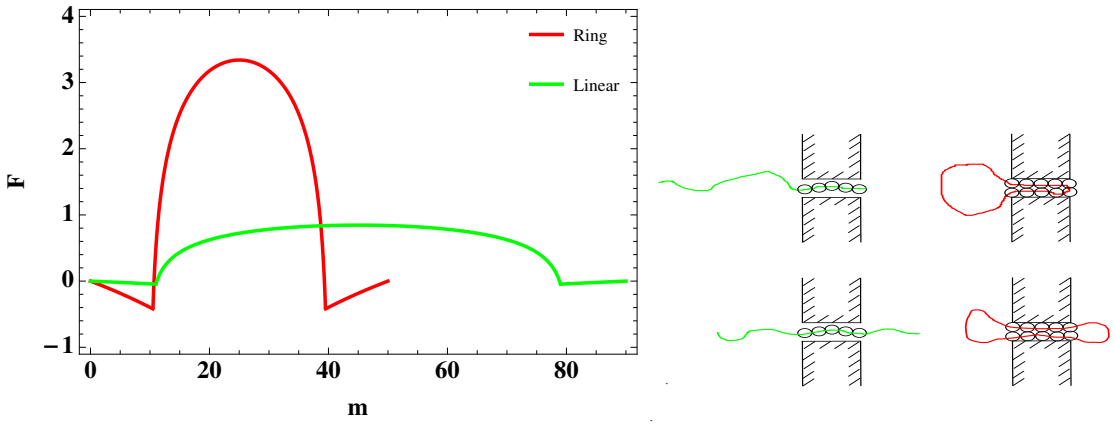

(a) (b)

Figure 3.4. Polymers pass through a small tube. (**??**) Pure entropic free energy without driving force. (**??**)Demonstration of how monomers pass through a tube under strong confinement.

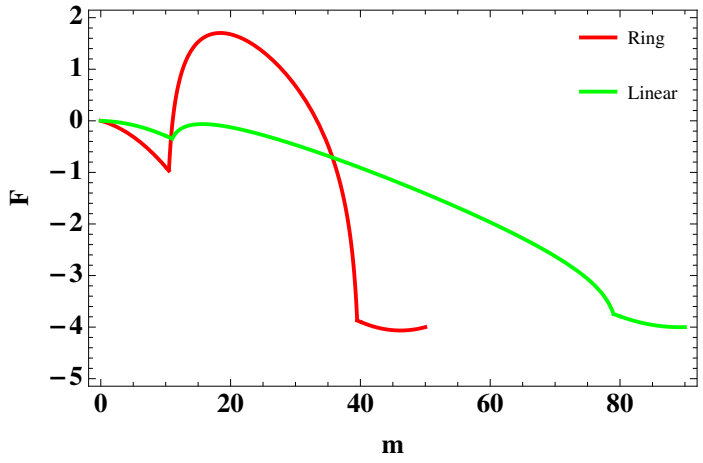

(a)

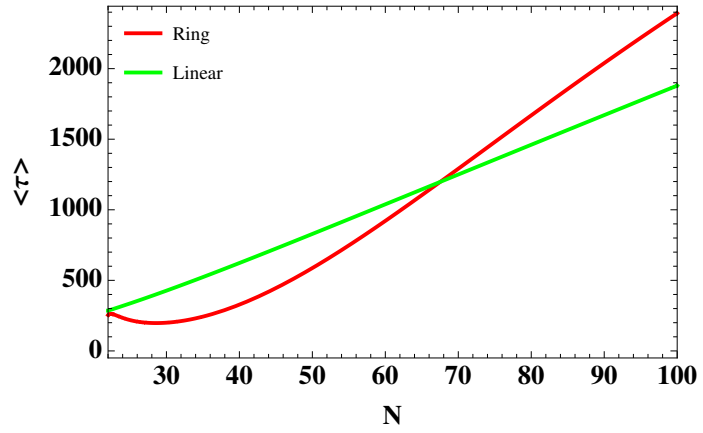

(b)

Figure 3.5. Comparison of ring and linear polymer translocation with $f = 0.005$, $\epsilon = 0$, $M = 10$. (**??**) Free energy landscape with $N = 80$. (**??**) Translocation time as a function of N.

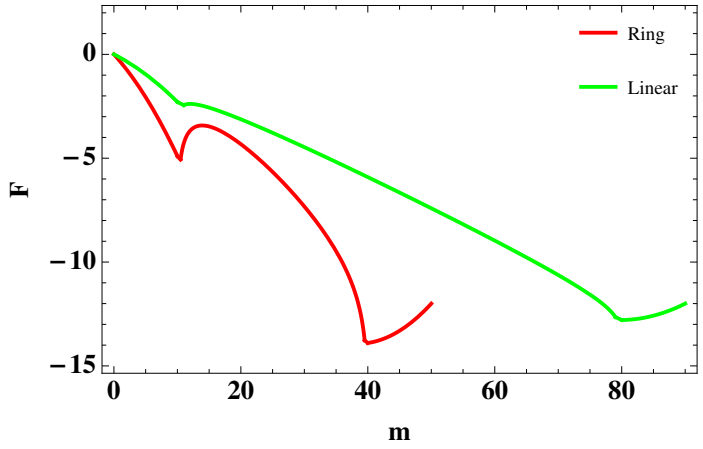

(a)

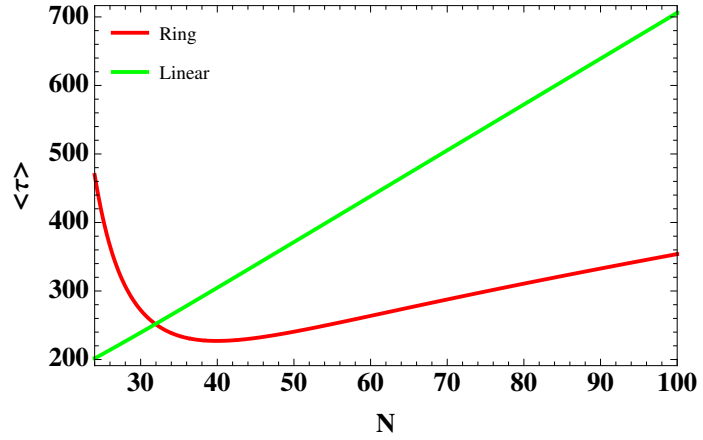

(b)

Figure 3.6. Comparison of ring and linear polymer translocation with $f = 0.015, \epsilon = -0.15, M = 10$. (**??**) Free energy landscape with $N = 80$. (**??**) Translocation time as a function of N.

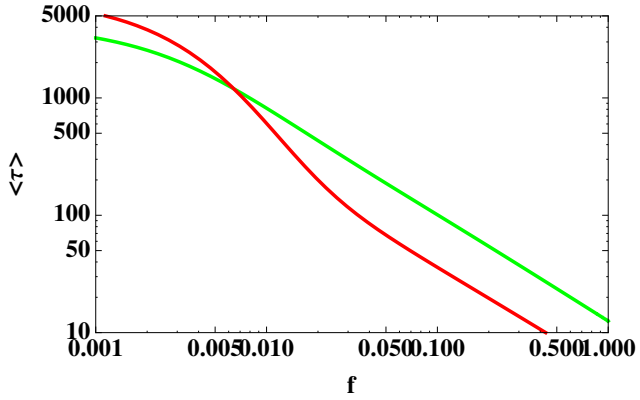

(a)

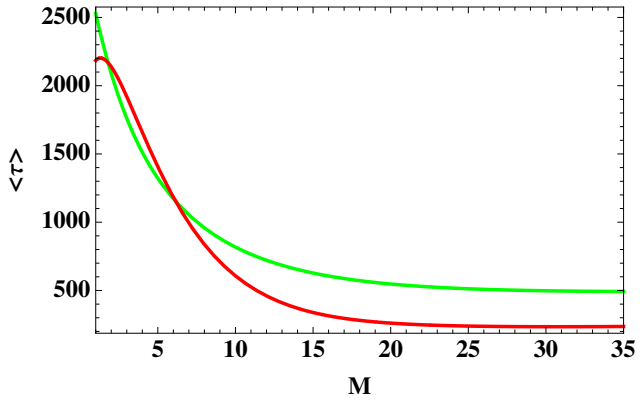

(b)

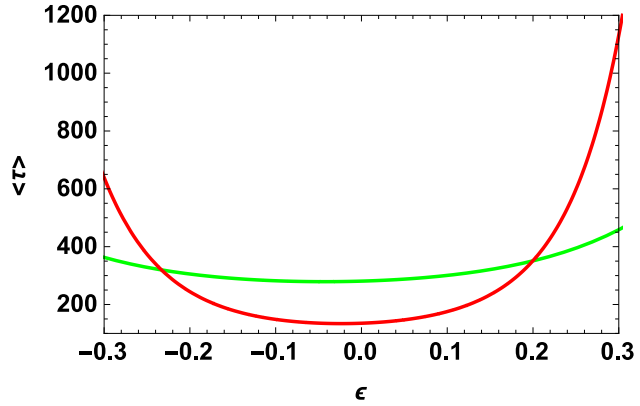

(c)

Figure 3.7. Comparison of ring and linear polymer translocation in terms of: (**??**) electric field strength f with $N = 80, \epsilon = 0$ and $M = 10$; (**??**) pore length M with $\epsilon = 0.0, N = 80, f = 0.01$;(**??**) polymer-pore interaction ϵ with $N = 50, f = 0.02$ and $M = 10$. Red curve for ring polymer, gree curve for linear polymer.

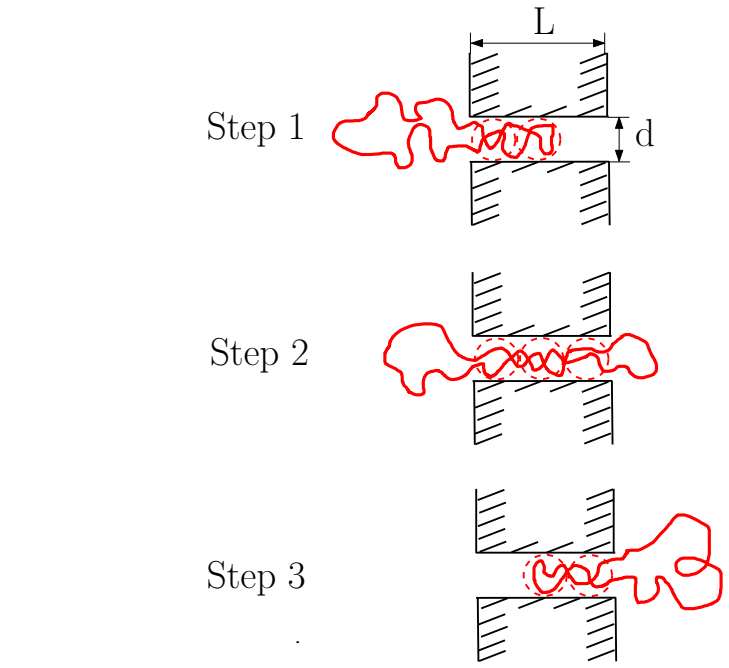

(a)

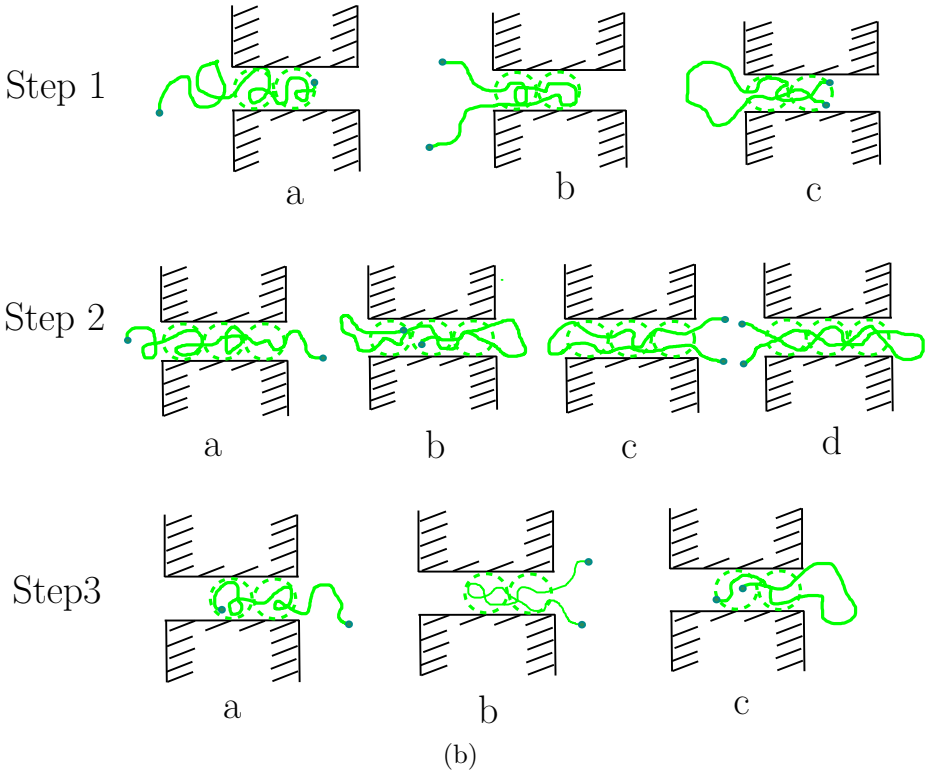

(b)

Figure 3.8. (a)The three steps of ring polymer translocation through wider pore; (b) The three steps of linear polymer translocation with possible conformations.

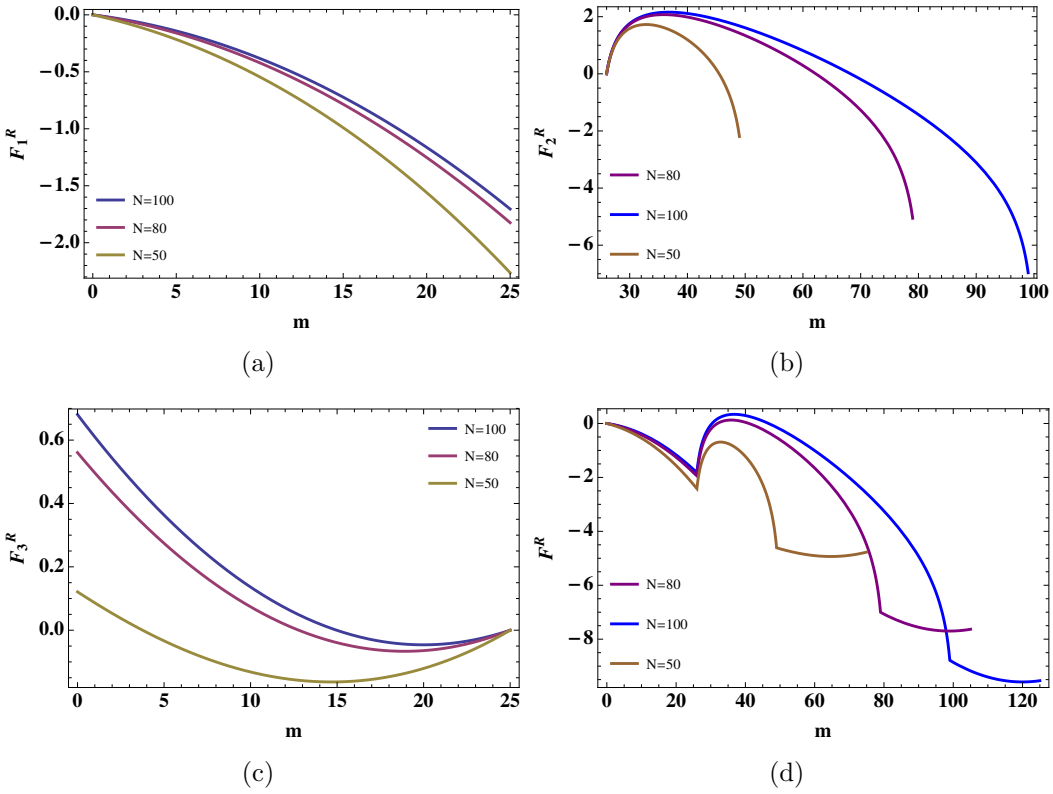

Figure 3.9. Free energy landscape in three steps for ring polymer translocation of different polymer length N, where $d = 4$, $M = 25$, $f = 0.01$ and $\epsilon = -0.1$.

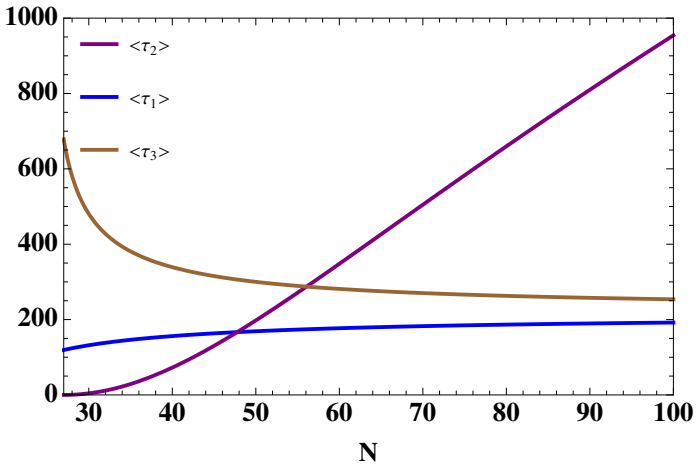

(a)

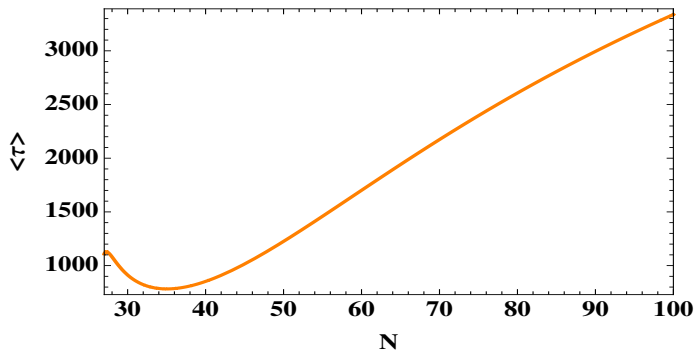

(b)

Figure 3.10. (a)Mean translocation times of ring polymer for step1, step2 and step3. (b)Mean total translocation time, where $d = 4$, $M = 25$, $f = 0.01$ and $\epsilon = -0.1$.

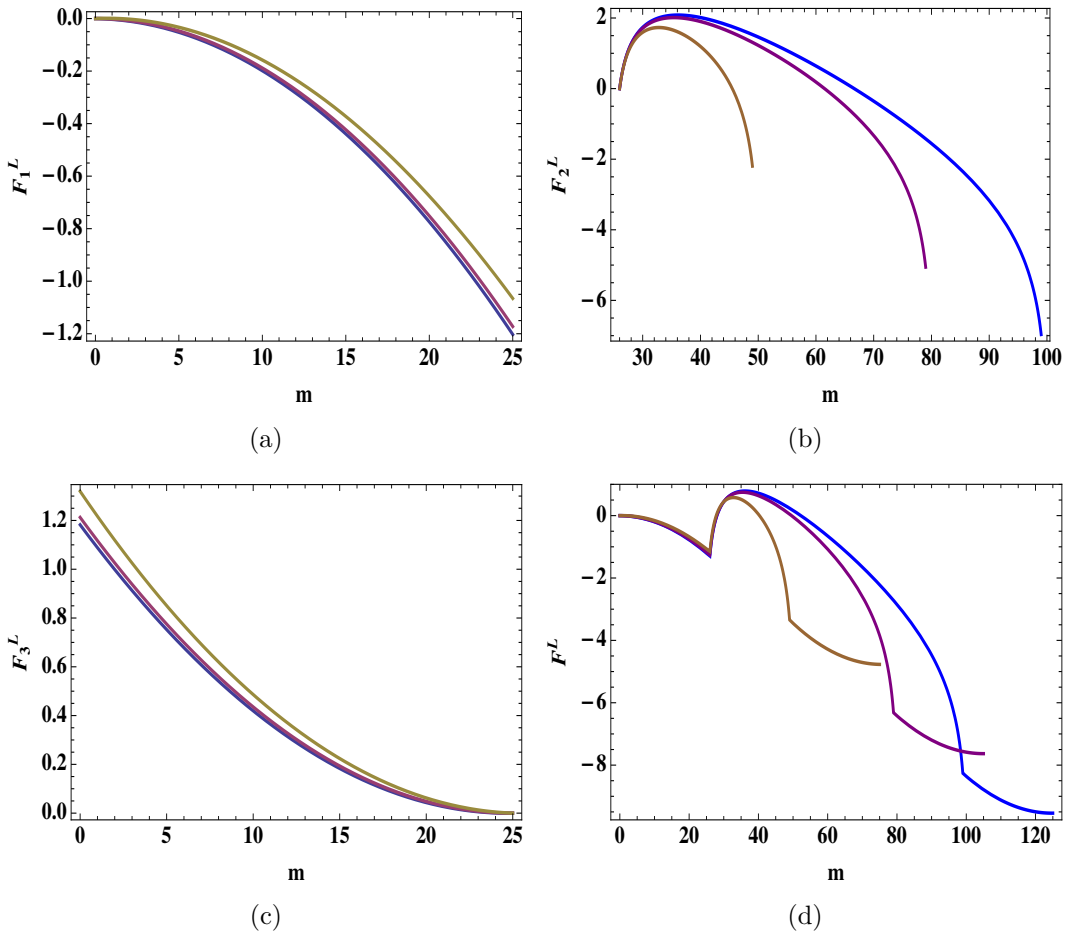

Figure 3.11. Free energy landscape in three steps for linear polymer translocation of different polymer length N: blue, purple and brown curves are for $N = 100$, $N = 80$, and $N = 50$ respectively, where $d = 4$, $M = 25$, $f = 0.01$ and $\epsilon = -0.1$.

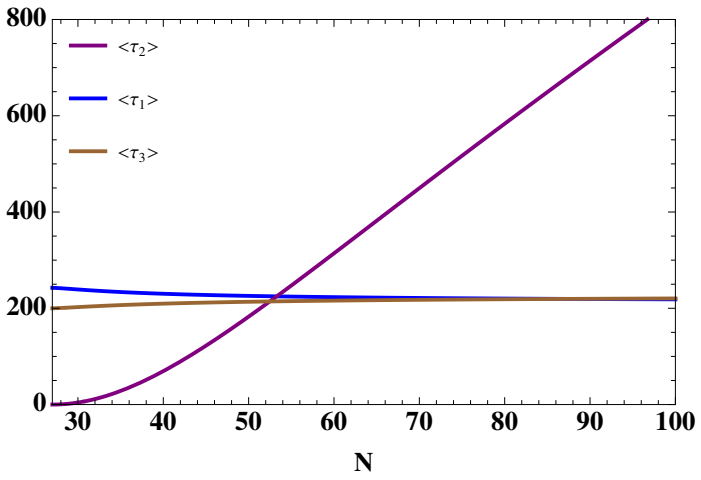

(a)

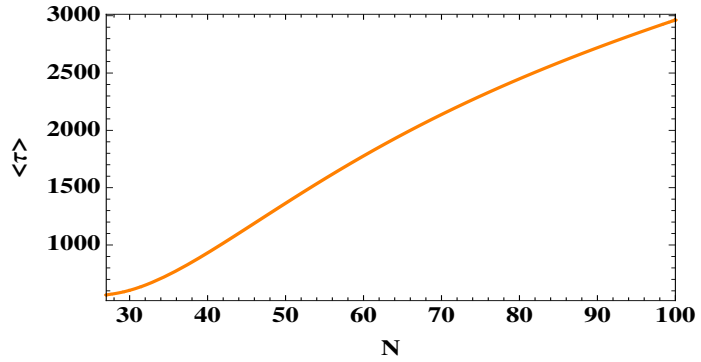

(b)

Figure 3.12. (a)Mean translocation times of linear polymer for step1, step2 and step3. (b)Mean total translocation time, where $d = 4$, $M = 25$, $f = 0.01$ and $\epsilon = -0.1$.

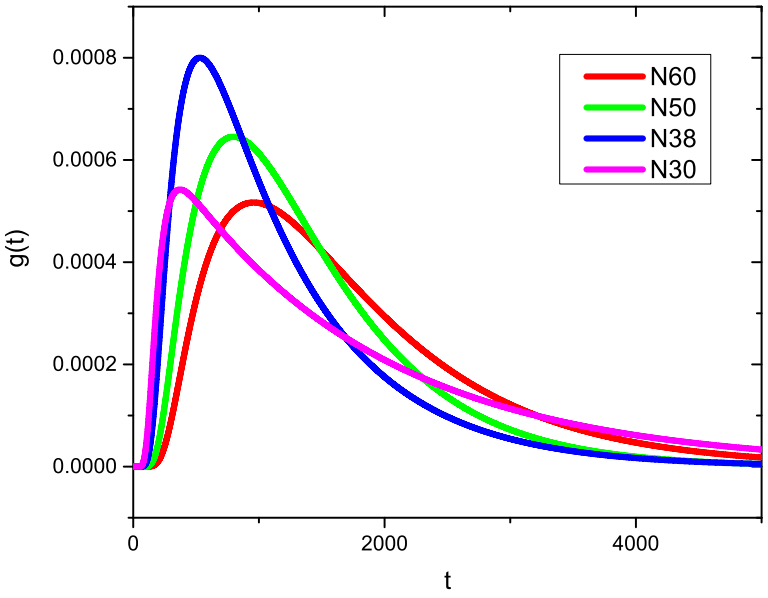

Figure 3.13. The probability distribution function of translocation time τ for ring polymer of different polymer length N, with $d = 4$, $M = 25$, $\epsilon = -0.1$ and $f = 0.01$.

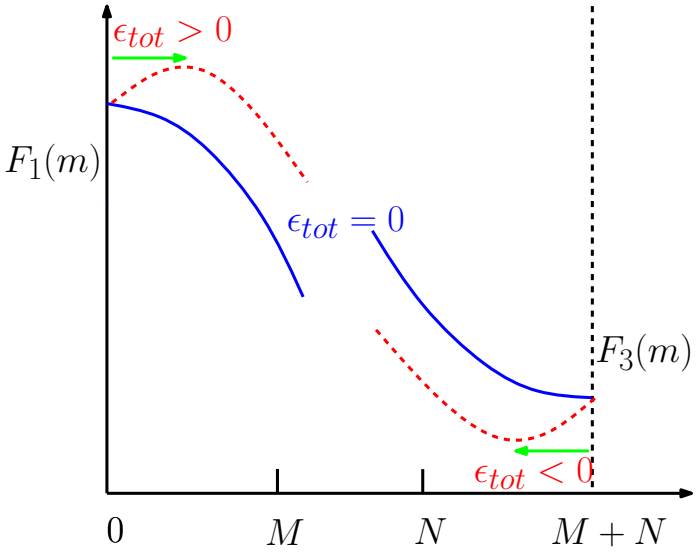

(a)

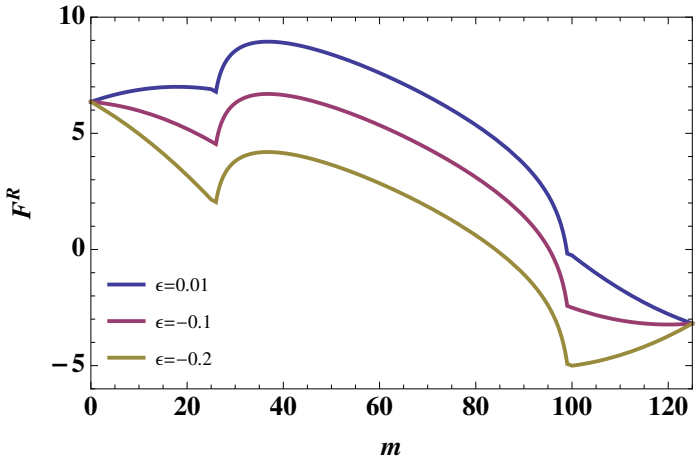

(b)

Figure 3.14. (a)Demonstration of free energy in the first and third step. (b)The total free energy of a ring polymer translocation for different pore attraction ϵ,with $N = 100$, $d = 4$, $M = 25$, and $f = 0.01$.

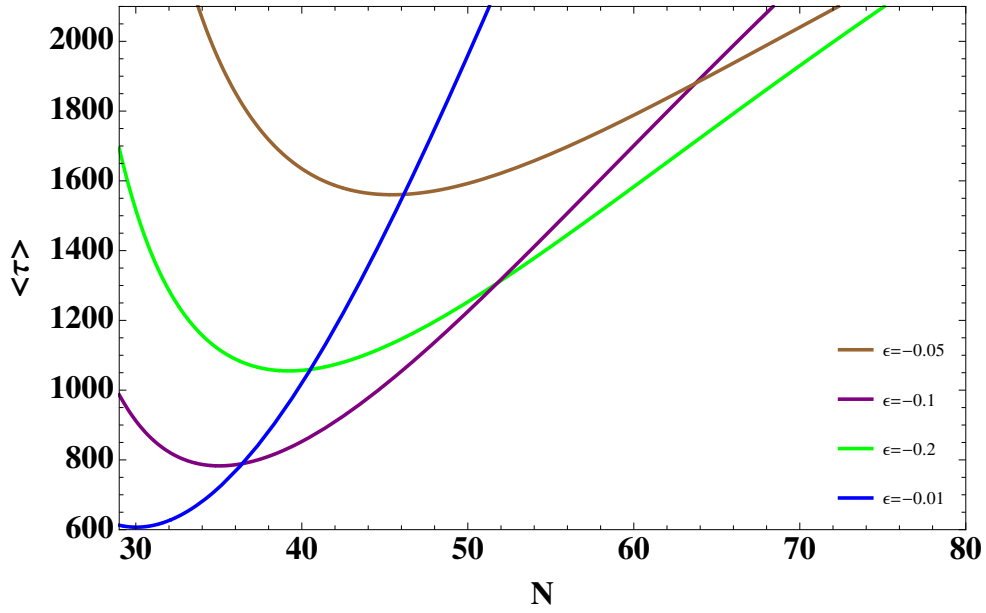

(a)

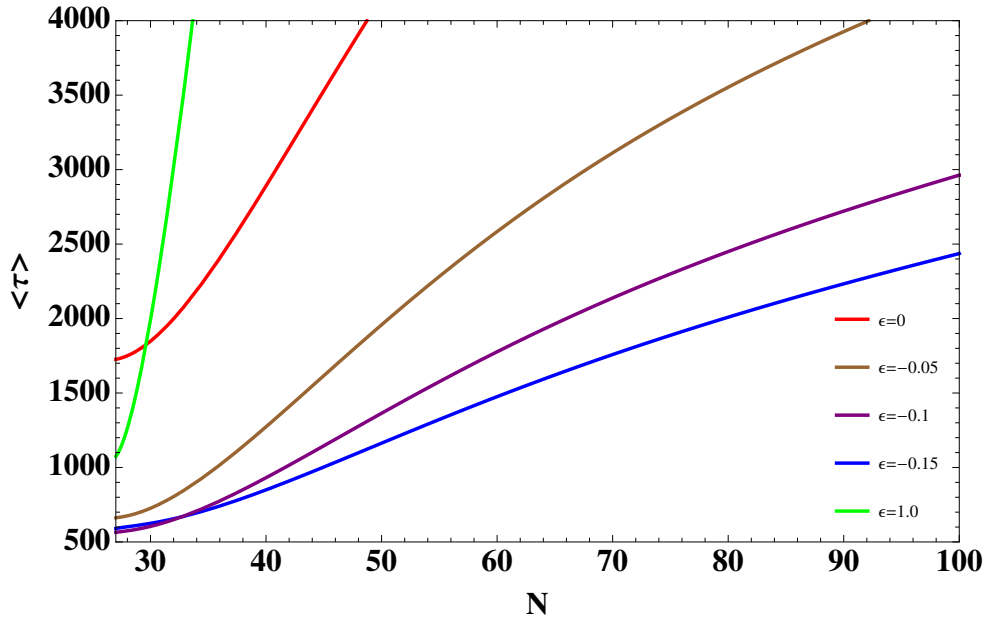

(b)

Figure 3.15. (a) The average translocation time of a ring polymer for different pore attraction energy ϵ; (b) The linear polymer translocation time with for different pore-polymer interaction ϵ, with $d = 4$, $M = 25$, and $f = 0.01$.

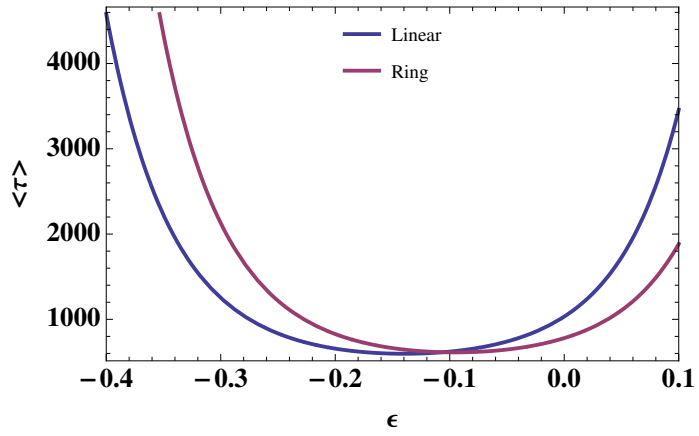

(a)

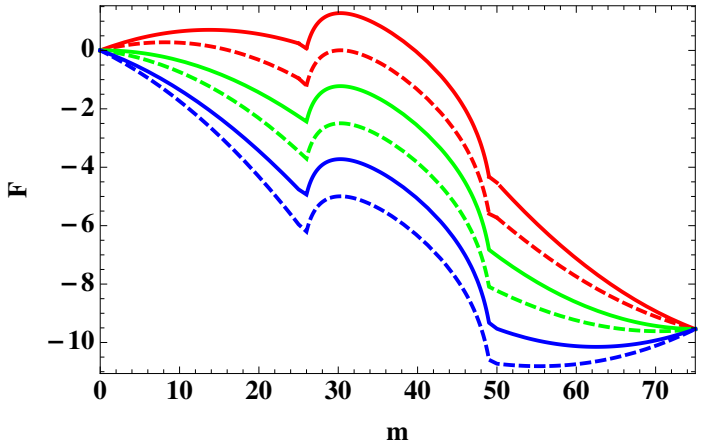

(b)

Figure 3.16. Comparison of ring and linear polymer with $N = 50$, $f = 0.02$, $d = 4$, $M = 25$. (a) Translocation time for ring and linear polymer as a function of ϵ. (b) Free energy of linear polymer (solid) and ring polymer (dashed) for $\epsilon = 0$(red), $\epsilon = -0.1$(green) and $\epsilon = -0.2$(blue).

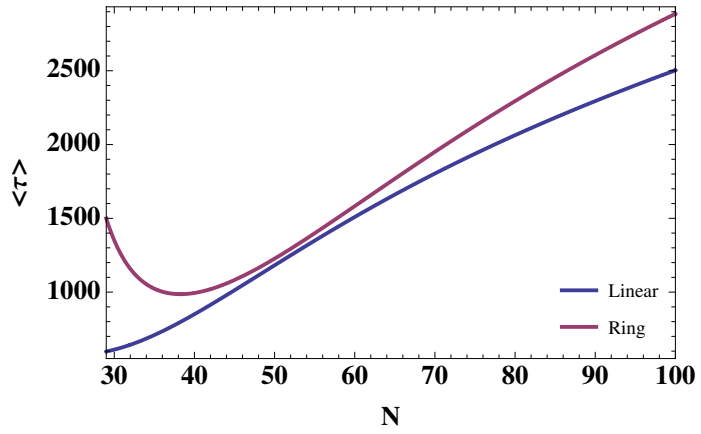

(a)

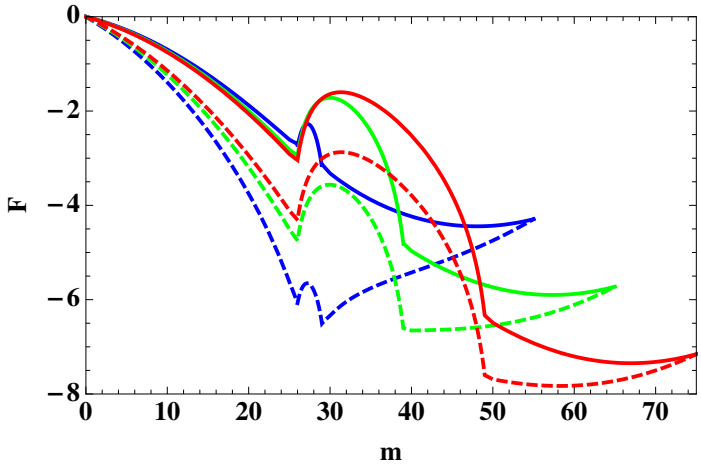

(b)

Figure 3.17. Comparison of ring and linear polymer translocation with $\epsilon = -0.15$, $f = 0.01$, $d = 4$, $M = 25$. (a) Translocation time for ring and linear polymer as a function of N. (b) Free energy of linear polymer (solid) and ring polymer (dashed) for $N = 50$(red), $N = 40$(green) and $N = 30$(blue).

CHAPTER 4

INTRODUCTION TO POLYMER BRUSH THEORY

4.1 Introduction to polymer brushes

Polymer brushes are formed by grafting long linear chains densely to a surface. When these polymers carry charges, the type of polymer brushes is referred as polyelectrolyte brush. Polymer brushes are featured as a dense layer of polymers confined by a surface. The surface can take different geometries, such as sphere and cylinder, in addition to flat surface. Limited space that can be explored by polymer chains leads to stretched conformations of brushes.

The adaptive nature of brush in accordance with its environment makes it an excellent candidate in practical application as functional material. For example, its sensitive swelling-shrinking conversion possesses good potential as "smart surfaces"[**?** **?**]. There are a variety of research areas where polymer brushes are used to achieve certain functions[**?**]. The practical use of grafted chains includes colloidal stabilization, friction reduction, tuning surface properties as adhesion and wetting[**?**]. Witten and Pincus theoretically showed the effective repulsion of two colloidal particles with grafted polymers[**?**]. This stabilization property leads to application in biomaterials, from controlling bacterial and cell adhesion[**?**] to bioelectronic systems[**?**]. The reduction of friction between surfaces with the help of tethered PE layers leads to a promising lubricant for joints or other organs in human body[**?** **?**]. Klein et al have pioneered the measurement of lateral forces in rubbing surfaces with tethered polymer chains[**?**], which indicated a strikingly low friction coefficient. They attributed the

effect to long-ranged repulsion originated from entropy that holds the surfaces apart. Raviv et al have shown that grafted polyelectrolytes is a superior lubricant[**?**].

Theories on neutral brushes have been studied as well. The credit goes to Alexander[**?**] and de Gennes[**?**] for their seminal work on neutral polymer brush, which attribute importance of excluded volume interaction in brush swelling and step function profile of monomer distribution. The scaling theory uses Flory argument and global energy balance. The equilibrium brush height balances the pair-wise excluded volume interaction with the free energy to stretch the chain from grafting surface. An alternative way to derive the brush height is to treat the densely grafted chain as a sequence of interacting blobs, which have radius of the grafting spacing. Self-consistent field method was first implemented by Milner, Witten and Cates[**?**], where they derived the monomer density self-consistently.

In the regard of polyelectrolyte brush, Pincus[**?**] was one of the pioneers in charged polymer brush theory, who pointed out that most counterions are trapped in brush phase in osmotic brush and the power law for salted brush. The two (osmotic and salted) regions are distinguished by different behaviors of brush height in salty solution. When the salt concentration is low, the brush height is independent of salt concentration because of the strong electrical repulsion of the charges carried by the polymer backbones. As the salt concentration increases, the electric interaction is screened by ion clouds. Thus the brush height decreases with salt concentration. Zhulina[**?**] extended the scaling theory to weak polyelectrolyte brush, by incorporating the dissociation balance of protons and Donnan equilibrium. Later, a semi self-consistent field theory was developed for polyelectrolyte brush [**?** **?**] following the lines of that for neutral brush. The effective electric potential for PE brush is quadratic[**?**], in accordance to the effective potential for neutral brush. Later Zhulina[**?**] developed a full self-consistent field theory for weak polyacid brush, which accounted for the position dependence of degree of ionization. Szleifer[**?**] also

considered the position dependent permitivity in their self-consistent theory, and they found such dependence is visible for grafted chains on curved surfaces, but negligible for flat polyelectrolyte brush.

Due to rich physics in polymer brushes, many experiments have been done and compared to theories at the same time. The brush height was first measured by X-ray reflectometry[**?**]. Dynamical measurement was also made by SFA[**?**]. In these experiments, two PE brushes slowly approach each other and the force between them was measured. It shows that the distance where repulsive force occurs is twice the brush height. Trirrell and co-workers observed attractive forces after the brushes compress and separate in multivalent salt[**?**]. There is also a non-monotonic behavior of brush height depending on added salt concentration for non-monovalent salt. On the other hand, different geometries of the surface, such as flat, spherical, cylindrical surface surfaces, have also been discussed and investigated in the literatures of polymer brush. Experimentally, Guo et al was the first to report that polyelectrolyte chains can be grafted to colloidal spheres by photo-emulsion polymerization[**?**].

In the following sections, we will present the existing theories for neutral brush and charged brush respectively.

4.2 Neutral polymer brush

4.2.1 Alexander brush

A simple scaling argument of a neutral polymer brush is Alexander brush[**?**]. It assumes a densely grafted polymer layer is immersed in a good solvent. The polymer chains are uniformly grafted with one end on a substrate and uniformly stretched. Segment concentration is also assumed constant (step-like function), with segment volume fraction being $\frac{Nl^3}{hd^2}$, where l is the monomer size, d is the space between two grafting positions, $\sigma = 1/d^2$ is the grafting density, and h is brush height. The Flurry

free energy is made up with pair-wise monomeric excluded volume interaction (first term) and chain stretching energy (second term):

$$\frac{F}{k_BT} = w(\frac{Nl^3}{hd^2})^2\frac{hd^2}{l^3} + \frac{h^2}{Nl^2} \tag{4.1}$$

Minimize the free energy with respect to h,

$$\frac{1}{k_BT}\frac{dF}{dh} = -\frac{wl^3N^2}{h^2d^2} + \frac{2h}{Nl^2} = 0, \tag{4.2}$$

$$h = Nl(w\sigma)^{1/3}. \tag{4.3}$$

The brush is stretched and the brush height increases with grafting density.

4.2.2 de Gennes brush

The de Gennes brush[**?**] distinguishes two regions in grafting density. When the grafting space d between two chains is less than the radius of gyration R_g, there is no overlap. This region is called "mushroom". When the grafting density is large enough to evoke strong interaction, especially repulsion for neutral brush, the correlation length ξ (i.e. the size of a interacting blob) equals to the spacing d. Figure**??** depicts the blob model of a neutral brush. The number of segments in one blob is $g = (\xi/l)^{1/\nu}$, where ν is the Flory exponent. The brush height is

$$h = \frac{N}{g}\xi = \frac{N}{(d/l)^{1/\nu}}d = Nl^{1/\nu}d^{1-1/\nu}. \tag{4.4}$$

In good solvent $\nu = 3/5$, the brush height h turns out to be proportional to $Nl\sigma^{1/3}$, which is in agreement to Alexander brush.

4.2.3 Self-consistent field theory (SCFT)

Milner, Witten and Cates[**?**] presented a self-consistent field method that is appropriate for brushes with high grafting density. Exact solution given by "classical

limit" suggested a parabolic concentration profile rather than a step-function. We will present self-consistent field method in the similar way we handle polyelectrolyte brush in Chapter**??**. We will also show that the result we got is consistent with [**?**].

The partition sum of a polymer brush is multiplication of all chains in the brush system:

$$\begin{aligned}\mathscr{Z} = \int \Pi_{i=1}^{n} \mathcal{D}[\mathbf{r}_i(s)] \exp\{-\frac{3}{2l^2}\sum_{i=1}^{n}\int_0^N ds(\frac{d\mathbf{r}_i(s)}{ds})^2 \\ - \frac{1}{2}\sum_{i=1}^{n}\sum_{i'=1}^{n}\int_0^N ds\int_0^N ds' V_{pp}(\mathbf{r}_i(s) - \mathbf{r}_{i'}(s'))\}\end{aligned} \tag{4.5}$$

where V_{pp} is the interaction between pair-wised monomers. We define the discrete monomer density as:

$$\hat{\rho}_p(\mathbf{r}) = \sum_{i=1}^{n}\int_0^N ds\delta(\mathbf{r} - \mathbf{r}_i(s)),$$

and the pair-wise interaction as:

$$V_{pp}(\mathbf{r} - \mathbf{r}') = w_{pp}\delta(\mathbf{r} - \mathbf{r}'),$$

Hereafter, we will omit vector notation for $\mathbf{r}$ as r, which means a $3D$ vector.

$$\mathscr{Z} = \int \Pi_{i=1}^{n} \mathcal{D}[r_i(s)] \exp\{\frac{3}{2l^2}\sum_{i=1}^{n}\int_0^N ds(\frac{dr_i(s)}{ds})^2 - \frac{1}{2}\int dr\omega_{pp}\hat{\rho}_p^2(r),$$

Insert the identities:

$$1 = \int \delta\rho_p\delta(\rho_p(r) - \hat{\rho}_p(r)) \tag{4.6}$$

into the equation and parameterized with $\phi_p(r)$:

$$1 = \int \delta\rho_p\delta\phi_p \exp\left[-i\int \phi_p(r)(\rho_p(r) - \hat{\rho}_p(r))dr\right] \tag{4.7}$$

Then the partition function becomes:

$$\begin{aligned}\mathscr{Z} &= \int \delta\rho_p\delta\phi_p \int \Pi_{i=1}^{n}\mathcal{D}[r_i(s)] \exp\Big[\int_0^N ds\Big(-\frac{3}{2l^2}\sum_{i=1}^{n}(\frac{dr_i(s)}{ds})^2 \\ &\quad \phi_p(r_i(s)) - \phi_p(r)\rho_p(r)\Big)\Big] \\ &= \int \delta\rho_p\delta\phi_p \left(\int D[r(s)] \exp\left[\int_0^N ds\left(-\frac{3}{2l^2}\left(\frac{dr(s)}{ds}\right)^2 + \phi_p(r_i(s))\right)\right]\right)^n \\ &\quad \exp\{-\phi_p(r)\rho_p(r)\} \\ &\approx \int \delta\rho_p\delta\phi_p e^{-\mathscr{F}(\phi_p,\rho_p)}\end{aligned}$$

With excluded volume interaction, the path integral of a chain in the brush is modified by a potential $\phi_p(r)$:

$$G = \int \mathcal{D}[r(s)] \exp\{-\frac{3}{2l^2}\int_0^N ds(\frac{d}{ds}r(s))^2 - i\int_0^N ds\phi_p(r(s))\}. \tag{4.8}$$

By saddle point approximation:

$$\frac{\delta\mathscr{F}}{\delta\phi_p} = \frac{\delta\mathscr{F}}{\delta\rho_p} = 0, \tag{4.9}$$

we have $i\phi_p = \rho_p$, which is in agreement with [**?**]. This means the effective potential imposed on any single chain in the brush is coming from the influence all other chains. Moreover, this potential is equal to the monomer density. Since we expect translational invariance parallel to the grafting surface, it is essentially a one-dimension problem, and the propagator of a chain can be written as:

$$G = \int \mathcal{D}[z(s)] \exp\left[-\frac{3}{2l^2}\int_0^N ds\left(\frac{d}{ds}z(s)\right)^2 - i\int_0^N ds\phi_p(z(s))\right]. \tag{4.10}$$

By classical limit, Milner et al[**?**] concluded that $i\phi_p$ has a quadratic form. The argument can be put in simple words. The path integral of **??** is same as that of

a frictional, classical particle that starts at some position z and ends at the surface $z = 0$, within time N. It requires every path of any initial position and velocity finishes in an equal time. It implies the particle is under a harmonic potential with period of $4N$.

Muthukumar[**?**] also derived a parabolic potential for polyelectrolyte brush by constraints from an equivalent classical system with Lagragian $\mathscr{L} = T - V$, where $T = -\frac{3}{2l^2}(\frac{d}{ds}z(s))^2$ and $V = i\phi_p(z)$. By energy conservation $E = T + V$ and free end zero force, we have

$$V = i\phi_p(z) = \left(\frac{h}{h_0}\right)^2 - (\frac{z}{h_0})^2 \tag{4.11}$$

with

$$h_0^2 = \frac{8l^2N^2}{3\pi^2}. \tag{4.12}$$

This effective potential under which the polyelectrolyte chain lives, is a combination effect from other chains, as well as counterions, anions, and solvent. One should be careful that in the context of polyelectrolyte, $i\phi_p = \rho_p$ no longer holds when there are other interactions, such as electric interaction.

4.3 Polyelectrolyte brush

4.3.1 Pincus brush

Similar to neutral polymer brush, scaling argument of polyelectrolyte brush was first brought up by Pincus[**?**] using force balance technique: the osmotic pressure from free ions balances with the elastic pressure from chain backbone. The assumption of step-like segment density profile is inherited from Alexander brush. Excluded volume interaction, which plays an important role in neutral brush, is ignored in polyelectrolyte brush, because it is relatively weaker compared to electric interaction. Pincus brush also has fixed fraction of charged monomers α.

4.3.1.1 Without added salt

The osmotic pressure scales as the counterion concentration:

$$\Pi_{count} \propto \alpha c_p = \frac{\alpha N}{hd^2}. \tag{4.13}$$

The elastical pressure scales as

$$P_{elast} \propto \frac{h^2}{Nl^2}\frac{1}{hd^2} = \frac{h}{Nl^2d^2}. \tag{4.14}$$

Let $\Pi_{count} = P_{elast}$, we have $h \propto \alpha^{1/2}Nl$. With finite fraction of charges, the brush is highly stretched and independent of grafting density.

4.3.1.2 With added salt

When the added salt is very low compared with counterion density, the screen length from salt $\kappa_s^{-1} \propto c_s$ is too small compared to that from counterions. The brush height is dictated by the osmotic pressure from counterions inside the brush. The low salt concentration does not affect the overall brush height. However, when the added salt increases and becomes comparable to counterion density, the brush height is determined by the osmotic pressure difference between counterions and salt ions. The osmotic pressure difference between brush phase and solution phase scales as:[**?**]

$$\Pi_{count} \propto \frac{c_{count}^2}{c_s} = \frac{(\alpha c_p)^2}{c_s}. \tag{4.15}$$

Force balance of $\pi_{count} = P_{elast}$ gives

$$h \propto \alpha^{2/3}Nlc_s^{-1/3}, \tag{4.16}$$

where the brush height decreases with salt concentration. The $-1/3$ scaling law has been confirmed by many experiments[**?**].

4.3.2 Self-consistent field methods

Self-consistent field method was applied to polyelectrolyte brush in many different ways as discussed in introduction. The application of self-consistent field method, similar to what is described in Section**??** to polyelectrolyte brush in monovalent salt will be discussed in details in next chapter.

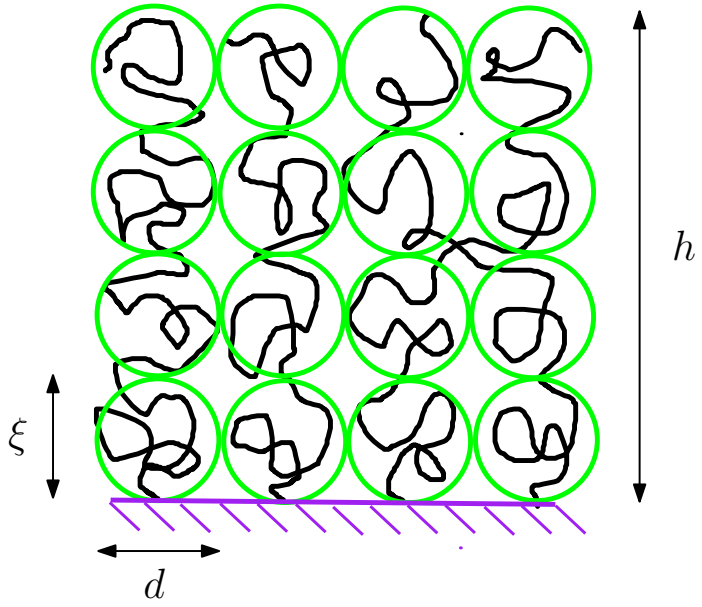

Figure 4.1. Blob model for a neutral brush.

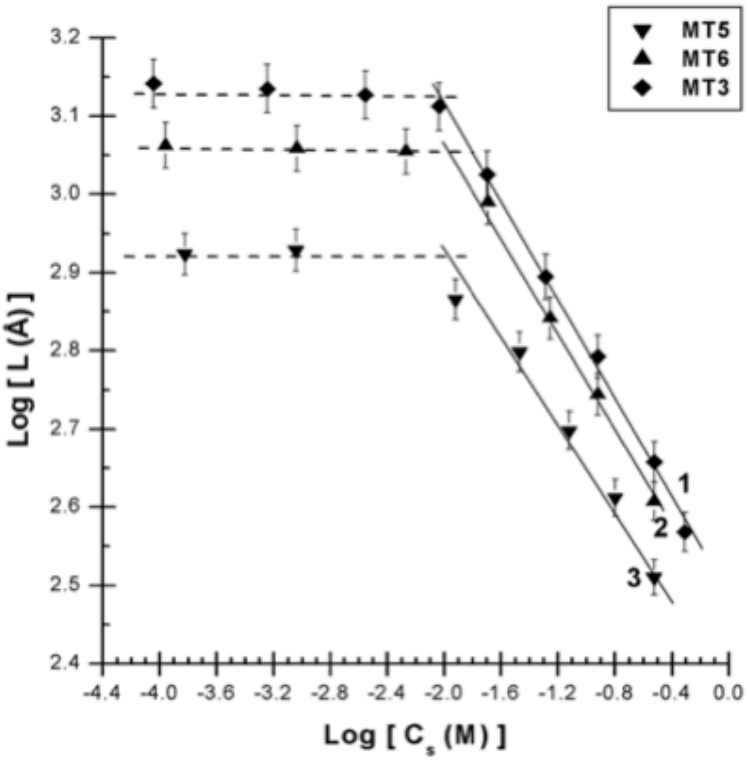

Figure 4.2. Salt concentration dependence of the brush height for three different brushes.[**?**].

CHAPTER 5

SELF-CONSISTENT FIELD THEORY OF POLYELECTROLYTE BRUSH IN MONOVALENT SALT

5.1 Introduction

The polyelectrolyte brushes are distinguished from their neutral counterpart due to the long range, electrostatic interaction. Their adaption to surrounding conditions, such as solvent quality, salt concentration, pH and temperature, makes them even more interesting with diverse properties and potential applications in functional materials and technologies. The reduction of friction between surfaces with help of tether PE layers leads to a promising lubricant for joints or other organs in human body[**?** **?**]. The stronger swelling-shrinking transformation can be applied to "smart surfaces" engeering[**?** **?**].

The scaling theory or semi-self-consistent field theory of charged brush are all based on a fixed degree of ionization. From many studies about counterion condensation[**?** **?**], we know that the degree of ionization is self-adaptable quantity as the entropy and energy of the system changes. Even those strong polyelectrolytes have variable degree of ionization in different salt concentrations and at different positions along the chain. Later Zhulina[**?**] developed a full self-consistent field theory for weak polyacid brush, which accounted for the position dependence of degree of ionization. Szleifer[**?** **?**] also considered the position dependent permittivity in their self-consistent theory, and they found such dependence is visible for grafted chains on curved surfaces, but negligible for flat PE brush. In the above SCFT, as the chain is much easier to adsorb protons than other salt ions, there is no exchange of adsorption

of counterions with added salt. Besides, the solvent quality is omitted for the stronger interaction from electric potential.

In this chapter, we follow the lines of self-consistent field theory for polymer brush, and developed a scheme for PE brush with monovalent salt solution. By employing saddle point approximation, we derive the free energy. It is demonstrated that even for strong PE brush, the degree of ionization is adjustable to salt concentration. This is because for any charged polymer, salt ions screen the electric repulsion of charges on the chain and its radius of gyration shrinks with added salt. Increase in local monomer density makes the local permittivity even smaller. Thus more counterions tend to adsorb to the chain, resulting in even more collapsed chain. We also confirm the assumption by scaling theory, that counterions are mostly trapped inside the brush, by calculating the distributions of monomers and ions in a seft-consistent way. By including the excluded volume interaction, our results observe phase transition in brush height in accordance with Ross and Pincus' theory[**?**].

5.2 SCFT set-up

In a polyelectrolyte brush system, suppose there are n polyelectrolyte (e.g. $NaPSS$) bristles, with degree of polymerization N and bond length l, grafted to a flat surface and immersed in monovalent salt solution (e.g. $NaCl$) with salt concentration n_i (cation or anion number density). The whole system has a volume of $V = SL$, with surface area of S and length of L. It can be divided into two phases: the brush phase and the solution phase. We treat the partition of each phase separately. Using self-consistent field theory and saddle point approximation, we can write down free energy for both phases separately. By the free energy minimization we can find the equilibrium macroscopic properties of the brush system, such as the brush height h, the degree of ionization α, as well as microscopic distributions of small molecules and

Table 5.1. Notations in SCFT set-up

Brush phase	Solution phase	Definition
ρ_+^B	ρ_+^S	number density of monovalent cations (e.g. Na^+)
ρ_-^B	ρ_-^S	number density of monovalent anions (e.g. Cl^-)
ρ_s^B	ρ_s^S	number density of solvent molecules (e.g. water)
ρ_p		number density of monomers
$\rho_0 = 1/l^3$		maximum density of each lattice point
n_+^B	n_+^S	number of positive ions
n_-^B	n_-^S	number of negative ions
n_s^B	n_s^S	number of solvent molecules

monomers in the system. Some functions and variables are defined in the following table.

5.3 Brush phase

5.3.1 Partition function

To include all the interactions between all components in the system, i.e. electric interaction and excluded-volume-interaction among monomers, salt ions and solvent molecules, as well as the connectivity of the chain, we write the partition sum of brush phase as:

$$
\begin{aligned}
e^{-\frac{F^B}{k_BT}} \;=\; & \frac{\int \Pi_{\beta=s,+,-}\Pi_{m=1}^{n_\beta} d\mathbf{r}_{\beta m}}{\Pi_{\beta=s,+,-} n_\beta!} \int \Pi_{i=1}^{n} \mathcal{D}[\mathbf{r}_i(s)] \exp\Big[-\frac{3}{2l^2}\sum_{i=1}^{n}\int_0^N ds (\frac{d\mathbf{r}_i(s)}{ds})^2 \\
& -\frac{1}{2}\sum_{m=1}^{n_s}\sum_{m'=1}^{n_s} V_{ss}(\mathbf{r}_m - \mathbf{r}_{m'}) - \frac{1}{2}\sum_{i=1}^{n}\sum_{i'=1}^{n}\int_0^N ds \int_0^N ds' V_{pp}(\mathbf{r}_i(s) - \mathbf{r}_{i'}(s')) \\
& -\sum_{i=1}^{n}\sum_{\beta=s,+,-}\int_0^N ds \sum_{m=1}^{n_\beta} V_{p\beta}(\mathbf{r}_{\beta m} - \mathbf{r}_{i'}(s)) \\
& -\frac{1}{2}\sum_{\beta=+,-}\sum_{\beta'=+,-}\sum_{m=1}^{n_\beta}\sum_{m'=1}^{n_{\beta'}} V_{\beta\beta'}(\mathbf{r}_{\beta m} - \mathbf{r}_{\beta' m'})\Big] \\
& \Pi_r \delta(\hat{\rho}_p(\mathbf{r}) + \hat{\rho}_s^B(\mathbf{r}) - \rho_0).
\end{aligned}
$$

From now on, we will use r for $3D$ vector instead of $\mathbf{r}$.

Substitute in the above equation the exclude-volume interactions among monomerss and solvent molecules, and electrostatic interactions among monomers and free ions, and then substitute the following density operators:

$$\hat{\rho}_p(r) = \sum_{i=1}^{n} \int_0^N ds\delta(r - r_i(s)),$$

$$\hat{\rho}_\beta^B(r) = \sum_{m=1}^{n_\beta} \delta(r - r_{\beta m}), with \beta = s, +, -$$

$$\hat{\rho}_e^B(r) = \sum_{\beta=+,-} z_\beta \hat{\rho}_\beta(r) + z_p \alpha \hat{\rho}_p(r),$$

$$\begin{aligned} e^{-\frac{F^B}{k_B T}} &= \frac{\int \Pi_{\beta=s,+,-} \Pi_{m=1}^{n_\beta} dr_{\beta m}}{\Pi_{\beta=s,+,-} n_\beta!} \int \Pi_{i=1}^{n} \mathcal{D}[r_i(s)] \exp\Big[-\frac{3}{2l^2} \sum_{i=1}^{n} \int_0^N ds (\frac{dr_i(s)}{ds})^2 \\ &\quad -\frac{1}{2} \int dr \omega_{ss} (\hat{\rho}_s^B)^2(r) - \frac{1}{2} \int dr \omega_{pp} \hat{\rho}_p^2(r) - \int dr \omega_{ps} \hat{\rho}_p(r) \hat{\rho}_s(r) \\ &\quad -\frac{l_B}{2} \int dr \int dr' \frac{\hat{\rho}_e(r) \hat{\rho}_e(r')}{|r - r'|} \Big] \Pi_r \delta(\hat{\rho}_p(r) + \hat{\rho}_s(r) - \rho_0). \end{aligned}$$

Using chi parameter $\chi = 2\omega_{ps} - \omega_{pp} - \omega_{ss}$, the partition function becomes:

$$\begin{aligned} e^{-\frac{F^B}{k_B T}} &= \frac{\int \Pi_{\beta=s,+,-} \Pi_{m=1}^{n_\beta} dr_{\beta m}}{\Pi_{\beta=s,+,-} n_\beta!} \int \Pi_{i=1}^{n} \mathcal{D}[r_i(s)] \exp\Big[- \frac{3}{2l^2} \sum_{i=1}^{n} \int_0^N ds (\frac{dr_i(s)}{ds})^2 \\ &\quad -\chi \int dr \hat{\rho}_p(r) \hat{\rho}_s^B(r) - \frac{l_B}{2} \int dr \int dr' \frac{\hat{\rho}_e^B(r) \hat{\rho}_e^B(r')}{|r - r'|} - \frac{\rho_0}{2} (\omega_{pp} n N + \omega s s n_s^B) \Big] \\ &\quad \Pi_r \delta(\hat{\rho}_p(r) + \hat{\rho}_s^B(r) - \rho_0). \end{aligned}$$

Insert into the equation with identities:$1 = \int \delta\rho_\beta \delta(\rho_\beta(r) - \hat{\rho}_\beta(r))$, with $\beta = p, s, +, -$, and parameterize $\rho_\beta(r)$ with $\phi_\beta(r)$ and $\eta(r)$,

$$
\begin{aligned}
e^{-\frac{F^B}{k_BT}} &= \frac{\int \Pi_{\beta=s,c,+,-}\Pi_{m=1}^{n_\beta} dr_{\beta m}}{\Pi_{\beta=s,+,-} n_\beta!} \int \Pi_{i=1}^{n}\mathcal{D}[r_i(s)] \int \Pi_{\beta=s,+,-}\delta\rho_\beta^B\delta\phi_\beta^B\delta\rho_p\delta\phi_p\delta\eta^B \\
&\exp\Big[-\frac{3}{2l^2}\sum_{i=1}^{n}\int_0^N ds(\frac{dr_i(s)}{ds})^2 - \chi\int dr\rho_p\rho_s^B - \frac{l_B}{2}\int dr\int dr'\frac{\rho_e^B(r)\rho_e^B(r')}{|r-r'|} \\
&-\frac{\rho_0}{2}(\omega_{pp}nN + \omega ssn_s^B) - i\int dr\big(\eta(\rho_p+\rho_s^B-\rho_0) + \phi_p(\hat{\rho}_p-\rho_p) \\
&+\sum_{\beta=s,+,-}\phi_\beta^B(\hat{\rho}_\beta^B-\rho_\beta^B)\big)\Big].
\end{aligned}
$$

Re-organize the exponent in the partition function:

$$
\begin{aligned}
e^{-\frac{F^B}{k_BT}} &= \int \Pi_{\beta=s,+,-}\delta\rho_\beta^B\delta\phi_\beta^B\delta\rho_p\delta\phi_p\delta\eta^B \int \Pi_{i=1}^{n}\mathcal{D}[r_i(s)]\exp\Big[-\frac{3}{2l^2}\sum_{i=1}^{n}\int_0^N ds(\frac{dr_i(s)}{ds})^2 \\
&-i\sum\int ds\phi_p(r(s))\Big]\frac{\int\Pi_{\beta=s,+,-}\Pi_{m=1}^{n_\beta}dr_{\beta m}}{\Pi_{\beta=s,+,-}n_\beta!}\exp\Big[-i\sum_{\beta=s,+,-}\sum_{m=1}^{n_\beta}\phi_\beta^B(r_{\beta m})\Big] \\
&exp\Big[-\chi\int dr\rho_p\rho_s^B - \frac{l_B}{2}\int dr\int dr'\frac{\rho_e^B(r)\rho_e^B(r')}{|r-r'|} - \frac{\rho_0}{2}(\omega_{pp}nN+\omega ssn_s^B) \\
&+i\int dr\Big(\eta(\rho_0-\rho_p-\rho_s^B)+\phi_p\rho_p+\sum_{\beta=s,+,-}\phi_\beta^B\rho_\beta^B\Big)\Big].
\end{aligned}
$$

Define:

$$
\begin{aligned}
G &= \int_{R_0}^{R}\mathcal{D}[r(s)]\exp\left(-\frac{3}{2l^2}\int_0^N ds(\frac{\dot{\mathrm{r}}(s)}{\dot{\mathrm{s}}})^2 - i\int_0^N ds\phi_p(r(s))\right), \\
Q_\beta^B &= \int dr e^{-i\phi_\beta^B(r)}, with \beta = s,+,-.
\end{aligned}
$$

Then the partition function becomes:

$$
e^{-\frac{F^B}{k_BT}} = \int \Pi_{\beta=s,+,-}\delta\rho_\beta^B\delta\phi_\beta^B\delta\rho_p\delta\phi_p\delta\eta^B e^{-f^B(\rho_\beta^B,\phi_\beta^B,\rho_p,\phi_p,\eta^B)}. \tag{5.1}
$$

where

$$
\begin{aligned}
f^B &= -\ln\left(\int dRG\right)^n - \sum_{\beta=s,+,-}\ln\frac{(Q_\beta^B)^{n_\beta}}{n_\beta!} + \chi\int dr\rho_p\rho_s^B + \frac{l_B}{2}\int dr\int dr'\frac{\rho_e^B(r)\rho_e^B(r')}{|r-r'|} \\
&-\frac{\rho_0}{2}(\omega_{pp}nN+\omega ssn_s^B) - i\int dr[\eta(\rho_0-\rho_p-\rho_s^B)+\phi_p\rho_p+\sum_{\beta=s,+,-}\phi_\beta^B\rho_\beta^B].
\end{aligned}
$$

5.3.2 Saddle point approximation

The path integral in the partition sum should be dominated by the minimal of the functional $f(\rho_\beta^B, \phi_\beta^B, \rho_p, \phi_p, \eta^B)$, due to the nature of exponential functions. We can use saddle point approximation for this integral:

$$e^{-\frac{F^B}{k_B T}} = \int \Pi_{\beta=s,+,-} \delta\rho_\beta^B \delta\phi_\beta^B \delta\rho_p \delta\phi_p \delta\eta^B e^{-f(\rho_\beta^B, \phi_\beta^B, \rho_p, \phi_p, \eta^B)} \approx e^{-f^*(\rho_\beta^{B*}, \phi_\beta^{B*}, \rho_p^*, \phi_p^*. \eta^{B*})},$$

Then we have $\frac{F^B}{k_B T} \approx f^{B*}$. To find the saddle point, we take variation of f with respect to each functions to be zero.

$$\begin{aligned} \frac{\delta f^B}{\delta \eta^B} &= \rho_0 - \rho_p - \rho_s^B = 0, \\ => \rho_0 &= \rho_p + \rho_s^B. \end{aligned} \tag{5.2}$$

$$\begin{aligned} \frac{\delta f}{\delta \phi_p} &= (-\frac{n}{\int dR\ G}) \frac{\delta \int dR\ G}{\delta\ \phi_p} - i\rho_p = 0, \\ => \rho_p &= \frac{n}{\int dR\ G} \int dR \int_0^N ds G(R_0, r(s), 0, s) G(r(s), R, s, N). \end{aligned} \tag{5.3}$$

$$\begin{aligned} \frac{\delta f^B}{\delta \phi_\beta^B} &= -i\rho_\beta^B - \frac{n_\beta^B}{Q_\beta^B} \frac{\delta Q_\beta^B}{\delta \phi_\beta^B} = 0, \\ => \rho_\beta^B &= \frac{n_\beta^B}{Q_\beta^B} e^{-i\phi_\beta^B},\ \beta = s, +, -. \end{aligned} \tag{5.4}$$

$$\begin{aligned} \frac{\delta f^B}{\delta \rho_p} &= \eta + \chi\rho_s^B - i\phi_p^B + l_B \int dr' \frac{\alpha z_p \rho_e^B(r')}{|r - r'|} = 0, \\ => i\phi_p &= \chi\rho_s^B + \eta + \alpha z_p \psi^B,\ where\ \psi^B = l_B \int dr' \frac{\rho_e^B(r')}{|r - r'|}. \end{aligned} \tag{5.5}$$

$$\begin{aligned} \frac{\delta f^B}{\delta \rho_s^B} &= \eta^B + \chi\rho_p - i\phi_s^B = 0, \\ => i\phi_s^B &= \chi\rho_p + \eta^B. \end{aligned} \tag{5.6}$$

$$\begin{aligned} \frac{\delta f^B}{\delta \rho_\beta^B} &= -i\phi_\beta^B + l_B \int dr' \frac{z_\beta \rho_e(r')}{|r - r'|} = 0, \\ => i\phi_\beta^B &= z_\beta \psi^B, \ \beta = +, -. \end{aligned} \tag{5.7}$$

5.3.3 Free energy of adsorbed counterions

When the polyelectrolyte chain (NaPSS) is immersed in monovalent salt (NaCl), some sodium atoms will disassociate from the backbone of the chain and become free cations in the solution. Because of thermal fluctuation, the sodium atoms on the backbone could move along the chain. The translational entropy of adsorbed ions is $S_{ad} = k_B \ln Z_{ad}$ with

$$Z_{ad} = \frac{(nN)!}{M!(nN - M)!},$$

where M is the number of adsorbed Na atoms. The corresponding free energy is

$$\begin{aligned} & \frac{F_{ad}}{k_B T} = -\ln Z_{ad} \\ = \ & -(nN)\ln(nN) + nN + M\ln(M) - M + (nN - M)\ln(nN - M) - (nN - M) \\ = \ & [\alpha \ln(\alpha) + (1 - \alpha)\ln(1 - \alpha)]nN. \end{aligned}$$

where $\alpha = \frac{M}{nN}$.

Beside the entropy, there is also electrostatic energy associated with the counterion condensation. It can be represented with a dielectric mismatch parameter δ:

$$\delta = \frac{\epsilon l}{\epsilon_l d_l}, \tag{5.8}$$

where ϵ_l is the local dielectric constant, and d_l is the local adsorption distance between the ion and charged monomer. Therefore, the free energy due to adsorption can be written as:

$$\frac{F_{ad}}{k_BT} = \left[\alpha \ln(\alpha) + (1-\alpha)\ln(1-\alpha) - (1-\alpha)\delta\frac{l_B}{l}\right] nN, \tag{5.9}$$

where δ is the dielectric mismatch parameter for monovalent cation adsorption.

Taking everything into consideration, the free energy in brush phase becomes:

$$\begin{aligned} F^B &= -n\ln\left(\int dRG\right) + \sum_{\beta=s,+,-}\int dr\rho_\beta^B(r)\left[\ln\rho_\beta^B(r)-1\right] + \chi\int dr\rho_p\rho_s^B \\ &+\frac{l_B}{2}\int dr\int dr'\frac{\rho_e^B(r)\rho_e^B(r')}{|r-r'|} + \frac{\rho_0}{2}\left(\omega_{pp}nN + \omega ssn_s^B\right) \\ &-i\int dr\phi_p\rho_p + \left[\alpha\ln\alpha + (1-\alpha)\ln(1-\alpha) - (1-\alpha)\delta\frac{l_B}{l}\right] nN. \end{aligned} \tag{5.10}$$

5.3.4 Green's function: propagator of polymer chains

5.3.4.1 Effective polymer potential

The propagator of one polymer chain is:

$$G(R_0,R,0,N) = \int_{R_0}^{R} D[r(s)]\exp\left[-\frac{3}{2l^2}\int_0^N ds(\frac{dr(s)}{ds})^2 - \int_0^N ds\phi_p(r(s))\right]. \tag{5.11}$$

The effective potential varies only along the direction perpendicular to the surface, i.e. $\phi_p(r(s)) = \phi_p(z(s))$. Our problem is essentially one-dimensional.

$$G(Z_0,Z,0,N) = \int_{Z_0}^{Z} D[z(s)]\exp\left[-\frac{3}{2l^2}\int_0^N ds(\frac{dz(s)}{ds})^2 - \int_0^N ds\phi_p(z(s))\right]. \tag{5.12}$$

Muthukumar pointed out in [**?**] that the quadratic potential should also apply to the polyelectrolyte brush. So we have $\phi_p(z) = V(z) = (h^2 - z^2)/h_0^2$ with $h_0 = \sqrt{\frac{8l^2N^2}{3\pi^2}}$.

5.3.4.2 Deriving Green's function

The one dimensional Green's function in the brush phase($0 < z < h$) in Equation**??** is equivalent to the solution of a Schordinger-equation-like equation in confined in half space:

$$\left(\frac{\partial}{\partial N} - \frac{l^2}{6}\frac{\partial^2}{\partial z^2} + V(z)\right) G(Z_0, Z, 0, N) = \delta(Z - Z_0)\delta(N). \tag{5.13}$$

By reflection principle, the probability $G(Z_0, Z, 0, N)$ of a chain starting fromZ_0 to Z in positive half space equals to the probability $G^f(Z_0, Z, 0, N)$ in full space subtracted by the probability $G^f(-Z_0, Z, 0, N)$ from image point $(-Z_0)$ to Z in full space[**?**], i.e.

$$G(Z_0, Z, 0, N) = G^f(Z_0, Z, 0, N) - G^f(-Z_0, Z, 0, N). \tag{5.14}$$

By analogy with harmonic oscillator, the solution to Equation **??** in full space reads[**?**]:

$$\begin{aligned} G^f(Z_1, Z_2, s, N) = & \left(\frac{\sqrt{3}}{\sqrt{2}\pi l h_0 \sin\zeta}\right)^{\frac{1}{2}} \\ & \exp\left[-\sqrt{\frac{3}{2}}\frac{1}{l h_0 \sin\zeta}\left((Z_1^2 + Z_2^2)\cos\zeta - 2Z_1 Z_2\right)\frac{(N-s)h^2}{h_0^2}\right], \end{aligned} \tag{5.15}$$

with $\zeta = \sqrt{\frac{2}{3}}\frac{(N-s)l}{h_0}$. Ignore the first monomer attached to the wall. The Green's function for a chain starting at $Z_0 = l$ to reach Z in $N-1$ steps, with $\zeta = \sqrt{\frac{2}{3}}\frac{Nl}{h_0} = \frac{\pi}{2}$, is

$$G^f(l, Z, 0, N) = \left(\frac{\sqrt{3}}{\sqrt{2}\pi l h_0}\right)^{\frac{1}{2}} \exp\left(\frac{\sqrt{6}}{h_0}Z - \frac{Nh^2}{h_0^2}\right). \tag{5.16}$$

Since $N \ll 1$, $N - 1 \approx N$. Therefore the Green's function in half space is:

$$\begin{aligned} G(l, Z, 0, N) &= G^f(l, Z, 0, N) - G^f(-l, Z, 0, N) \\ &= 2\left(\frac{\sqrt{3}}{\sqrt{2}\pi l h_0}\right)^{\frac{1}{2}} \exp\left(-\frac{Nh^2}{h_0^2}\right)\sinh\left(\frac{\sqrt{6}Z}{h_0}\right). \end{aligned} \tag{5.17}$$

The normalization factor in the denominator of monomer density function (Equation **??**)is:

$$\begin{aligned}\int_0^h dZG(l,Z,0,N) &= 2\left(\frac{\sqrt{3}}{\sqrt{2}\pi l h_0}\right)^{\frac{1}{2}}\exp\left(-\frac{Nh^2}{h_0^2}\right)\int_0^h dZ\sinh\left(\frac{\sqrt{6}Z}{h_0}\right)\\ &= \left(\frac{\sqrt{2}h_0}{\sqrt{3}\pi l}\right)^{\frac{1}{2}}\exp\left(-\frac{Nh^2}{h_0^2}\right)\left[\cosh\left(\frac{\sqrt{6}h}{h_0}\right)-1\right]. \quad (5.18)\end{aligned}$$

5.3.4.3 Deriving monomer density

From saddle point approximation and Equation**??**, we have the expression for monomer density as

$$\rho_p(r) = \frac{n}{\int dR\ G(R_0,R,0,s)}\int dR\int_0^N dsG(R_0,r,0,N)G(r,R,s,N).$$

Due to one-dimensionality,

$$\rho_p(z) = \frac{n}{\int dZ\ G(Z_0,Z,0,N)}\int dZ\int_0^N dsG(Z_0,z,0,N)G(z,Z,s,N). \quad (5.19)$$

We have derived the denominator $\int dZG$. Now we only need to deal with the numerator:

$$\begin{aligned}\int dZG(z(s),Z,s,N) &= \int dZG^f(z(s),Z,s,N) - G^f(-z(s),Z,s,N)\\ &= 2\left(\frac{\sqrt{3}}{\sqrt{2}\pi l h_0\cos\theta}\right)^{\frac{1}{2}}\exp\left[-\frac{\sqrt{3}z^2}{\sqrt{2}lh_0}\tan\theta - \frac{(N-s)h^2}{h_0^2}\right]\\ &\quad \int_0^h dZ\exp\left[-\frac{\sqrt{3}Z^2}{\sqrt{2}lh_0}\tan\theta\right]\sinh\left(\frac{\sqrt{6}zZ}{lh_0\cos\theta}\right).\end{aligned}$$

with $\theta = \sqrt{\frac{2}{3}}\frac{sl}{h_0}$. To solve this integral we use:

$$\int_0^h dZ e^{-aZ^2}\sinh(bZ) =$$
$$\frac{1}{4}\sqrt{\frac{\pi}{a}}e^{\frac{b^2}{4a}}\left(2\,\mathrm{erf}\left[\frac{b}{2\sqrt{a}}\right]+\mathrm{erf}\left[\sqrt{a}\left(h-\frac{b}{2\sqrt{a}}\right)\right]-\mathrm{erf}\left[\sqrt{a}\left(h+\frac{b}{2\sqrt{a}}\right)\right]\right).$$

Then we get the brush profile:

$$\begin{aligned}\rho_p(z) &= \frac{nC}{\int dRG}\left(\frac{\sqrt{3}}{\sqrt{2}\pi l h_0}\right)^{\frac{1}{2}} e^{-\frac{Nh^2}{h_0^2}}\int_0^N ds\frac{\sinh(\sqrt{6}z/h_0\sin\theta)}{\sin\theta}\exp\left(-\frac{\sqrt{3}l}{\sqrt{2}h_0\tan\theta}\right)\\ &\quad\Big(2\,\mathrm{erf}\left[\left(\frac{\sqrt{6}z^2}{lh_0\sin(2\theta)}\right)^{\frac{1}{2}}\right]+\mathrm{erf}\left[\left(\frac{\sqrt{3}\tan\theta}{\sqrt{2}lh_0}\right)^{\frac{1}{2}}\left(h-\frac{z}{\sin\theta}\right)\right]\\ &\quad-\mathrm{erf}\left[\left(\frac{\sqrt{3}\tan\theta}{\sqrt{2}lh_0}\right)^{\frac{1}{2}}\left(h-\frac{z}{\sin\theta}\right)\right]\Big).\end{aligned}$$

It is shown in Figure**??** that, the more stretched a brush, the monomer profile is more uniform (Figure**??**). For highly stretched limit, step-function is a good approximation for monomer density.

5.4 Solution phase

5.4.1 Partition function

In solution phase, $h < z < L$, there are only small molecules, including salt ions and solvent molecules. The partition function in solution phase is similar to that in brush phase without polymers:

$$\begin{aligned}e^{-\frac{F^S}{k_BT}} &= \frac{\int\Pi_{\beta=s,+,-}\Pi_{m=1}^{n_\beta}dr_{\beta m}}{\Pi_{\beta=s,+,-}n_\beta!}\exp\Big[-\frac{1}{2}\sum_{m=1}^{n_s}\sum_{m'=1}^{n_s}V_{ss}(r_m-r_{m'})\\ &\quad-\frac{1}{2}\sum_{\beta=+,-}\sum_{\beta'=+,-}\sum_{m=1}^{n_\beta}\sum_{m'=1}^{n_{\beta'}}V_{\beta\beta'}(r_{\beta m}-r_{\beta' m'})\Big]\Pi_r\delta(\hat{\rho}_s^S(r)-\rho_0)\\ &= \frac{\int\Pi_{\beta=s,+,-}\Pi_{m=1}^{n_\beta}dr_{\beta m}}{\Pi_{\beta=s,+,-}n_\beta!}\exp\Big[-\frac{l_B}{2}\int drdr'\frac{\hat{\rho}_e^S(r)\hat{\rho}_e^S(r')}{|r-r'|}\\ &\quad-\frac{\omega_{ss}}{2}\int drdr'\hat{\rho}_s^S(r)\hat{\rho}_s^S(r')\Big]\Pi_r\delta(\hat{\rho}_s^S(r)-\rho_0).\end{aligned}$$

With similar field transformations we have:

$$\begin{aligned} e^{-\frac{F^S}{k_BT}} &= \frac{\int \Pi_{\beta=s,+,-}\Pi_{m=1}^{n_\beta} dr_{\beta m}}{\Pi_{\beta=s,+,-} n_\beta!} \int \Pi_{\beta=s,+,-}\delta\rho_\beta^S \delta\phi_\beta^S \delta\eta^S \exp\Big[-\frac{l_B}{2}\int dr dr' \frac{\hat{\rho}_e^S(r)\hat{\rho}_e^S(r')}{|r-r'|} \\ &\quad -\frac{\omega_{ss}}{2}\int dr(\hat{\rho}_s^S(r))^2 - i\int dr\Big(\eta^S(\hat{\rho}_s^S-\rho_0) + \sum_{\beta=s,+,-}\phi_\beta^S(\hat{\rho}_\beta^S-\rho_\beta^S)\Big)\Big] \\ &= \int \Pi_{\beta=s,+,-}\delta\rho_\beta^S\delta\phi_\beta^S\delta\eta^S \frac{\int \Pi_{\beta=s,+,-}\Pi_{m=1}^{n_\beta} dr_{\beta m} e^{-i\phi_\beta^S(r_{\beta m})}}{\Pi_{\beta=s,+,-} n_\beta!} \exp\Big[-\frac{l_B}{2}\int dr dr' \frac{\hat{\rho}_e^S(r)\hat{\rho}_e^S(r')}{|r-r'|} \\ &\quad -\frac{\omega_{ss}}{2}\int dr(\hat{\rho}_s^S(r))^2 + i\int dr\Big(\eta^S(\rho_0-\rho_s^S) + \sum_{\beta=s,+,-}\phi_\beta^S\rho_\beta^S\Big)\Big]. \end{aligned}$$

Simply,

$$e^{-\frac{F^S}{k_BT}} = \int \Pi_{\beta=s,+,-}\delta\rho_\beta^S\delta\phi_\beta^S\delta\eta^S e^{-f^S}.$$

Define:

$$Q_\beta^S = \int dr e^{-i\phi_\beta^S(r_{\beta m})},$$

where $\beta = s,+,-$. Then

$$\begin{aligned} f^S = \quad & -\sum_{\beta=s,+,-}\ln\frac{(Q_\beta^S)^{n_\beta^S}}{n_\beta^S!} + \frac{l_B}{2}\int dr dr' \frac{\hat{\rho}_e^S(r)\hat{\rho}_e^S(r')}{|r-r'|} - i\int dr\Big[\eta^S(\rho_0-\rho_s^S) \\ & + \sum_{\beta=s,+,-}\phi_\beta^S\rho_\beta^S)\Big] + \frac{\omega_{ss}}{2}\rho_0^2 S(L-h). \end{aligned} \tag{5.20}$$

5.4.2 Saddle point approximation

$$\begin{aligned} \frac{\delta f^S}{\delta\rho_s^S} &= i\eta^S + -i\phi_s^S = 0, \\ => \phi_s^S &= \eta^S. \end{aligned} \tag{5.21}$$

$$\begin{aligned} \frac{\delta f^S}{\delta\rho_\beta^S} &= -i\phi_\beta^S + l_B\int dr' \frac{z_\beta\rho_e^S(r')}{|r-r'|} = 0, \\ => i\phi_\beta^S &= z_\beta\psi^S,\ where\ \beta = +,-\ and\ \psi = l_B\int dr' \frac{\rho_e^S(r')}{|r-r'|}. \end{aligned} \tag{5.22}$$

$$\begin{aligned}\frac{\delta f^S}{\delta\phi^S_\beta} &= -i\rho^S_\beta - \frac{n^S_\beta}{Q^S_\beta}\frac{\delta Q^S_\beta}{\delta\phi^S_\beta}e^{-\phi^S_\beta} = 0,\\ => \rho^S_\beta &= \frac{n^S_\beta}{Q^S_\beta}e^{-i\phi^S_\beta},\ \beta = s,+,-. \end{aligned} \tag{5.23}$$

With saddle point approximation $\frac{F^S}{k_BT} \approx f^{S*}$, the free energy in solution phase is:

$$\frac{F^S}{k_BT} = \sum_{\beta=s,+,-}\int dr\rho^S_\beta(r)[\ln\rho^S_\beta(r) - 1] + \frac{l_B}{2}\int dr\int dr'\frac{\rho^S_e(r)\rho^S_e(r')}{|r-r'|} + \frac{\omega_{ss}}{2}\rho_0^2 S(L-h).$$

5.4.3 Total free energy

The total free energy is the sum of free energy of brush phase and solution phase $F = F^B + F^S$:

$$\begin{aligned}\frac{F}{k_BT} &= -n\ln(\int_0^h dZG) + \sum_{\beta=s,+,-} S\int_0^h dz\rho^B_\beta(z)[\ln\rho^B_\beta(z) - 1] + S\chi\int_0^h dz\rho_p\rho^B_s\\ &+\frac{S}{2}\int dz\rho^B_e(z)\psi^B(z) - S\int_0^h dz\phi_p\rho_p + [\alpha\ln\alpha + (1-\alpha)\ln(1-\alpha)]nN\\ &-(1-\alpha)nN\frac{\delta l_B}{l} + \sum_{\beta=s,+,-} S\int_h^L dz\rho^S_\beta(z)[\ln\rho^S_\beta(z) - 1] + \frac{S}{2}\int_h^L dz\rho^S_e(z)\psi^S_e(z)\\ &+\frac{\omega_{ss}}{2}\rho_0^2 SL + \frac{\rho_0}{2}(\omega_{pp} - \omega_{ss})nN.\end{aligned}$$

5.4.4 Electrostatic potential

To get the electric potential in solution phase we employ the Gouy-Chapman theory, along with matching conditions at brush interface.

The saddle point approximation, which has been discussed for brush phase and solution phase separately, is implying Poisson-Boltzmann equations of two phases:

$$\begin{aligned}\frac{d^2}{dz^2}\psi^B(z) &= -4\pi l_B\rho^B_e(z) = -4\pi l_B\left[\frac{n^B_+}{Q^B_+}e^{-\psi^B(z)} - \frac{n^B_-}{Q^B_-}e^{\psi^B(z)} - \alpha\rho_p(z)\right],\\ \frac{d^2}{dz^2}\psi^S(z) &= -4\pi l_B\rho^S_e(z) = -4\pi l_B\left[n_ie^{-\psi^S(z)} - n_ie^{\psi^S(z)}\right].\end{aligned}$$

The matching conditions at brush-solution interface $z = h$ are:

1)ψ is continuous, $\psi^B(h) = \psi^S(h) = \psi_0$;

2)ψ' is also continuous, $\psi'^B(h) = \psi'^S(h) = \psi'_0$;

3)ρ_+ and ρ_- are continuous: $\rho_+^B(h) = \rho_+^S(h)$ and $\rho_-^B(h) = \rho_-^S(h)$, so that $n_+^B = n_i Q_+^B$ and $n_-^B = n_i Q_-^B$.

From Gouy-Chapman theory, the electric potential in solution phase is:

$$\psi^S(z) = 2\ln\left(\frac{1+\gamma_0 e^{-\kappa(z-h)}}{1-\gamma_0 e^{-\kappa(z-h)}}\right), \tag{5.24}$$

where $\gamma_0 = \tanh(\frac{\psi_0}{4})$, $\kappa = \sqrt{8\pi n_i l_B}$.

From saddle point approximation in brush phase, we have

$$\psi^B = -\frac{1}{\alpha}\left[\phi_p(z) + 2\chi\rho_p(z) - \chi\rho_0 - \phi_s(z)\right],$$

$$\phi_s^B(z) = \ln n_s^B - \ln Q_s^B - \ln\left[\rho_0 - \rho_p(z)\right].$$

Eventually, we have

$$\psi^B(z) = -\frac{1}{\alpha}\left(\phi_p(z) + 2\chi\rho_p(z) + \ln\left[\rho_0 - \rho_p(z)\right] + \ln Q_s^B - \ln n_s^B - \chi\rho_0\right),$$

with $\ln Q_s^B$ to be determined.

Using matching condition 2), we have:

$$\begin{aligned}\psi'_0 &= \psi'^B(h) = -\frac{1}{\alpha}\left[\phi'_p(h) + 2\chi\rho'_p(h) - \frac{\rho'_p(h)}{\rho_0 - \rho_p(h)}\right] \\ &= \psi'^S(h) = -\frac{4\kappa\gamma_0}{1-\gamma_0^2},\end{aligned}$$

and

$$\gamma_0 = \frac{2\kappa}{\psi'_0} + -\sqrt{\left(\frac{2\kappa}{\psi'_0}\right)^2 + 1}.$$

Since $-1 < \gamma_0 < 1$, the real solution of γ_0 is:

$$\begin{cases} \gamma_0 = \frac{2\kappa}{\psi_0'} + \sqrt{(\frac{2\kappa}{\psi_0'})^2 + 1}, \ when \ \psi_0' < 0; \\ \gamma_0 = \frac{2\kappa}{\psi_0'} - \sqrt{(\frac{2\kappa}{\psi_0'})^2 + 1}, \ when \ \psi_0' > 0, \end{cases} \tag{5.25}$$

Then the constant Q_s^B is determined by:

$$-\ln Q_s^B = 2\alpha \ln\left(\frac{1+\gamma_0}{1-\gamma_0}\right) + 2\chi\rho_p(h) + \ln(\rho_0 - \rho_p(h)) - \ln n_s^B - \chi\rho_0.$$

The final solution of $\psi^B(z)$ is:

$$\psi^B(z) = -\frac{1}{\alpha}\left(\phi_p(z) + 2\chi[\rho_p(z) - \rho_p(h)] + \ln\left[\frac{\rho_0 - \rho_p(z)}{\rho_0 - \rho_p(h)}\right] - 2\alpha \ln\left[\frac{1+\gamma_0}{1-\gamma_0}\right]\right).$$

5.4.5 Electroneutrality

The electroneutrality of the whole system requires

$$n_+^B - n_-^B - \alpha n N = Q^B = -Q^S, \tag{5.26}$$

where Q^B and Q^S are total charge in brush phase and solution phase respectively. Therefore, we have an equation for the only two unknown variables left, i.e. brush height h and degree of ionization α:

$$n_i(Q_+^B - Q_-^B) - \alpha n N = -\frac{S\psi^B(h)}{4\pi l_B}. \tag{5.27}$$

We can solve this equation numerically for any given h, i.e. $\alpha = \alpha(h)$. Then the total free energy is reduced to have one variable h, i.e. $F(h)$. Finally, we only need to do one dimensional minimization of this free energy.

5.5 Results

5.5.1 Brush height

The complicated competition between the entropy and energy of each components of the system gives rise to a self-consistent brush height after minimization of free energy with respect of h. The results are shown in Figure**??**. At low salt concentration, the brush height is independent of salt concentration, which is consent with Pincus brush. AT high salt concentration, the brush height decrease exponential with salt concentration. For poor solvent, the decrease is even sharper. Compare to Pincus brush in high salt, the scaling power law $(-1/3)$ is not followed in SCFT results. This is could be a mutual effect of changable degree of ionization and brush height. After self-consistently determining h and α (Figure **??**), one see a decreasing degree of ionization, instead of a fixed α in scaling argument. This would in turn lessens the charges on backbones and shrinks the chains more than Pincus brush does.

5.5.2 Degree of ionization

Following previous section, the first step of numerical calculation is to solve α from electroneutrality (Equation **??**). In this way, we can calculate α for any given h in any conditions. The Figure**??** shows that the degree of ionization of brush has similar trend as brush height, which is decreasing with salt concentration. That is independent of salt concentration and decrease with the chain collapsing. Therefore, it is confirmed that degree of ionization is a variable in polyelectrolyte brush system,

5.5.3 Solvent quality effect

From Figure **??**, although in low salt region, excluded volume interaction does not have effect on brushes, the rate of decrease in brush height is very different for different solvent qualities in high salt region. When χ parameter is small (~ 0.1), i.e. in a good solvent where the mixture energy is weak ($\chi \leq 0.5$), brush collapses in high salt in a way much more slower. This is similar to scaling theory, where the excluded

volume interaction is neglected. However, as the quality of solvent gets poorer, the mixture energy is no longer weak. This is because the contraction of the brush leads to the counterion condensation in general, and makes the chain less charged, thus weakens the electric potential. The influence of solvent quality is crucial in height salt region but negligible in height salt region. In some experiments, it is also observed that the shrinking rate at high salt region also depends on the properties of grafting substrate[**?**].

5.5.4 Dielectric constant mismatching effect

Figure**??** shows that the stronger the local electric interaction is (i.e. δ parameter is larger), the more collapsed the brush is. This is because counterions are bounded tighter to the polymer backbones. Hence the degree of ionization is accordingly smaller (as shown in Figure**??**). This parameter is an input of the theory, which is introduced by Muthukumar[**?**]. It can be a fitting parameter when compared with experiment results.

5.5.5 Electric field

Electric field is shown in Figure**??**, for different salt concentrations. The reference potential is zero at infinity, where the salt bath concentration is held constant. The electric potential is continuous across the brush-solution interphase. And the electric force (derivative of electric potential) is also continuous. As salt concentration increases, the chains are less charged. Hence the variation of electric field in shrunk brush is less than that in a swollen brush. Figure **??** shows the distribution of counterions in accordance with electric field. The counterion density is higher when there is a higher salt in bath, but as the brush is more or less neutral, the variation of counterion density is less compared to swollen brush region.

5.5.6 Ion distributions

Figure **??**, **??**, and **??** show the free ion densities at different salt concentrations. Most ion density variations happen within the brush, and the solution phase is essentially constant. This is consistent with the assumption of scaling argument that most counterions are trapped inside brush. For $n_i = 0.1$, the counterion density ρ_+ is high above zero, and the negative charge from brush is more than neutralized by counterions (ρ_+), which means there are excessive counterions in the brush phase. However, for low salt concentration $n_i = 0.01$ and $n_i = 0.0001$, only the part of the brush has excessive counterions, while part of the stretched brush does not have enough counterions to neutralize its negative charge.

5.6 Conclusions

We work through the SCFT for PE brush in monovalent salt. The results show that the brush height is sensitive to salt concentration, solvent quality, local dielectric mismatch. For compressed brush, the monomer profile is prone to hyperbolic shape, but resembles step function if in stretched state. The counterions are mostly trapped in the brush phase, which enormously excess the bulk salt concentration. This confirmed with the osmotic brush assumption.

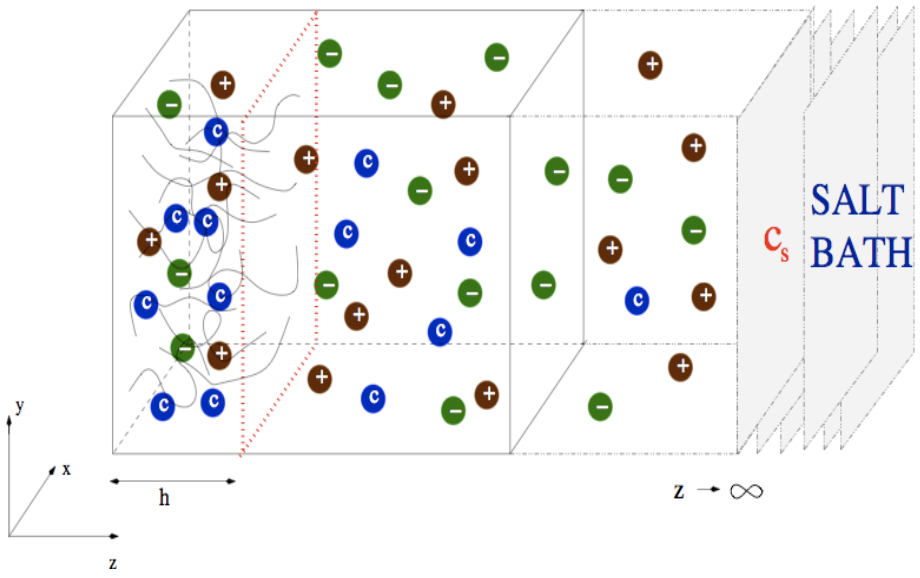

Figure 5.1. Demonstration of polyelectrolyte brush in monovalent salt.

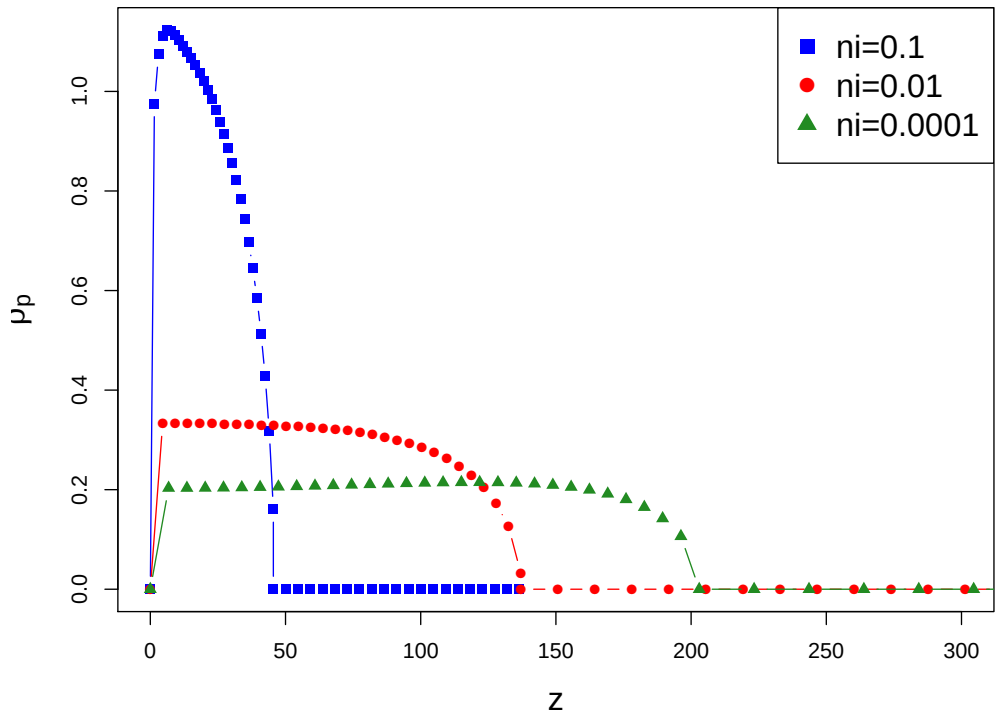

Figure 5.2. Density profile of brush with different brush heights (h) in different salt connectrations.

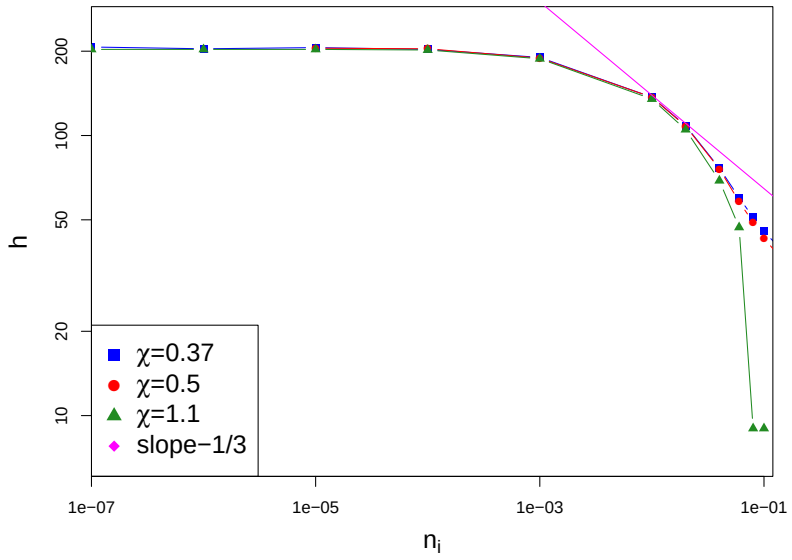

(a)

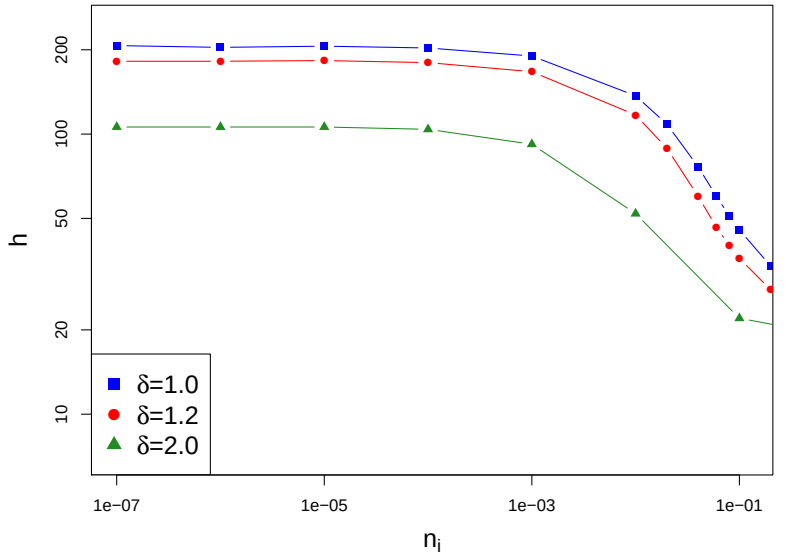

(b)

Figure 5.3. The results of brush height h as function of salt concentration n_i.

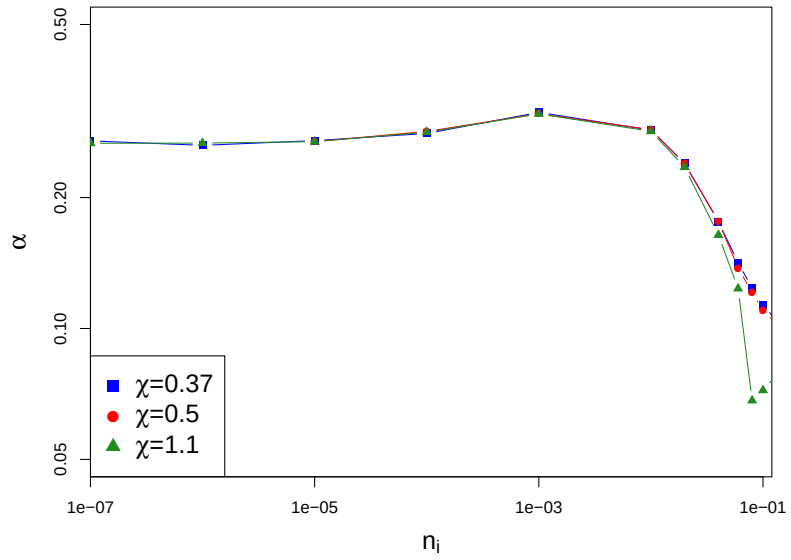

(a)

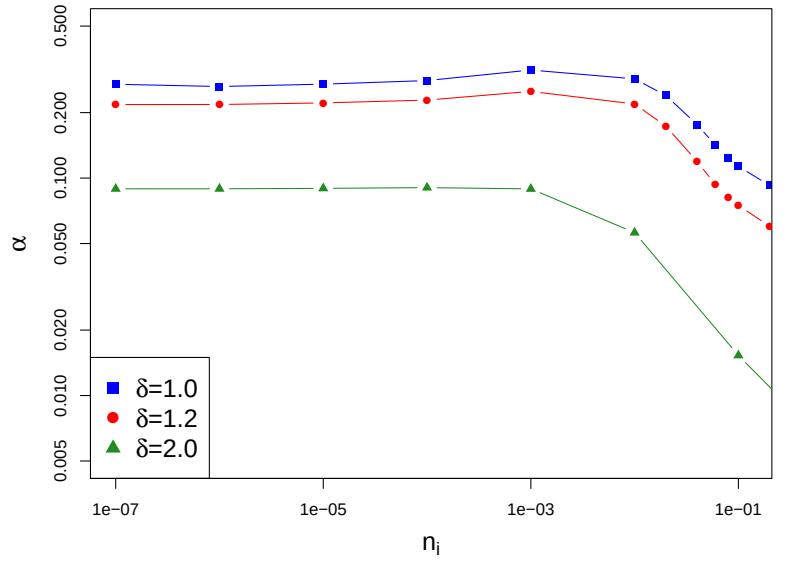

(b)

Figure 5.4. The results of degree of ionization α as function of salt concentration n_i.

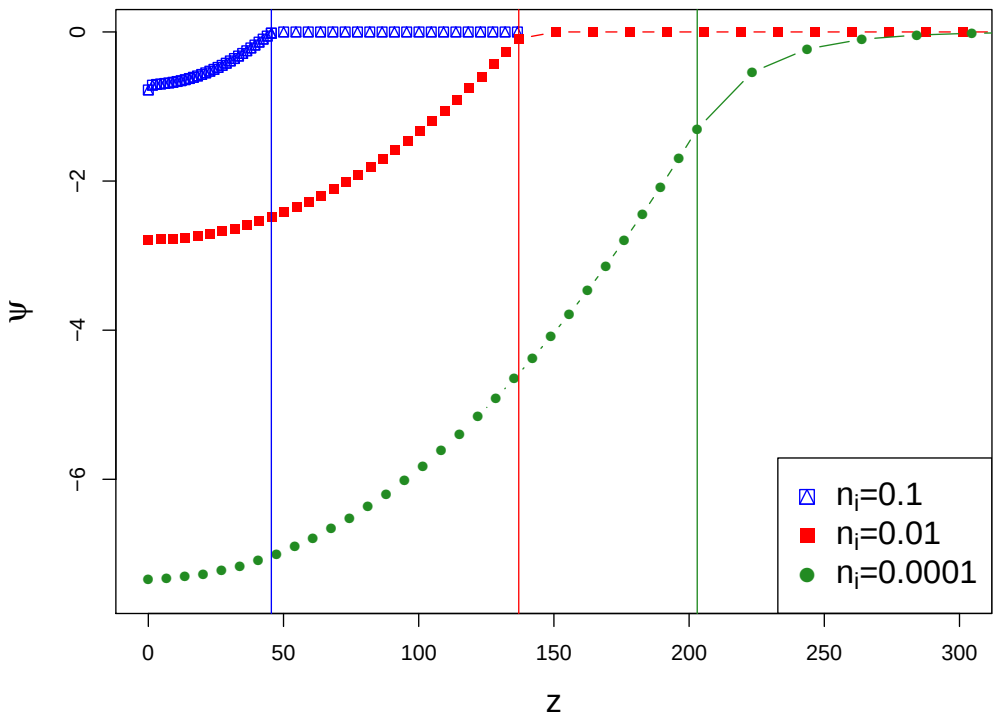

Figure 5.5. Electric field for different salt concentrations. The vertical lines indicate the corresponding brush height.

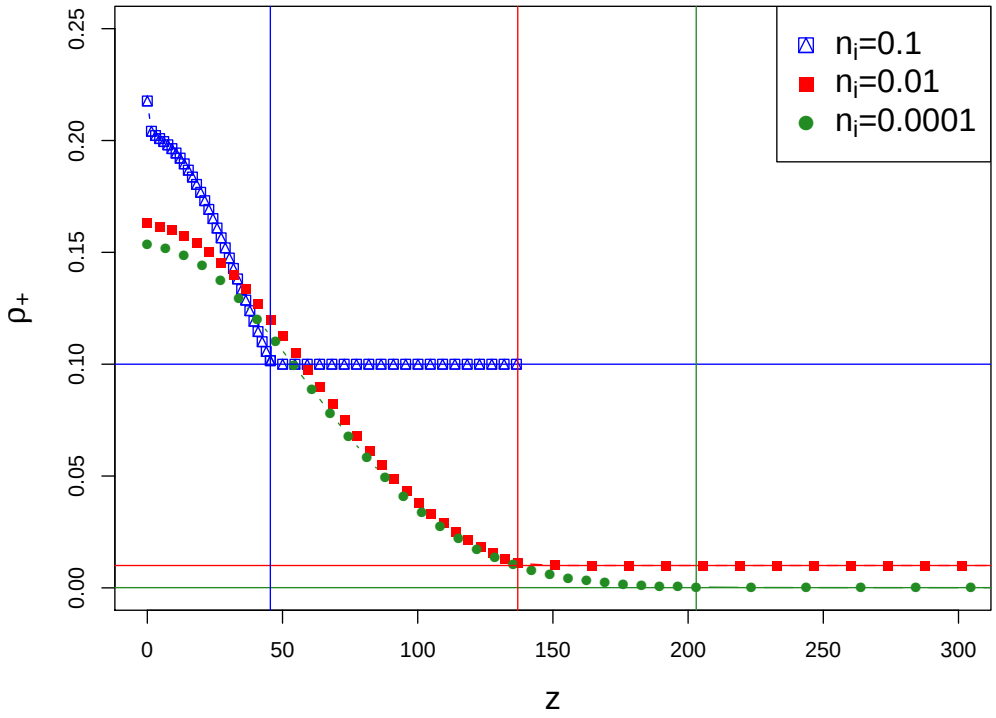

Figure 5.6. Counterion distributions for different salt concentrations. The horizontal lines indicate the corresponding salt concentration. The vertical lines indicate the corresponding brush height.

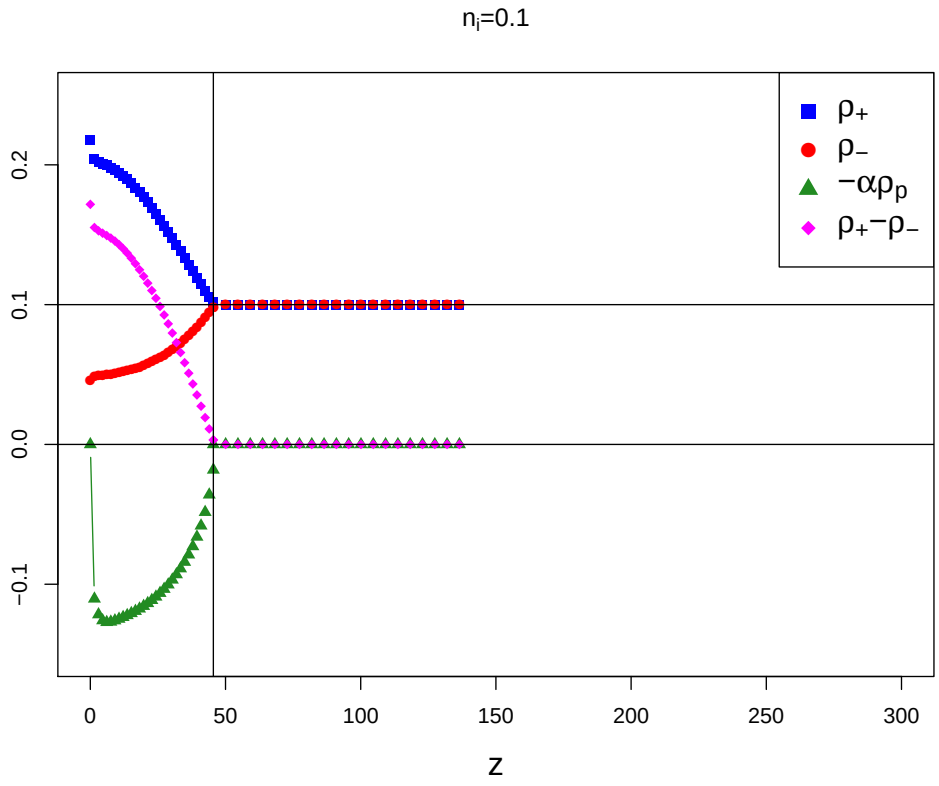

Figure 5.7. Ion distribution when $n_i = 0.1$. The vertical line indicates brush height. The horizontal lines indicate zero concentration and salt concentration respectively.

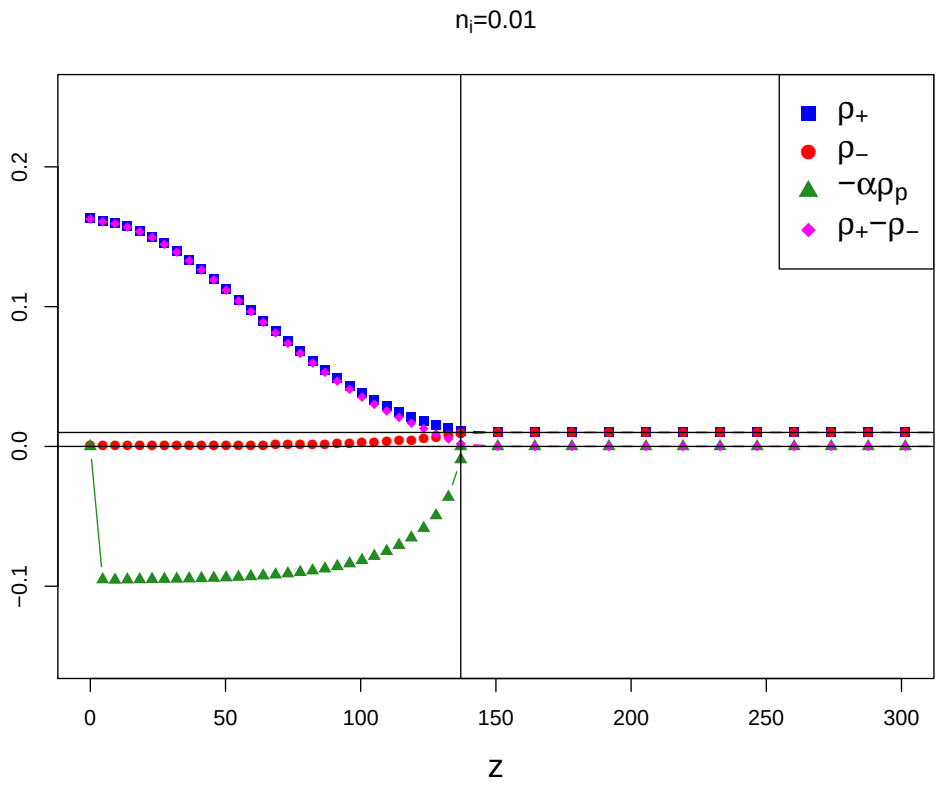

Figure 5.8. Ion distribution when $n_i = 0.01$. The vertical line indicates brush height. The horizontal lines indicate zero concentration and salt concentration respectively.

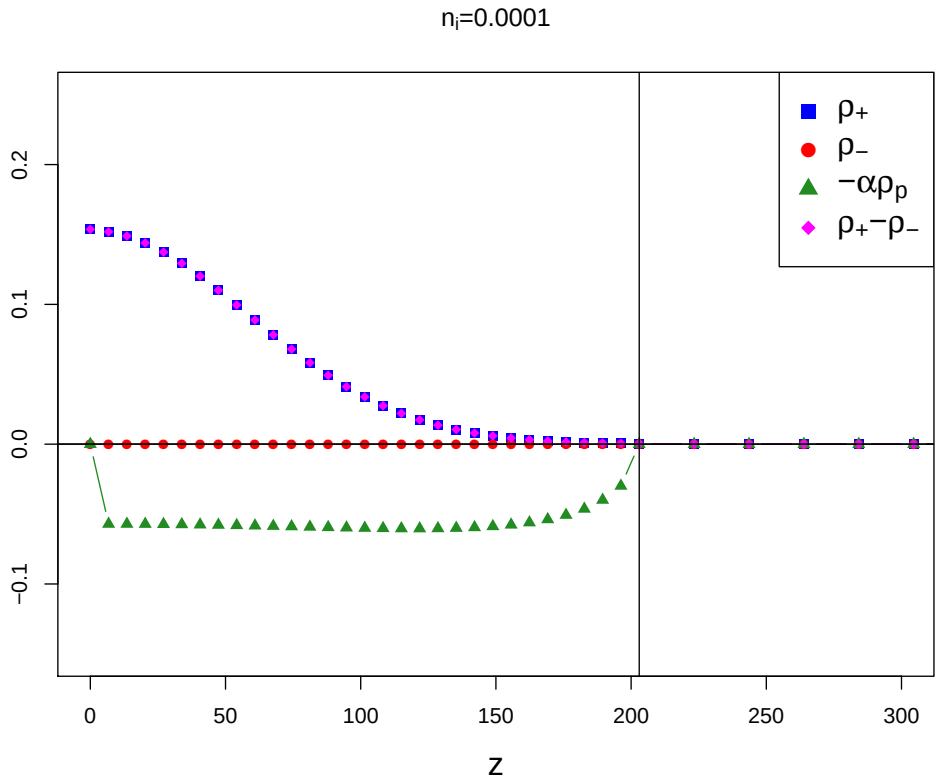

Figure 5.9. Ion distribution when $n_i = 0.0001$. The vertical line indicates brush height. The horizontal lines indicate zero concentration and salt concentration respectively.

CHAPTER 6

VARIATIONAL THEORY OF POLYELECTROLYTE IN DIVALENT SALT

6.1 Introduction

There has been a plenty of work on quantifying the properties and functions of PE brushes. It is crucial to understand and to predict the relation between macroscopic and microscopic structures and environmental conditions. Recently It has been interesting to more and more researchers that the properties of counterions have strong effect on the brush structure. And the valence of ions is an important one. In this chapter, we aim to understand the effect of divalent salt on a PE brush.

The SCFT method that we discussed in previous chapter, confirmed several assumptions in scaling argument. Firstly, in highly stretched brush, monomer density resembles uniform, step-like function. Secondly, counterions are trapped in brush phase, which makes the ion density in side the brush are much higher than solution phase. Therefore, we are going to assume uniform monomer density and high salt approximation directly without deriving. We implement this results as assumption to build a simpler and more transparent theory to describe PE brush. Beside the assumption of uniformly stretched chains and high salt limit, we also use Donnan conditions explicitly, which governs the physics of phase equilibrium. We constructed the free energy for both monovalent and divalent cases. After free energy minimization, we derive and discuss properties of PE brush in divalent salt solutions. Moreover, we reproduced the non-monotonic behavior of brush height as a function of salt concentration, which is observed in experiment[**?**].

6.2 Application to monovalent case

Without mentioning, many notations in this chapter are inherited from previous chapter (as in Table**??**). The salt concentration is denoted by c_s, which is same as n_i in previous chapter. We will show how to derive the free energy of the system by analyzing the microscopic conformations and interactions of the polymers and small molecules. The problem will also be turned into a problem of two dimensional minimization of free energy with respect to the brush height h and the degree of ionization α, taking advantage of Donnan equilibrium.

6.2.1 Free energy composition

We divide the total free energy of the system into two parts: brush phase and solution phase. For a certain salt concentration c_s, the free energy will be written given the brush height h and the degree of ionization α. We will determine α and h at the end, by free energy minimization.

6.2.1.1 Free energy of adsorbed counterions

The translational entropy and adsorption energy are taken care of similarly as in Chapter **??**, because in both methods the salt is assuming to be monovalent as $NaCl$ (Equation**??**):

$$\frac{F_{ad}}{k_BT} = \left[\alpha \ln(\alpha) + (1-\alpha)\ln(1-\alpha) - (1-\alpha)\delta\frac{l_B}{l}\right] nN.$$

6.2.1.2 Fluctuations of free ions

In the brush phase and solution phase respectively, the free energy due to the fluctuation of free ions in the solution, which arise from the Coulomb interaction among the free ions, can be written as[**?**]:

$$\frac{F^B_{fl,i}}{k_BT} = -\frac{Sh}{4\pi l^3}[\ln(1+\kappa^B l) - k^B l + \frac{1}{2}(\kappa^B l)^2],$$

$$\frac{F^S_{fl,i}}{k_BT} = -\frac{S(L-h)}{4\pi l^3}[\ln(1+\kappa^S l) - k^S l + \frac{1}{2}(\kappa^S l)^2],$$

where $\kappa^B = \sqrt{4\pi l_B(\rho^B_+ + \rho^B_-)}$ and $\kappa^S = \sqrt{4\pi l_B(\rho^S_+ + \rho^S_-)}$.

6.2.1.3 Translational entropy of small molecules

In brush phase, suppose we have a lattice of size l and assume free ions and solvent molecules all have same dimension l as monomers. The total number of configurations putting free ions and solvent molecules in the lattice is:

$$Z^B_{tr} = \frac{(Sh)^{\rho_0 Sh - nN}}{n^B_+! n^B_-! n^B_s!}.$$

The free energy due to the translation entropy is:

$$\begin{aligned}
&\frac{F^B_{tr}}{k_BT} = -\ln Z^B_{tr} \\
= \;& -(\rho_0 Sh - nN)\ln(Sh) + n^B_+\ln(n^B_+) - n^B_+ + n^B_-\ln(n^B_-) - n^B_- + n^B_s\ln(n^B_s) - n^B_s \\
= \;& Sh[\rho^B_+(\ln(\rho^B_+) - 1) + \rho^B_-(\ln(\rho^B_-) - 1) + (\rho_0 - \rho^B_+ - \rho^B_- - \rho_p)(\ln(\rho_0 - \rho^B_+ - \rho^B_- - \rho_p) - 1)].
\end{aligned}$$

In solution phase, similarly we have partition of salt ions and solvent:

$$Z^S_{tr} = \frac{(S(L-h))^{\rho_0 S(L-h)}}{n^S_+! n^S_-! n^S_s!}.$$

The corresponding free energy reads:

$$\begin{aligned}
&\frac{F^S_{tr}}{k_BT} = -\ln Z^S_{tr} \\
=& -\rho_0 S(L-h)\ln(S(L-h)) + n^S_+\ln(n^S_+) - n^S_+ + n^S_-\ln(n^S_-) - n^S_- + n^S_s\ln(n^S_s) - n^S_s \\
=& S(L-h)[\rho^S_+(\ln(\rho^S_+) - 1) + \rho^S_-(\ln(\rho^S_-) - 1) + (\rho_0 - \rho^S_+ - \rho^S_-)(\ln(\rho_0 - \rho^S_+ - \rho^S_-) - 1)].
\end{aligned}$$

6.2.1.4 Free energy for polymer backbones

1) Chain connectivity (assuming Gaussian statistics):

$$\frac{F_{cn}}{k_BT} = \frac{n}{2}\Big(\frac{h^2}{Nl^2} - \ln\Big(\frac{h^2}{Nl^2}\Big)\Big)$$

2) Excluded volume effect (with χ being the chi parameter):

$$\frac{F_{\chi}}{k_BT} = \chi l^3 \rho_p(\rho_0 - \rho_p)Sh$$

3) Electrostatic repulsion (high salt approximation[**?**]):

$$\frac{F_{el}}{k_BT} = \frac{2\pi l_B}{Sh}\Big(\frac{\alpha n N}{\kappa^B}\Big)^2$$

6.2.1.5 Constraints

1) Electroneutrality: In variational theory set-up, both brush phase and solution phase are assumed to be neutral.

$$\rho_+^B = \alpha\rho_p + \rho_-^B. \tag{6.1}$$

Moreover, we assume the salt concentration is fixed in solution phase. Thus we have

$$\rho_+^S = \rho_-^S = c_s. \tag{6.2}$$

2) Incompressibility: We assume free ions and solvent molecules are of same size l as monomers.

$$\rho_s^B + \rho_p + \rho_+^B + \rho_-^B = \rho_0,$$

$$\rho_s^S + \rho_+^S + \rho_-^S = \rho_0.$$

where ρ_0 is the maximum local occupation density.

6.2.1.6 Donnan equilibrium

In a general system of two phases: I and II, and two ion species: $+$ and $-$. The chemical potentials of each species are equal to the sum of a constant term depending on temperature, a log term of activity and electric potential due to that specie:

$$\begin{cases} \mu_i^I = \mu_i^0(T) + k_B T \ln a_i^I + z_i e\psi^I; \\ \mu_i^{II} = \mu_i^0(T) + k_B T \ln a_i^{II} + z_i e\psi^{II}, \end{cases}$$

where a_i^I and a_i^{II} are activities of ion species $i = +, -$, and z_i are valences of ion specie i. Donnan's conditions are such that: at equilibrium, the chemical potentials of two phases must be equal:

$$\mu_i^I = \mu_i^{II} \quad (i = +, -). \tag{6.3}$$

This implies

$$\begin{cases} \dfrac{a_+^I}{a_+^{II}} = \exp\left(\dfrac{e\psi}{k_B T}\right); \\ \dfrac{a_-^I}{a_-^{II}} = \exp\left(\dfrac{-e\psi}{k_B T}\right), \end{cases}$$

where $\psi = \psi^I - \psi^{II}$, and thus $a_+^I a_-^I = a_+^{II}, a_-^{II}$. Since activity of an ion specie is proportional to the density of that ion specie, we have

$$\rho_+^B \rho_-^B = \rho_+^S \rho_-^S. \tag{6.4}$$

With Donnan equilibrium (Equation **??**) and electroneutrality (Equation **??** and **??**), we can solve ρ_+^B and ρ_-^B:

$$\rho_+^B = \frac{1}{2}[\alpha\rho_p + \sqrt{(\alpha\rho_p)^2 + 4c_s^2}],$$

$$\rho_-^B = \frac{1}{2}[-\alpha\rho_p + \sqrt{(\alpha\rho_p)^2 + 4c_s^2}].$$

Substitute this results for ρ_+^B and ρ_-^B in the total free energy, which is a function of brush height h and degree of ionization $alpha$ now. Sum up all terms in free energy and in two phases, we can get equilibrium result by performing two-dimensional minimization of free energy:

$$\begin{aligned} \frac{1}{k_BT}F(h,\alpha) &= \frac{F^B}{k_BT} + \frac{F^S}{k_BT} \\ = \quad & \frac{F_{ad}^B}{k_BT} + \frac{F_{tr}^B}{k_BT} + \frac{F_{fl,i}^B}{k_BT} + \frac{F_\chi}{k_BT} + \frac{F_{el}}{k_BT} + \frac{F_{tr}^S}{k_BT} + \frac{F_{fl,i}^S}{k_BT}. \end{aligned}$$

simultaneous with respect to h and α.

6.2.2 Results

We present here plots for brush height h with $S = 10^4 nm^2, n = 10^4, N = 10^3, l = 0.3nm, \chi = 0.5, \delta = 1, l_B = 0.7nm, L = 2Nl$ in Figure**??**. We confirm here the there are two regions of monovalent salt concentration. In the low salt concentration, the polyelectrolyte brush is in a swollen state, where the brush height is independent of salt concentration. As the salt concentration meets some crossover concentration, the brush starts to shrink as salt concentration increases. The power law of the shrinkage is highly dependent on the solvent quality as in Figure**??**, which is consistent with the results from SCFT method. The degree of ionization is changing with added salt in a way similar to brush height. Figure**??** and Figure**??** are results for different δ parameter, which is a fitting parameter from the theory similar to SCFT method.

6.3 Variational theory for divalent case

With the technique used to study PE brush in monovalent salt, the divalent salt effects are investigated. The primary difference in the system comes from the possibility that, with high density of divalent salt ions. The adsorption of divalent ions to the oppositely charge chain backbones would make the brush charge reverse. Similar

to monovalent brush system, we still have n polyelectrolyte (e.g. $NaPSS$) bristles. But now the same polymer brush is exposed to a divalent salt solution (e.g. $CaCl_2$) with salt concentration c_s. Beside all the variables defined in monovalent case, we also have:ρ_{2+}^B and ρ_{2+}^S: the number density of divalent cations (e.g. Ca^{2+}) in the divalent case.

6.3.1 Free energy composition

6.3.1.1 Free energy of adsorbed counterions

With divalent counterions present in the system, we assume that there are three kinds of counterion adsorptions as shown in Figure**??**: I) one monovalent cation (Na^+) sticking to one negatively charged monomer, with N_1 being the number of adsorbed monovalent cations. II) one divalent cation (Ca^{2+}) sticking to one negatively charged monomer, with N_2 being the number of divalent cations appearing in two body association. III) one divalent cation (Ca^{2+}) and one monovalent anion (Cl^-) together sticking to one monomer, with N_3 being the number of divalent cation taking place in three-body association.

Then the translational entropy of adsorbed ions is $S_{ad} = k_B \ln Z_{ad}$ with

$$Z_{ad} = \frac{(nN)!}{N_1!N_2!N_3!(nN - N_1 - N_2 - N_3)!}.$$

The corresponding free energy is

$$\begin{aligned}
&\frac{F_{ad}}{k_BT} = -\ln Z_{ad} \\
=&-(nN)\ln(nN) + nN + N_1\ln(N_1) - N_1 + N_2\ln(N_2) - N_2 + N_3\ln(N_3) - N_3 \\
&+ (nN - N_1 - N_2 - N_3)\ln(nN - N_1 - N_2 - N_3) - (nN - N_1 - N_2 - N_3) \\
=&[\beta_1\ln(\beta_1) + \beta_2\ln(\beta_2) + \beta_3\ln(\beta_3) + (1 - \beta_1 - \beta_2 - \beta_3)\ln(1 - \beta_1 - \beta_2 - \beta_3)]nN,
\end{aligned}$$

where $\beta_1 = \frac{N_1}{nN}$, $\beta_2 = \frac{N_2}{nN}$, $\beta_3 = \frac{N_3}{nN}$. Average degree of ionization is $\alpha = 1 - \beta_1 - \beta_2 - 2\beta_3$.

Beside the entropy, there is also electrostatic energy associated with the counterion condensation. It can be represented through dielectric mismatch parameters. The free energy due to adsorption can be written as:

$$\begin{aligned}\frac{F_{ad}}{k_BT} &= nN\Big[\beta_1\ln(\beta_1) + \beta_2\ln(\beta_2) + \beta_3\ln(\beta_3) \\ &\quad +(1-\beta_1-\beta_2-\beta_3)\ln(1-\beta_1-\beta_2-\beta_3) \\ &\quad -(\beta_1\delta + 2\beta_2\delta + \beta_3\delta_2)\frac{l_B}{l}\Big]. \end{aligned} \tag{6.5}$$

where δ is the dielectric mismatch parameter for monovalent cation adsorption, 2δ for divalent cation pair adsorption and $\delta_2 = (2 + \frac{4}{\delta+1})\delta$ for three-body adsorption[**?**].

6.3.1.2 Fluctuations of free ions

In the brush phase and solution phase respectively[**?**],

$$\frac{F^B_{fl,i}}{k_BT} = -\frac{Sh}{4\pi l^3}\left[\ln(1+\kappa^B l) - k^B l + \frac{1}{2}(\kappa^B l)^2\right],$$

$$\frac{F^S_{fl,i}}{k_BT} = -\frac{S(L-h)}{4\pi l^3}\left[\ln(1+\kappa^S l) - k^S l + \frac{1}{2}(\kappa^S l)^2\right],$$

where $\kappa^B = \sqrt{4\pi l_B(\rho^B_+ + \rho^B_- + 4\rho^B_{2+})}$ and $\kappa^S = \sqrt{4\pi l_B(\rho^S_+ + \rho^S_- + 4\rho^S_{2+})}$.

6.3.1.3 Translational entropy of small molecules

In brush phase, the partition of small molecules is

$$Z^B_{ad} = \frac{(Sh)^{\rho_0 Sh - nN}}{n^B_+! n^B_-! n^B_{2+}! n^B_s!}.$$

Thus, free energy due to translational entropy in brush phase is:

$$\begin{aligned}
\frac{F_{tr}^B}{k_BT} &= -\ln Z_{tr}^B \\
&= -(\rho_0 Sh - nN)\ln(Sh) + n_+^B \ln(n_+^B) - n_+^B + n_-^B \ln(n_-^B) - n_-^B + \\
&\quad n_{2+}^B \ln(n_{2+}^B) - n_{2+}^B + n_s^B \ln(n_s^B) - n_s^B \\
&= Sh[\rho_+^B(\ln(\rho_+^B) - 1) + \rho_-^B(\ln(\rho_-^B) - 1) + \rho_{2+}^B(\ln(\rho_{2+}^B) - 1) \\
&\quad +(\rho_0 - \rho_+^B - \rho_-^B - \rho_{2+}^B - \rho_p)(\ln(\rho_0 - \rho_+^B - \rho_-^B - \rho_{2+}^B - \rho_p) - 1)].
\end{aligned}$$

In solution phase, similarly we have partition sum as

$$Z_{ad}^S = \frac{(S(L-h))^{\rho_0 S(L-h)}}{n_+^S! n_-^S! n_{2+}^S! n_s^S!},$$

and free energy as

$$\begin{aligned}
&\frac{F_{tr}^S}{k_BT} = -\ln Z_{tr}^S \\
= \;& -\rho_0 S(L-h)\ln(S(L-h)) + n_+^S \ln(n_+^S) - n_+^S + n_-^S \ln(n_-^S) - n_-^S \\
&+n_{2+}^S \ln(n_{2+}^S) - n_{2+}^S + n_s^S \ln(n_s^S) - n_s^S \\
= \;& S(L-h)[\rho_+^S(\ln(\rho_+^S) - 1) + \rho_-^S(\ln(\rho_-^S) - 1) + \rho_{2+}^S(\ln(\rho_{2+}^S) - 1) \\
&+(\rho_0 - \rho_+^S - \rho_-^S - \rho_{2+}^S)(\ln(\rho_0 - \rho_+^S - \rho_-^S - \rho_{2+}^S) - 1)].
\end{aligned}$$

6.3.1.4 Free energy for polymer backbones

Free energy for polymer backbones is unchanged compared to monovalent case.

1) Chain connectivity (assuming Gaussian statistics):

$$\frac{F_{cn}}{k_BT} = \frac{n}{2}\Big(\frac{h^2}{Nl^2} - \ln\Big(\frac{h^2}{Nl^2}\Big)\Big).$$

2) Excluded volume effect (with χ being the chi parameter):

$$\frac{F_\chi}{k_BT} = \chi l^3 \rho_p(\rho_0 - \rho_p)Sh.$$

3) Electrostatic repulsion:

$$\frac{F_{el}}{k_B T} = \frac{2\pi l_B}{Sh}\left(\frac{\alpha n N}{\kappa^B}\right)^2.$$

6.3.1.5 Constraints

1) Incompressibility:

$$\begin{cases} \rho_s^B + \rho_p + \rho_+^B + \rho_{2+}^B + \rho_-^B = \rho_0, \\ \rho_s^S + \rho_+^S + \rho_{2+}^S + \rho_-^S = \rho_0. \end{cases} \tag{6.6}$$

2) Mass conservation: With added divalent salt ($CaCl_2$) fixed in the whole system, all free monovalent cations (Na^+) are released from the polymer

$$\rho_+^B h + \rho_+^S (L - h) = (1 - \beta_1)\rho_p h,$$

and all Ca atoms come from the added divalent salt

$$\rho_{2+}^B h + 2\rho_{2+}^S (L - h) + (\beta_2 + \beta_3)\rho_p h = c_s L.$$

3) Electroneutrality:

$$\begin{cases} \rho_+^B + 2\rho_{2+}^B = \alpha\rho_p + \rho_-^B, \\ \rho_+^S + 2\rho_{2+}^S = \rho_-^S. \end{cases} \tag{6.7}$$

6.3.1.6 Donnan equilibrium

In a system of two phases: I and II, and three ion species: $2+$, $+$ and $-$, which contains divalent salt ions. The chemical potentials of each species are same as Equation**??**:

$$\begin{cases} \mu_i^I = \mu_i^0(T) + k_B T \ln a_i^I + z_i e\psi^I; \\ \mu_i^{II} = \mu_i^0(T) + k_B T \ln a_i^{II} + z_i e\psi^{II}, \end{cases}$$

where $i = 2+, +, -$. At equilibrium, the chemical potentials of two phases are required to be equal:

$$\mu_i^I = \mu_i^{II} \quad (i = 2+, +, -). \tag{6.8}$$

Thus we have

$$\begin{cases} \dfrac{a_+^I}{a_+^{II}} = \exp\left(\dfrac{e\psi}{k_B T}\right); \\ \dfrac{a_-^I}{a_-^{II}} = \exp\left(\dfrac{-e\psi}{k_B T}\right); \\ \dfrac{a_{2+}^I}{a_{2+}^{II}} = \exp\left(\dfrac{2e\psi}{k_B T}\right), \end{cases}$$

where $\psi = \psi^I - \psi^{II}$. Therefore

$$\begin{cases} a_+^I a_-^I = a_+^{II}, a_-^{II}; \\ a_{2+}^I (a_-^I)^2 = a_{2+}^{II}, (a_-^{II})^2. \end{cases}$$

Since activity of an ion specie is proportional to the density of that ion specie, eventually, Donnan's conditions for divalent salt are:

$$\begin{cases} \rho_+^B \rho_-^B = \rho_+^S \rho_-^S, \\ \rho_{2+}^B (\rho_-^B)^2 = \rho_{2+}^S (\rho_-^S)^2. \end{cases} \tag{6.9}$$

6.3.2 Results

The parameters used are as follows: $l = 0.3nm$, $N = 1000$, $n = 10^4$, $S = 2.5 \times 10^5 nm^2$, $L = 2Nl$, $\delta = 2.5$, $\chi = 0.5$, $l_B = 0.7$. After minimizing free energy with respect to $(\beta_1, \beta_2, \beta_3, h)$ under the constraints and conditions listed as above, we derive the values of them at particular divalent salt concentration in equilibrium.

6.3.2.1 Non-monotonic brush height

As shown in Figure**??**, there appears a stage of re-swelling of the brush with added divalent salt, which is absent with only monovalent salt. Similar to the monovalent case, at low salt limit the brush is expected to swell, as there are not much ions in the solution. While at high salt, the brush shrinks due the same electric screening in monovalent system. However, in some intermediate region, the brush also contracts to a minimal height.

In experiments, non-monotonic brush height with divalent salt has been reported[**?**] in Figure**??**. As salt concentration decreases, the brush first swells and then collapses. However, the lower salt region has not been investigated. We conjecture that if the measurement is carried in non-salt or extremely low salt region, where nearly no divalent ions present, one should see the brush swells again. In the experiment the salt concentration was measured only in the bulk. The corresponding average salt concentration (in the whole system) should be higher than that in the bulk, because charged brush attracts much more salt ions. To compare with our theory, the low salt region in Figure**??** is actually an intermediate salt concentration.

6.3.2.2 Charge reversal

The non-monotonic behavior of brush height in the intermediate salt region can be explained by examining the adsorbing fraction of each specie of small ions. Figure**??** shows that at low salt, the adsorbed ions are mostly monovalent (Na^+), as there is not many divalent ions (Ca^{2+}) available in the solution. As the divalent salt increases, more and more Ca^{2+} caught by the chain, because the type II and III adsorption have lower energy ($-2\delta l_B/l$ and $-\delta_2 l_B/l$) than type I adsorption energy ($-\delta l_B/l$). Meanwhile, the total degree of ionization α is decreasing as the chains shrink. Once it hits the zero line, the brush becomes essentially neutral and collapses to the minimal height (although there are still local charge due to type II adsorption

and bare backbones). Since the neutral chain is not as attractive to type III adsorption as type I, it is easier to convert type II adsorption to type III or simply make type III adsorption. Therefore, β_2 decreases and β_3 increases after α reaches zero. After this stage, the overall degree of ionization α keeps decreasing and becomes negative, while the brush becomes positive. This process is called charge reversal, which is the main reason for brush re-swelling.

Figure**??** shows the log-transform of each adsorption fraction. The monovalent ion (Na^+) adsorption is continuously decreasing and replaced by the divalent ions (Ca^{2+}). In the increase of divalent ion adsorption, there are in fact two stages. The first stage is when type II adsorption is growing fast until the overall charge of brush is zero (i.e. degree of ionization α is zero). The second stage is when the type III adsorption takes over from type II (i.e. more anions Cl^- enter the brush and form three-body adsorption), and continues to increase and makes the brush close to neutral again in high salt limit.

6.3.2.3 Solvent quality effect

We also observe the solvent effect by changing χ parameter in Figure**??**. It is predicted from our result that in poor solvent, one will not see brush re-swell, because the phase transition happens at lower salt concentration before divalent ions play a role. In poor solvent, when phase separation takes place, β_1 suddenly increases (Figure**??**). To contract, brush chains suddenly collect a large amount of monovalent counterions which are available at relatively lower salt concentrations. Figure**??** and Figure**??** shows transition of α, i.e. the overall degree of ionization, for different solvent qualities. In poor solvent ($\chi = 1.0$ and 1.5), where α takes sharp transition coincides with where brush collapses. This is indicating excluded volume interaction is collaborating with electric interaction through charge regularization.

Through all χ parameters we examine, at low and intermediate salt concentration, degree of charges α is dominating the brush height h. In this region of salt concentration, electric interaction is dominating. However, in very hight salt concentration, brushes are surrounded by neutralizing ions and nearly uncharged. In this region, the excluded volume interaction is playing a very important role. Because the interaction strength among monomers are not negligible compared to electric interaction.

6.3.2.4 Dielectric constant mismatch

Dielectric constant mismatch parameter is a theoretical input that represents the local ion adsorption strength. Larger δ means tighter bindings of all types of adsorption (I, II, and III). Figure**??** shows that non-monotonicity is absent for smaller δ. This means δ parameter is also playing a role in determining whether there would be non-monotonicity in physical region of salt concentration. (It would not make any sense to go to higher concentration than $c_s = 1.0$, which is not feasible in reality. Because excessive salt will cause solubility problem of polymer.) When δ is small, the bindings of counterions are not strong enough to attract enough C_a^{2+} to neutralize and reverse the charge of the brush. Thus the brush shrinkage and re-swelling require much higher salt concentration, which is out of a physical range. In Figure**??** and Figure**??**, the degree of ionization is much larger for smaller δ. Thus in the physical region of salt concentration, non-monotonicity is not observed for smaller δ.

6.4 Conclusions and Discussion

We build up the free energy with explicit Donnan equilibrium, and we have similar results as the SCFT in monovalent case. For divalent, we observe charge reversal and non-monotonic behavior in the brush height. This explains the experimental observation of PE brush with divalent salt. Moreover, we conclude from the χ effect that, other than electric interaction, the excluded volume interaction is also important. Es-

pecially when solvent quality is poor, the excluded volume interaction overrides the electric interaction. This effect was usually omitted when polyelectrolyte brush being discussed in previous theoretical work. On the other hand, the dielectric mismatching (δ) is also tuning the fraction of counterion adsorption, which is in turns tuning the shrinking and swelling behavior of brush. Therefore, the non-monotonicity is only observed in certain range of solvent quality and dielectric mismatching.

In this work, bridging between two monomers mediated by a divalent ion is ignored, in light of previous work of similar system. However, the experiments [**?**] of PE brushes in trivalent salt suggest that some intra-chain bridges should form. And this bridging effect is strong for trivalent case. We have already seen effects from counterion species, and this work is focusing specifically on divalent counterions. Therefore, a natural follow-up of this work is to extent the theory to incorporate trivalent counterions and bridging effect.

Both SCFT method and variational method are realization of mean field approximation. Future improvement of the theory can be in the direction of including fluctuations with higher order approximation.

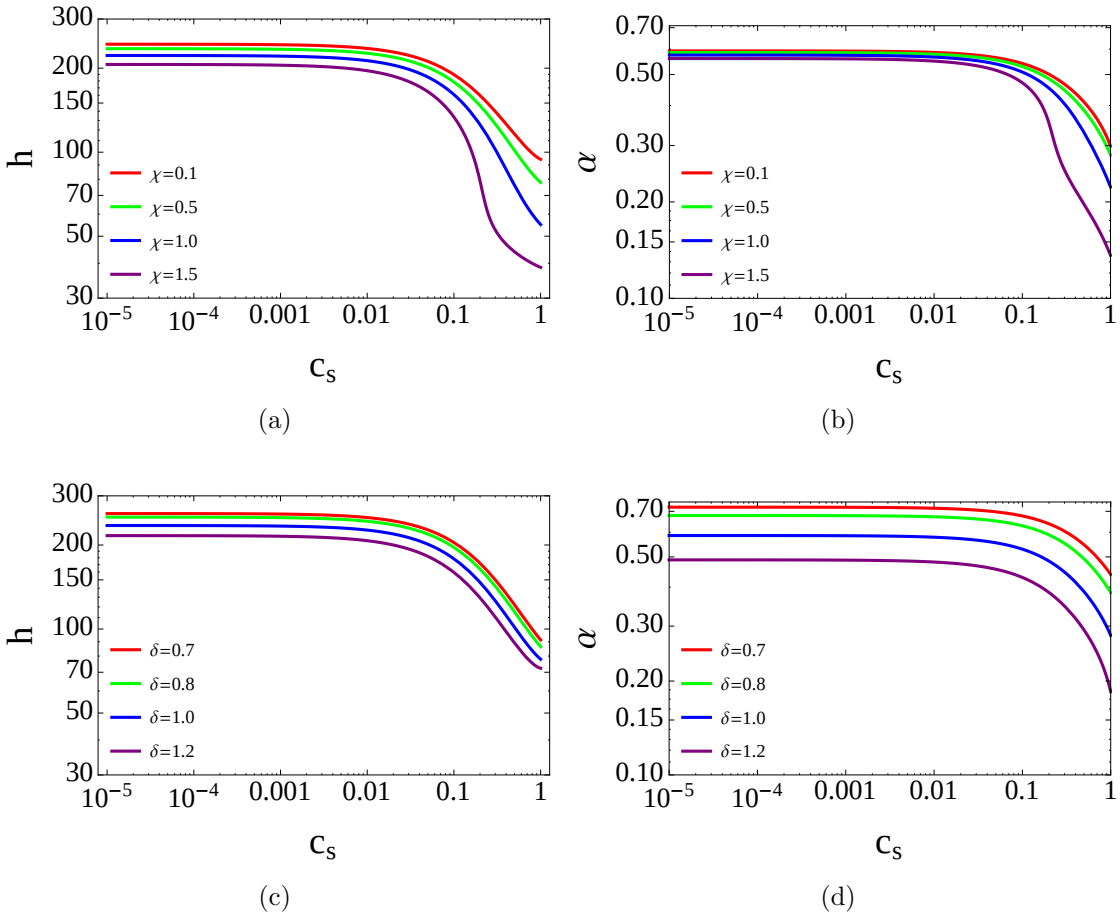

Figure 6.1. Numerical results for the brush height h and degree of ionizationα.

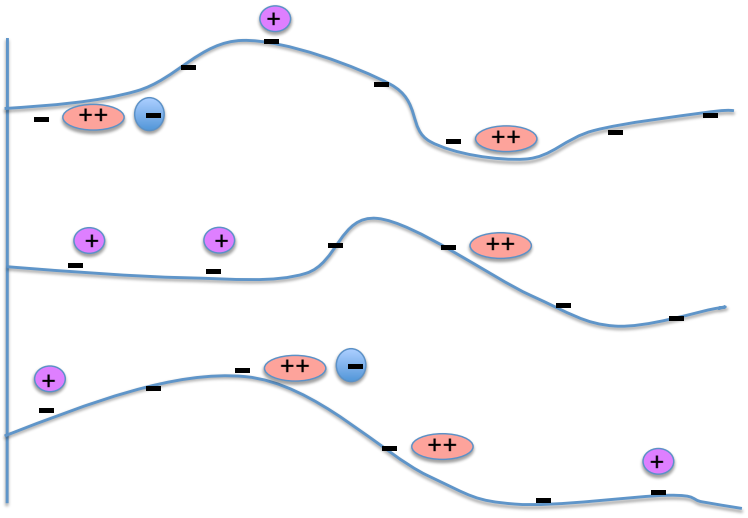

Figure 6.2. Demonstration of counterions' associations without bridging.

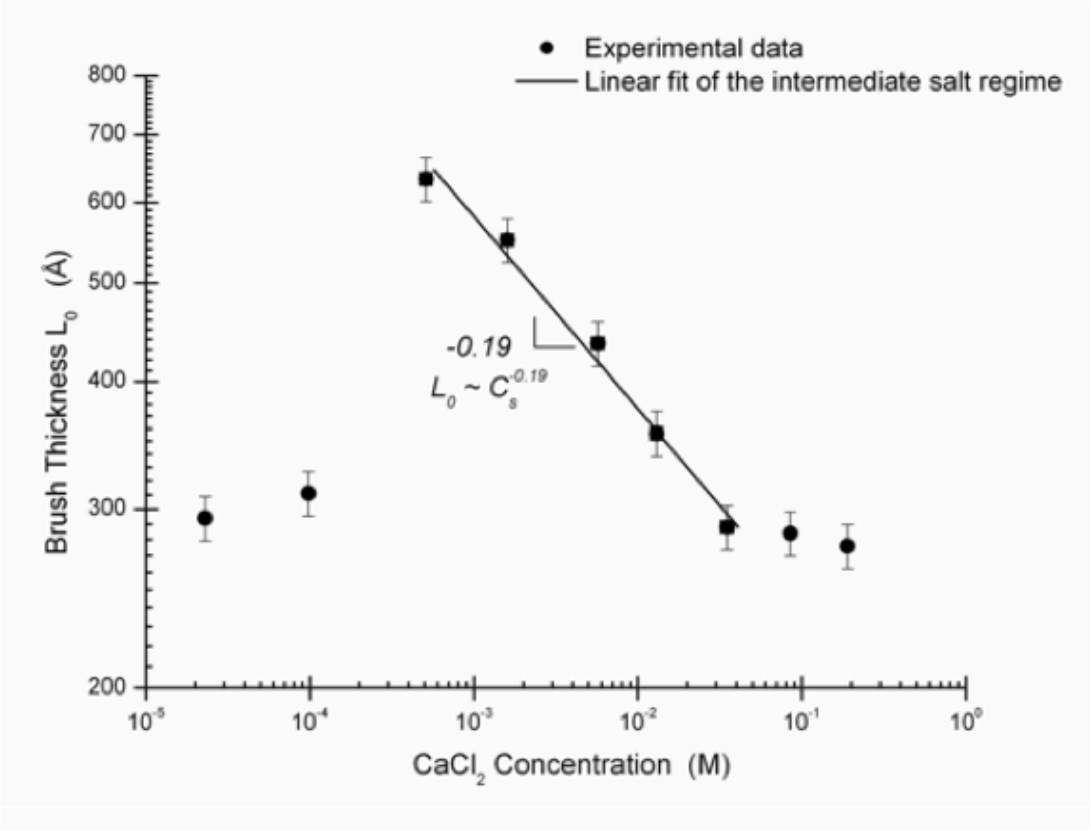

Figure 6.3. The dependence of the brush height on the concentration of $CaCl_2$[**?**].

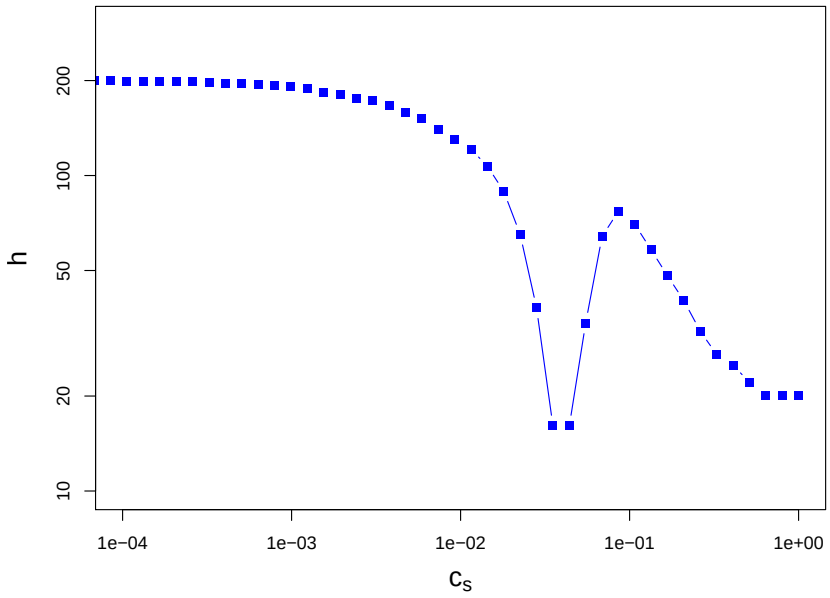

(a)

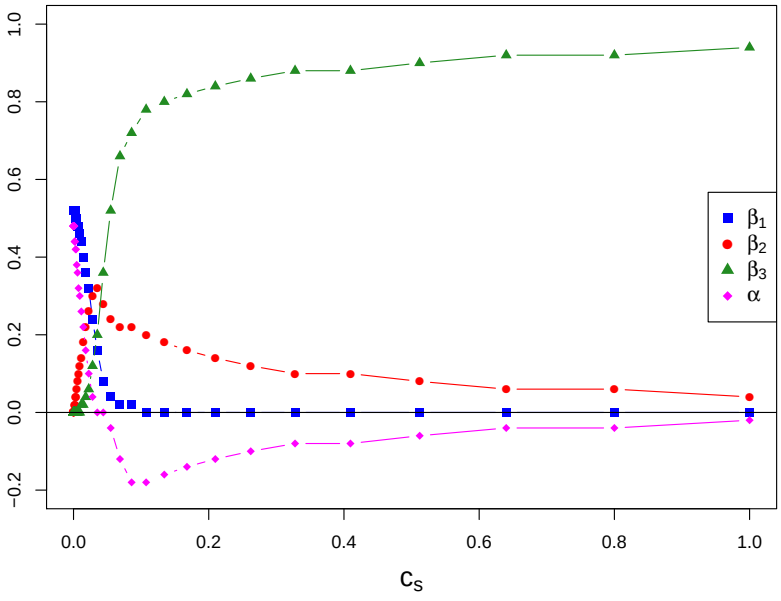

(b)

Figure 6.4. Results of divalent case: (**??**) The brush height as function of salt concentration. (**??**) The degree of ionization as function of salt concentration.

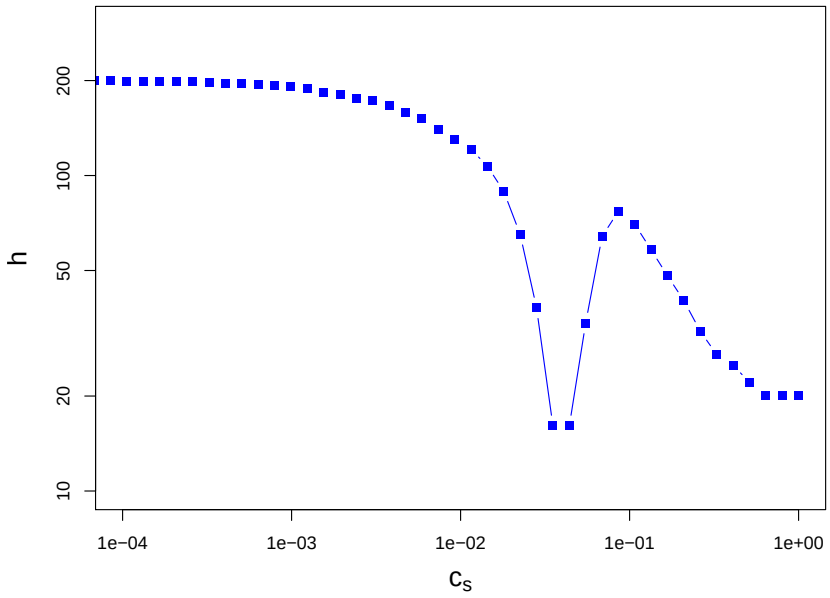

(a)

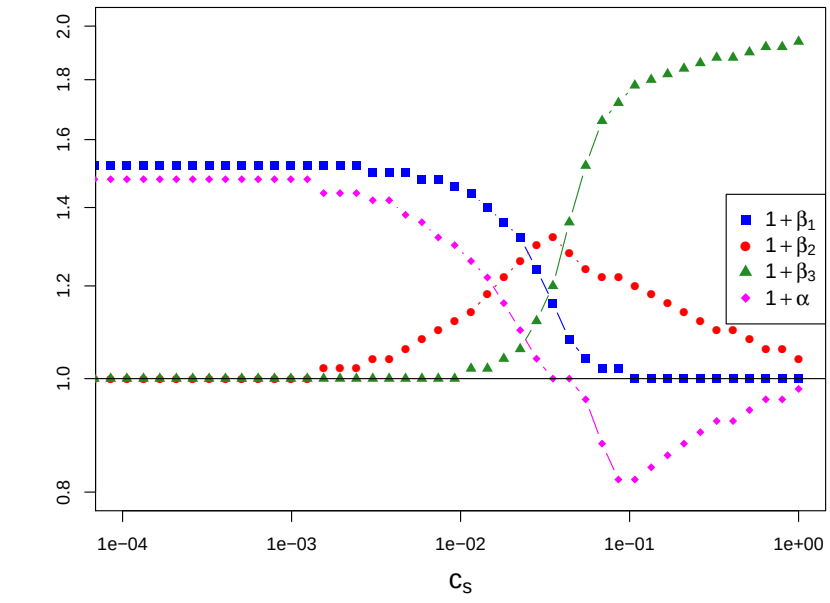

(b)

Figure 6.5. Results of divalent case: (**??**) The brush height as function of salt concentration. (**??**) Log-transform of degree of association for different ions.

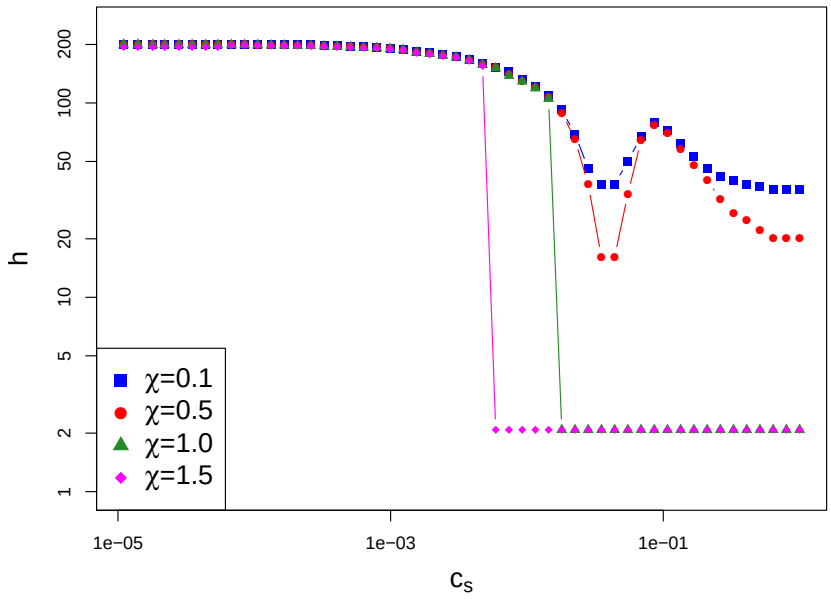

(a)

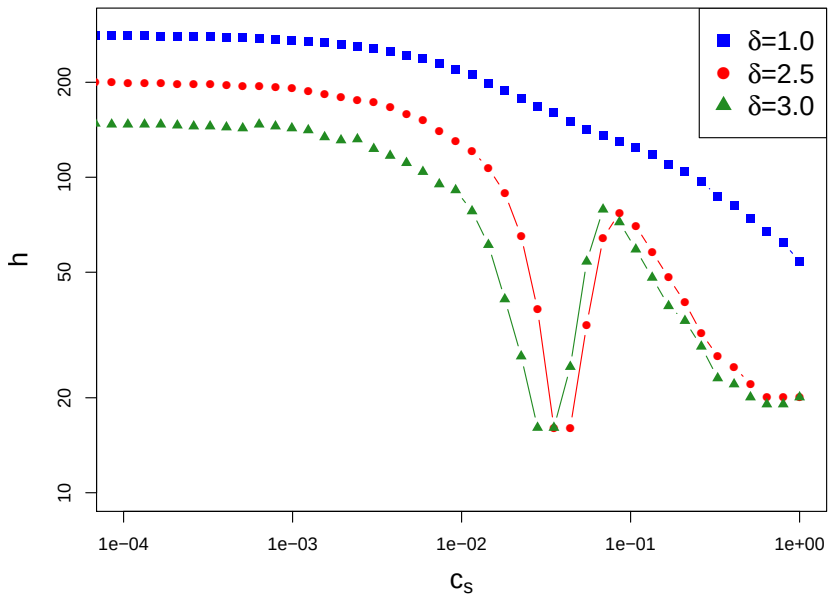

(b)

Figure 6.6. (**??**)The brush height as function of salt concentration for different χ parameter. (**??**)The brush height as function of salt concentration for different δ parameter.

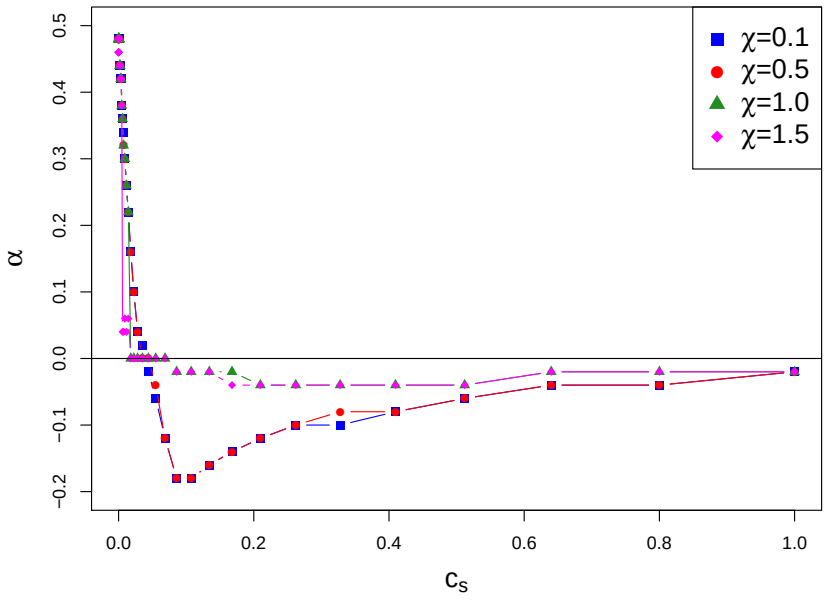

(a)

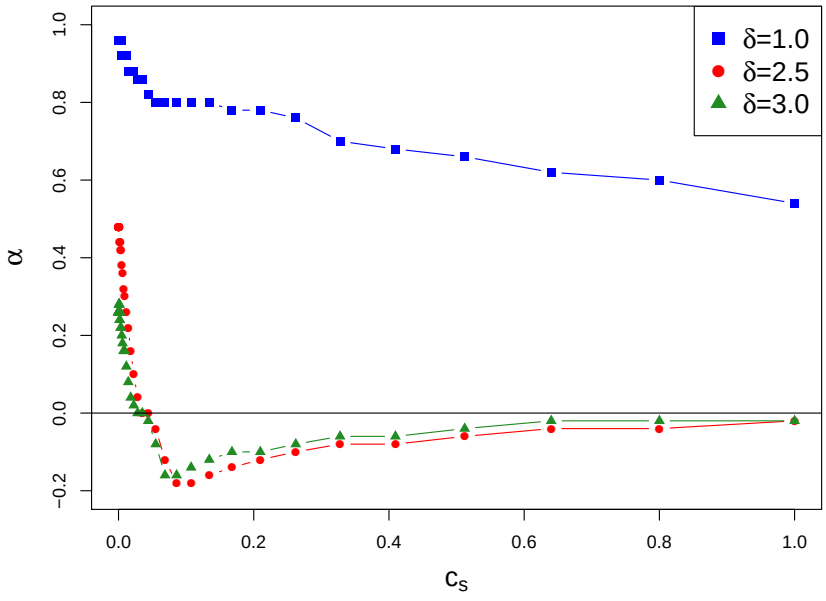

(b)

Figure 6.7. (**??**)The brush height as function of salt concentration for different χ parameter. (**??**)The brush height as function of salt concentration for different δ parameter.

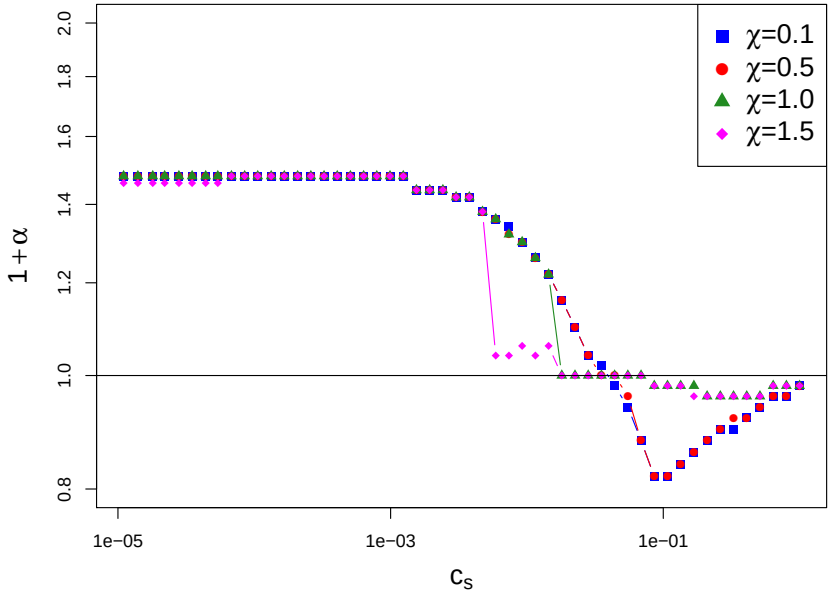

(a)

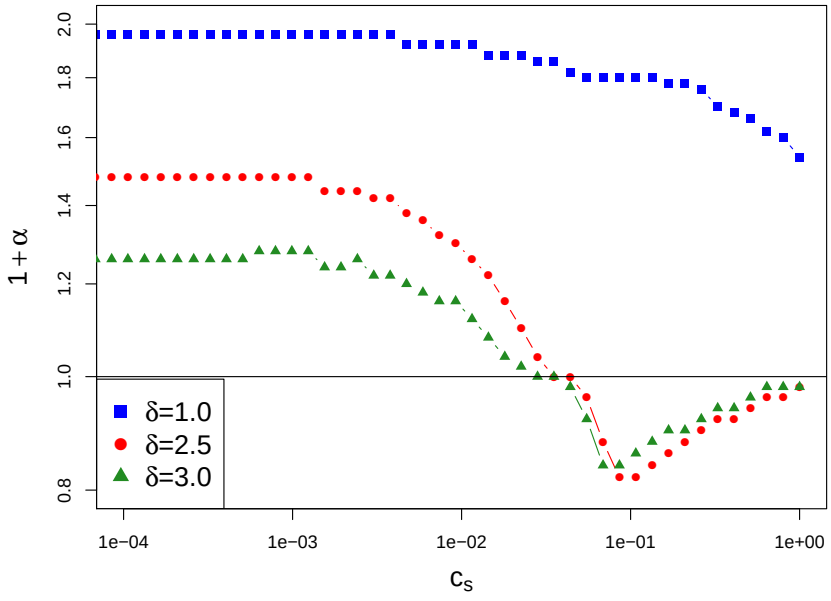

(b)

Figure 6.8. Log-transformed degree of ionization: (a)for different χ parameters; (b)for different δ parameters.

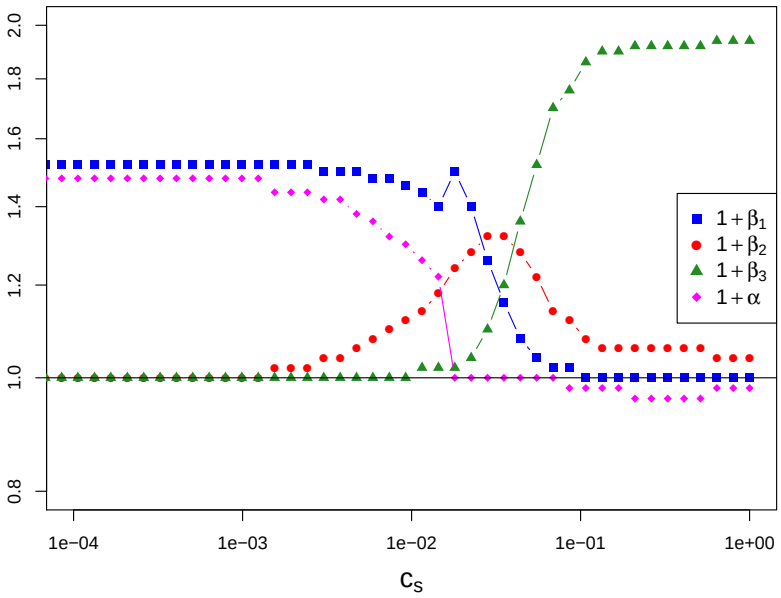

(a)

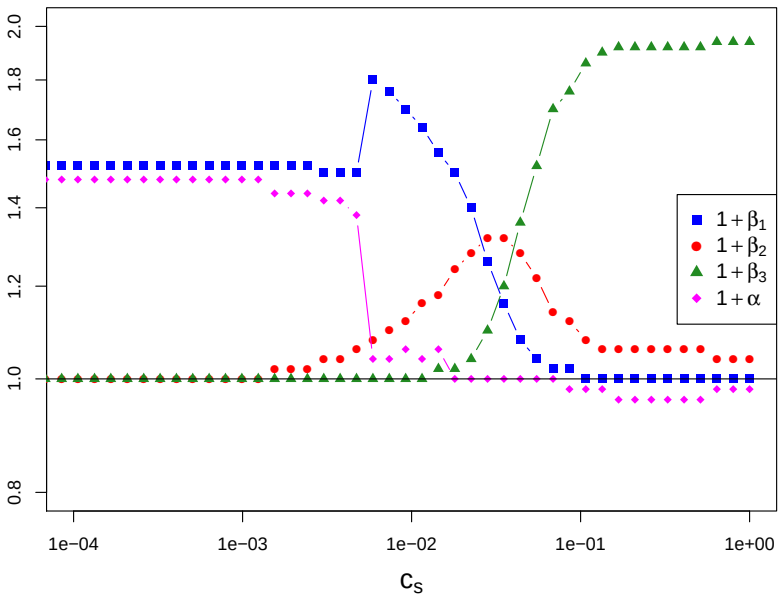

(b)

Figure 6.9. Log-transformed degree of ionization. (a)$\chi = 1.0$; (b)$\chi = 1.5$.

BIBLIOGRAPHY

[] J. Li et al. *Nat. Mater*, 2:611, 2003.

[] F. Li. *Polyelectrolyte brushes at interfaces: properties, structure and interactions*. UCSB, 2005.

[] M. Muthukumar. *Polymer Translocation*. CRC Press, Boca Raton, FL, 2011.

[] B. Alberts et al. *Molecular Biology of the Cell*. Garland Science, New York, 3rd edition, 1994.

[] R. V. Miller. *Scientific American*, 1:66, 1998.

[] C. Dekker. *Nat. Nanotechnol.*, 2:209, 2007.

[] A. Aksimentiev. *Nanoscale*, 2:468, 2010.

[] B. Jeon and M. Muthukumar. *J. Chem. Phys.*, 140:015101, 2014.

[] V. V. Palyulin et al. *Soft Matter*, 10:9016, 2014.

[] A. Meller et al. *Phys. Rev. Lett.*, 86:3435, 2001.

[] H. Bayley. *Clin. Chem.*, 61:25, 2015.

[] M. Muthukumar and C. Y. Kong. *Proc. Natl. Acad. Sci.*, 103:5273, 2006.

[] C. Forrey and M. Muthukumar. *J. Chem. Phys.*, 127:15102, 2007.

[] C. T. A. Wong and M. Muthukumar. *J. Chem. Phys.*, 133:45101, 2010.

[] H. H. Katkar and M. Muthukumar. *J. Chem. Phys.*, 140:135102, 2014.

[] K. Luo et al. *Phys. Rev. Lett.*, 100:058101, 2008.

[] K. Luo et al. *J. Chem. Phys.*, 126:145101, 2007.

[] M. Muthukumar. *Annu. rev. BioPhys.*, 36:435, 2007.

[] M. Muthukumar. *J. Chem. Phy.*, 11:10371, 1999.

[] E. Slonkina and A. B. Kolomeisky. *BioPhy. J.*, 95:3619, 2008.

[] D.K. Lubensky and D. R. Nelson. *BioPhy. J.*, 77:1824, 1999.

[] Y. Kantor and M. Kardar. *Phys. Rev. E*, 69:021806, 2001.

[] E. Eisenriegler et al. *J. Chem. Phys.*, 77:6296, 1982.

[] P. G. de Gennes. *Scaling Concepts in Polymer Physics*. Cornell University Press, Ithaca, NY, 1979.

[] E. A. DiMazio. *J. Chem. Phys.*, 42:308, 1965.

[] K. F. Freed. *Renormalization Group Theory of Macromolecules*. John Wiley & Sons, Inc., Canada, 1987.

[] H. E. Daniels. *J. Chem. Phys.*, 21:290, 1952.

[] J. J. Hermans and R. Ullman. *Physica*, 18:951, 1952.

[] H. Yamakawa. *Helical Wormlike Chains in Polymer Solutions*. Springer-Verlag Berlin, Heidelberg, 1997.

[] K. Freed. *Adv. in Chem. Phys.*, 22, 2007.

[] S. M. Bhattacharjee and M. Muthukumar. *J. Chem. Phys.*, 86(1):411, 1986.

[] Y. Tagami. *Macromolecules*, 2:8, 1969.

[] J. B. Lagowski and J. Noolandi. *J. Chem. Phys.*, 95:1266, 1991.

[] R. P. Feynman and A. R. Hibbs. *Quantum Mechanics and Path Integrals*. McGraw-Hill, Inc., USA, 1965.

[] E. M. Lifshitz and L. P. Pitaevskii. *Physical Kinetics*. Pergamon Press, New York, NY, 1989.

[] C. W. Gardiner. *Handbook of Stochastic Methods for Physics, Chemistry, and the Natural Sciences*. Springer-Verlag, Berlin, 1983.

[] H. Riskin. *The Fokker-Planck Equation*. Garland Publishing, 1994.

[] C. T. A. Wong and M. Muthukumar. *BioPhy. J.*, 95:3619, 2008.

[] W. Fiers and R. L. Sinsheimer. *J. Mol. Bio.*, 5:424, 1962.

[] R. Dulbecco and M. Vogt. *Proc. Natl. Acad. Sci. U.S.A.*, 50:236, 1963.

[] H. Jacobson and W. H. Stockmayer. *J. Chem. Phys.*, 18:1600, 1950.

[] H. Jacobson et al. *J. Chem. Phys.*, 18:1607, 1950.

[] G. Wilemski and M. Fixman. *J. Chem. Phys.*, 60:866, 1974.

[] G. Wilemski and M. Fixman. *J. Chem. Phys.*, 60:878, 1974.

[] M. Doi. *Chem. Phys.*, 11:107, 1975.

[] M. Doi. *Chem. Phys.*, 11:115, 1975.

[] A. Szabo et al. *J. Chem. Phys.*, 72:4350, 1980.

[] J. Roovers and P. M. Toporowski. *Macromolecules*, 16:843, 1983.

[] S. Obukov et al. *Phys. Rev. Lett.*, 73:1263, 1994.

[] J. Sheng and K. Luo. *arXiv*, 1212.1047v1, 2014.

[] S. Obukov et al. *Phys. Rev. Lett.*, 73:1263, 1994.

[] P. G. de Gennes. *J. Chem. Phys.*, 55:572, 1971.

[] R. M. Robertson et al. *PNAS*, 103:7310, 2006.

[] R. M. Robertson and D. E. Smith. *Macromolecules*, 40:3373, 2007.

[] C. D. Chapman et al. *Soft Matter*, 8:9177, 2012.

[] B. van Lent et al. *Macromolecules*, 20:366, 1986.

[] G. Stratouras and M. Kosmas. *J. Chem. Phys.*, 25:3307, 1991.

[] J. Sheng and K. Luo. *RSC Adv.*, 5:2056, 2015.

[] Z. Tang et al. *Small*, 10:4332, 2014.

[] C. A. Merchant et al. *Nano Letters*, 10:2915, 2010.

[] C. T. A. Wong and M. Muthukumar. *J. Chem. Phys.*, 128:154903, 2008.

[] J. Sheng and K. Luo. *Soft Matter*, 8:367, 2012.

[] K. Luo et al. *PRL*, 99:148102, 2007.

[] A. Meller et al. *Proc. Natl. Acad. Sci.*, 97:1079, 2000.

[] A. Meller and D. Branton. *Electrophoresis*, 23:2583, 2002.

[] O. V. Krasilnikov et al. *Phys. Rev. Lett.*, 97:018301, 2006.

[] R. J. Murphy and M. Muthukumar. *J. Chem. Phys.*, 126:051101, 2007.

[] P. G. de Gennes. *Flexible Polymers in Nanopores.* Springer-Verlag Berlin, Heidelberg, 1999.

[] T. Kenneth et al. *Nature*, 261:512, 1976.

[] A. V. Vologodskii et al. *Nucleic Acids Res.*, 6(3):967, 1979.

[] D. E. Pulleyblank et al. *Proc. Nat. Acad. Sci. USA*, 72(11):4280, 1975.

[] L. F. Liu et al. *Proc. Nat. Acad. Sci. USA*, 84:7042, 1987.

[] F. Zhou et al. *Phys Chem Chem Phys*, 8(33):3815, 2006.

[] P. Uhlmann et al. *Prog. in Org. Coat.*, 55:168, 2006.

[] O. Azzaroni. *J. of Poly. Sci. A: Poly. Chem.*, 50:3225, 2012.

[] T. Chen et al. *Prog. in Poly. Sci.*, 35:94, 2010.

[] T. A. Witten and P. A. Pincus. *Macromolecues*, 19:2509, 1986.

[] O. H. Kwon et al. *Biomaterials*, 24:1223, 2003.

[] T. K. Tam et al. *Langmuir*, 26(6):4506, 2010.

[] M. Kobayashi et al. *Soft Matter*, 7:740, 2007.

[] M. Kobayashi et al. *Faraday Discussion*, 156:403, 2012.

[] J. Klein et al. *Nature*, 370:643, 1994.

[] U. Raviv et al. *Nature*, 425:163, 2003.

[] S. Alexander. *J. Phys. (France)*, 38:983, 1977.

[] P. G. de Gennes. *Macromolecules*, 13:1069, 1980.

[] S. T. Milner et al. *Macromolecules*, 21:2610, 1988.

[] P. A. Pincus. *Macromolecues*, 24:2919, 1991.

[] E.B. Zhulina and T. M. Birshtein. *Macromolecules*, 28:1491, 1995.

[] S. Misra et al. *Macromolecules*, 22:4173, 1989.

[] M. Muthukumar. *Adv. Chem. Phys.*, 149, 2012.

[] E. B. Zhulina et al. *Langmuir*, 27:10615, 2011.

[] R. Nap et al. *J. Poly. Sci.B*, 44:2638, 2006.

[] H. Ahrens et al. *Phys Rev Lett*, 81:4172, 1998.

[] M. Balastre et al. *Macromolecules*, 35:9480, 2002.

[] C. Schneider et al. *Langmuir*, 24:10612, 2008.

[] X. Guo et al. *Macromolecules*, 32:6043, 1999.

[] G. S. Manning. *J. Chem. Phys.*, 51:924, 1969.

[] M. Muthukumar. *J. Chem. Phys.*, 120:9343, 2004.

[] P. Gong et al. *Phys. Rev. Let.*, 98:18302, 2007.

[] R.S. Ross and P. A. Pincus. *Macromolecues*, 25:2177, 1992.

[] D. A. McQuarrie. *Statistical Mechanics*. Longman Education, USA, 1975.

[] A. Kundagrami and M. Muthukumar. *J. Chem. Phys.*, 128:244901, 2008.